technische universität dortmund

TÜRK-ALMAN ÜNİVERSİTESİ
TÜRKISCH-DEUTSCHE UNIVERSITÄT

Master Thesis

Thesis submitted for the degree of Master of Science in Manufacturing Technology

Development of intrinsic connection elements to join composite and metal components for automotive applications

by

Can Adalı

Student Number: 181241

Advisors:

Prof. Dr.-Ing. Markus Stommel

Asst. Prof. Dr. Selim Coşkun

Submitted on 26.03.2018

Table of Contents

Abstract

The lightweight construction is in great demand in the 21st century with the increasing need for fuel saving, safety concerns and customized material properties. For its high specific strength and customizable material properties, the composite materials have found its place as a major lightweight material in aerospace, marine and automotive industries. One fastening technique to join these composite parts to other components is bolted joining which requires drilling to form the holes. Nevertheless, drilling weakens the properties of the composite enormously. One technique to reinforce the joint is to place inserts in the bearing region during the production of the composite. In this work, three different reinforcement inserts were designed for joint region of a Mercedes-Benz Truck component, namely metal insert (M), polymer insert (P) and metal-polymer insert (MP). Four different types of glass/epoxy, plain weave textile composite (PWTC) specimens were designed. One specimen type is only drilled which is used as reference, and other three specimen types have inserts embedded between their layers. The specimens were tested under quasi-static loading conditions at a two-parallel pinned pull-through test. It is observed that all the inserted specimens have higher ultimate load capacity relative to the reference specimens (up to 44% improvement). Besides, the bearing strength increases up to 74.7% at the non-drilled specimen types. However, placement of inserts leads to significant delamination failure (up to 3mm delamination at polymer inserted specimen). Moreover, the pin pull-through test of reference specimen and metal inserted specimen were modeled in commercial Abaqus FEA software. Stiffness values from FE analysis is in relatively good correlation with experimental stiffness. The stiffness errors for reference and metal inserted specimens are 5% and 39.2% consequently. The non-elastic response of PWTC specimens were not properly represented in the FE models.

List of Figures

List of Tables

List of Abbreviations and Symbols

PMC – Polymer Matrix Composite

CFRP – Carbon Fiber Reinforced Plastic

GFRP – Glass Fiber Reinforced Plastic

CZM – Cohesive Zone Model

PW – Plain Woven

RTM – Resin Transfer Molding

FRP – Fiber reinforced polymer

PWTC – Plain woven textile composite

RVE – Representative Volume Element

RUC – Repetitive Unit Cell

WF – Woven Fabric

SEA – Specific Energy Absorption

FEA – Finite Element Analysis

FEM – Finite Element Method

PDE – Partial Differential Equation

1 Introduction

In Ch.1.1 a brief background information about the research question of this thesis is given. And then, the approach of this thesis to solve the research question is explained. The design, production, experiment and FE Analysis steps are explained briefly in Ch.1.2.

1.1 Background of the research question

The automotive industry has been facing two main challenges during the past decades, they are the reduction of fuel consumption and CO_2 emission. CO_2 is a greenhouse gas (GHG) which is harmful for environment, and it is emitted in excessive amounts by automobiles. By reducing the fuel consumption, CO_2 emission can be decreased.

Due to the increasing fuel prices and CO_2 emission regulations of governments, car manufacturers are forced to improve fuel efficiency. The fuel consumption is directly related to the vehicle weight. The fuel is consumed for accelerating the vehicle and to overcome the friction between the tire and the road. Reducing the vehicle weight lessens the fuel consumption significantly (Mallick, 2010, p.1-2). Therefore, car manufacturers seek methods to reduce the vehicle weight. According to the Brooke and Evans, the fuel efficiency can be increased up to 8% by reducing the weight of the vehicle by 10% (as cited in Mallick, 2010, p.2).

Besides, if the vehicle is lighter, the power necessary to accelerate and decelerate the vehicle drops. Therefore, smaller and lighter engine, brake system and transmission system can be used. Thus, this secondary benefit leads to further weight reduction opportunities (Mallick, 2010, p.2).

The methods for reducing the vehicle weight are downsizing an existing vehicle and reducing the weight of its components (Mallick, 2010, p.2). The downsizing is the redesign of some parts of a vehicle or whole of the vehicle in a smaller scale. The most frequently downsized component is the engine.

The component weight can be reduced by the following methods: using a lighter material, parts consolidation and design optimization for regional weight optimization. The commonly used lightweight materials are composites, high strength steels, aluminum, magnesium and zinc. Among those, the composites materials are the point of interest in this thesis work.

This thesis focuses on weight reduction of rear cab suspension bracket of a Mercedes Benz Truck by substituting its material from metal to composite material. The bracket is fastened to chassis with two bolts on a flat surface. Since drilling would weaken the composite at the joint region, alternative methods are necessary to reinforce the joint for a durable and safe design. Hybridization of metal and composite is a method to produce both durable and relatively light components. The intrinsic hybridization is a method to produce the hybrid component while

producing the composite. With this method, metal component of the hybrid can be placed between the layers of the composite. In addition, the contact zone between the metal and the composite can be customized to mechanically interlock the hybrid components to each other. Besides, with intrinsic production method, a metal or another material of any shape can be embedded in the composite, in which case the embedded material can be called an insert. In this work, three types of insert are designed to reinforce the joining region of the rear cab suspension bracket.

1.2 Purpose and Approach

There are three main purposes of this thesis work. First is to develop inserts to reinforce an actual metal-composite joint that is used at a Mercedes Benz Truck. Second is to place these designed inserts in the composite specimens that represent the joint area of the Mercedes Truck. And then identify the failure modes at the inserted bearing regions by pin pull-through tests. And finally, it is aimed to validate the pin pull-through tests by FE Analyses. The overall workflow can be seen in the Figure 1.1.

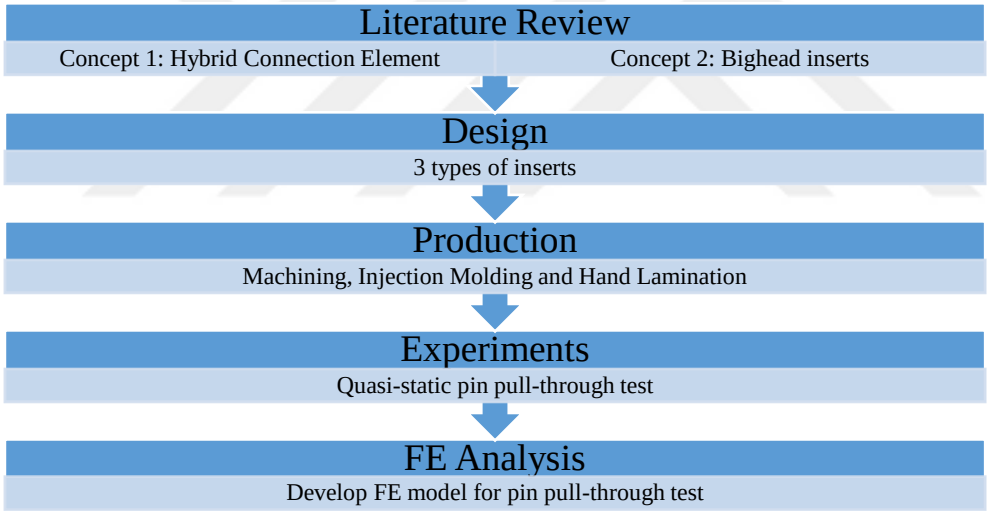

Figure 1.1. The workflow of the research

First a literature survey was conducted on metal-composite joining techniques. Two methods from the literature were used in the design of reinforcement inserts. First method that was inspired from is the hybridization technique with a polymeric material in the metal-composite interface (Pohl & Stommel, 2017). And second method that was inspired from is the commercial Bighead® insert concept (BigHead® Bonding Fasteners, 2015).

Three types of inserts were designed in this thesis. First type is metal insert (abbreviated as ‘M’) which is a sheet steel produced with laser cutting. Second type is polymer insert (abbreviated as ‘P’), which is a 33% short glass fiber reinforced polyamid material produced by injection molding. The third type is metal-polymer insert (abbreviated as ‘MP’) which is a combination

of metal and polymer inserts. It is produced by injection of thermoplastic material around the metal insert with injection molding which is an intrinsic hybridization method. The polymer and metal-polymer inserts have collars at their bearing regions to form a pin socket.

There are two main proposed benefits of the designed inserts. First, the contact zone between designed inserts and composite was intentionally made inclined. This inclined contact zone mechanically interlocks the insert and the composite to each other. Moreover, the inclined contact zone would reinforce the bearing region by distributing the force on the bearing along the inclined contact zone. Second proposed design benefit is the bearing collar. With the help of the designed bearing collars at the polymer and metal polymer inserts, the fiber tows of the plain woven glass fabric are directed around the bearing collar. Thus, a pin socket with hole is formed during composite production. This intrinsic production method removes the need for drilling of the composite, so that there would be less stress concentration at the bearing. Under this circumstance, the bearing is expected to endure higher forces without breaking.

To validate the expected design benefits, a pin pull-through experiment setup with two parallel pins was designed. The experiment setup represents the loading on the joint region of rear cab suspension bracket of a Mercedes Benz Truck. The purpose of the experiments is to observe the failure modes of inserted composites and to compare the effect of the inserts on the bearing durability.

Four types of composite specimens are produced with hand lamination. The material of specimens is glass/epoxy. The reinforcement fiber is plain weave textile fabric. Among those four types of specimens, one specimen type which is only drilled is used as reference. The other three specimen types have inserts embedded between their layers. Each specimen type has a different type of insert embedded between its layers. The inserts were placed with intrinsic hybridization method, which means inserts were placed while producing the composite with hand lamination. The metal inserted specimens are drilled. The polymer inserted, and metal-polymer inserted specimens are non-drilled, their pin socket were shaped during specimen production. The effect of inclined zone and intrinsically formed pin socket were tested under quasi-static loading conditions.

Lastly, the Finite Element Models of reference and metal inserted specimens were created in the commercial FE software Abaqus environment. The elastic material properties that were identified at the performed pin pull-through tests of reference specimens were used at the FE analysis as input material properties. The fracture toughness and strength properties were taken from the literature. The correlation of the load-displacement curves from the experiments and FE Analysis were compared. The failure modes of composite specimens were observed.

2 State-of-the-Art

This chapter informs the reader regarding up-to-date background information of the concepts used in this thesis work. The content of this chapter is mainly taken from the literature. First, a background information about composite materials is given in Ch.2.1. Then, multi-material design and hybridization methods were covered in Ch.2.2. And finally, basics of FE analysis in Abaqus software is mentioned with a focus on modeling of composite structures.

2.1 Composite Materials

Composites consist of a filler matrix and a reinforcing material which is immersed in the matrix. Basically, the reinforcement provides strength and the matrix provides flexibility to the composite material. The composite materials can be classified according to the matrix material or by the reinforcement material (Kaw, 2006).

2.1.1 Types of Composite Materials

According to the matrix material the types of composites are: polymer matrix (PMC), metal matrix and ceramic matrix composites. Among them polymer matrix composites are much common and feasible for automotive applications.

The polymeric material of the matrix could be either a thermoplastic (e.g. polyamide) or a thermoset (e.g. epoxy resin, polyester resin). Both thermoplastic and thermoset matrix (e.g. epoxy resin) composites are used in the automotive applications. In this thesis work, an epoxy resin was used as matrix material.

The reinforcement material is fundamentally stronger than matrix material. The main purpose of the reinforcement is to bear the major part of the applied load on the composite material. In addition, the shape and the material of the reinforcement highly affect the load bearing capacity of the composite. Therefore, according to the loads that will be applied on the composite material, the adequate type of composite should be selected.

Basically, there are three types of composites according to the shape of the reinforcement as shown in the following Figure 2.1. The particulate composites are basically the mechanically improved version of the matrix. The particles can be bulky balls, carbon Nano-tubes or chopped glass fibers. Body panels, dashboards and intake manifolds are example usages of particulate composites from automotive applications.

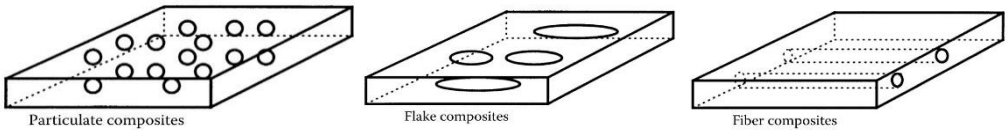

Figure 2.1. Composite types by shape of reinforcement material. (Left): Particulate Composite, (Middle): Flake composite, (Right): fiber composite. Retrieved from (Kaw, 2006).

The fiber reinforced composites (FRP) is maybe the most commonly used type of composite in the industry due to its high design flexibility. The fibers can be in continuous or discontinuous lengths. The examples of discontinuous fibers are chopped short fibers (can be also considered as particulates) or long fibers in random orientations (mat) Figure 2.2. The examples for the continuous fibers are unidirectional pre-pregs or weave fabrics (Figure 2.2 & Figure 2.3).

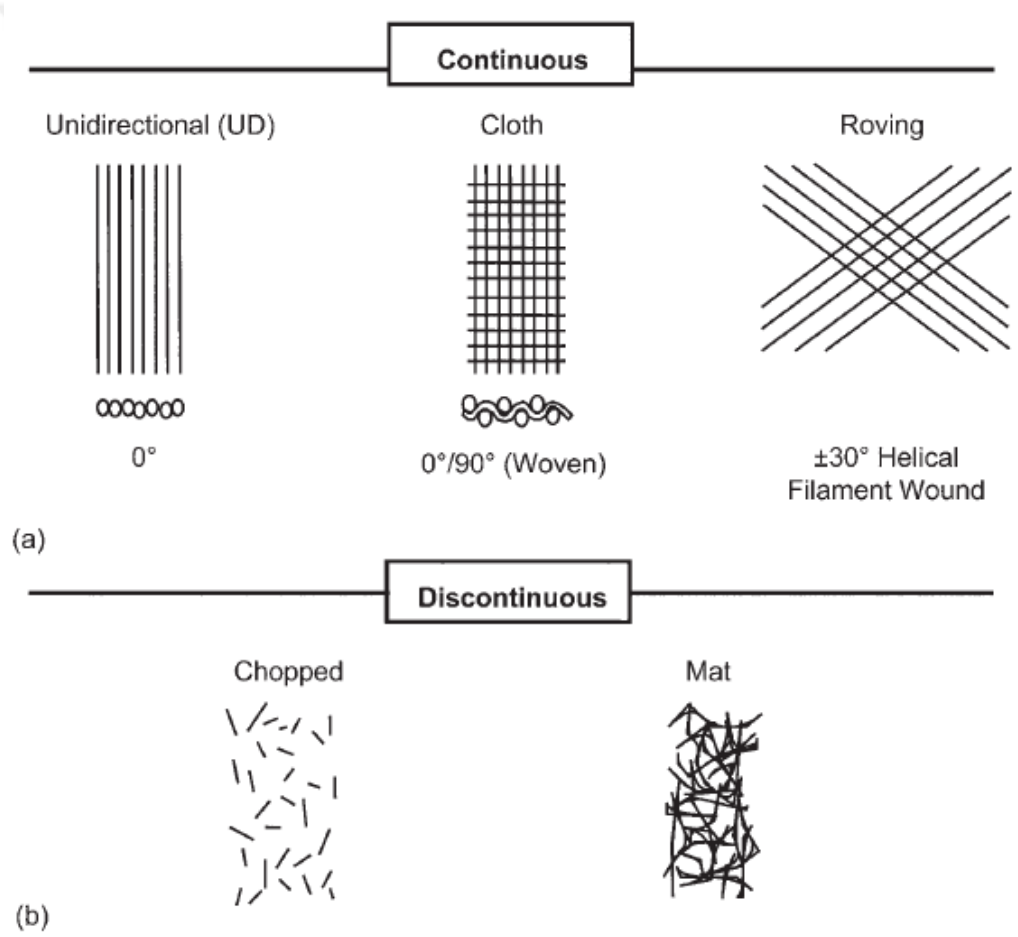

Figure 2.2. Types of reinforcement fiber. Retrieved from (Campbell, 2010, p.2).

In the unidirectional pre-pregs, the fibers are aligned in only one single direction where all off the continuous fibers are aligned parallel to each other. Differently, in woven fabric, the fibers

are weaved into each other, they are curved and aligned in two perpendicular dimensions perpendicular.

The strength and the elastic modulus of a composite is extremely higher in longitudinal fiber direction. For instance, the longitudinal modulus of a unidirectional carbon fiber/epoxy composite is more than 14 times higher than its transverse modulus. (E_{long}= 207 GPa, E_{trans}= 14 GPa). For this reason, the random fiber composites have more isotropic material properties whereas the unidirectional and bidirectional composites have clearly non-isotropic material properties (Mallick, 2010, p.18).

According to the specific loading conditions in which the composite structure will be used, the fiber orientation can be decided. Therefore, composites can be used at various industries such as automotive, aerospace, marine and renewable energy for various structures. In addition to its high specific strength, the design flexibility of the composites is one of the biggest advantages of the composite structures

The specific strength of a fiber is much higher than of a bulk material. The reason is that fiber has less defects thanks to its thin radius than a bulk material. The smaller the material volume is, less likely it is to have internal/external defects. Absence of defects is an important merit for durability.

Although the short fiber-polymer matrix composites are preferred most in the automotive industry due to its suitability for mass production (e.g. with Injection molding), short fiber composites do not have the highest strength-to-density ratio. On the other hand, continuous fiber composites have higher strength to density ratio, but they are less suitable for mass production.

The common fiber materials are Kevlar, carbon and glass. Natural fiber materials such as silk can also be used as reinforcement fibers. For its low cost and relatively high durability, glass fiber is frequently used in the industry.

In Table 2.1, the properties of carbon fiber reinforced plastic (CFRP) and glass fiber reinforced plastic (GFRP) are compared relative to the steel. The values in the table are not real values, instead they are representative values for comparison.

Table 2.1. *Representative costs of FRPs relative to the generic steel (Mallick, 2010, p.19)*

Material	Relative Density (ρ)	Relative Elastic Modulus (E)	Relative Tensile Strength	Relative Material Cost
Steel	1	1	1	1
CFRP	0.2	0.67	4.89	15-20
GFRP	0.23	0.19	3.04	8

As can be seen in the Table 2.1, the continuous fiber composites have higher specific strength comparison to steel. Besides, the density of the FRPs is only the 20% of the steel's density which is a great advantage for weight reduction. On the other hand, the cost of the FRPs is at least 8 times higher than the cost of the steel.

2.1.2 Mechanical Property Comparison between Woven Composites and Unidirectional Composites

The choice of reinforcement is a major step in the design of composites. As mentioned in the previous section, the two common fiber reinforcements are unidirectional and weave fabrics. The unidirectional fiber reinforcement consists of a sheet of non-undulated, parallel aligned fibers only one single direction. UD fiber layers have the maximum possible stiffness in the direction of the fiber alignment which is longitudinal direction, whereas very low stiffness in the transverse direction.

Woven fabrics consists of weaved fiber tows that are aligned both in longitudinal and transverse directions (Figure 2.3). Although that provides with stiffness in two directions, due to the undulation of the fiber tows, the maximum possible stiffness of woven composites is lower than their equivalent unidirectional conjugate.

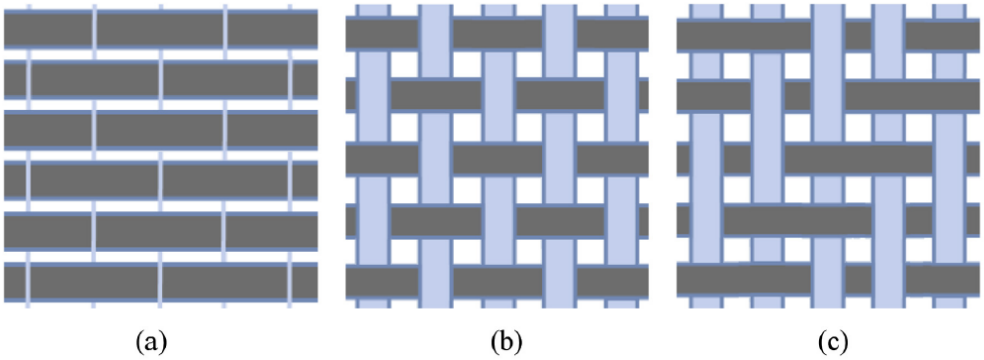

Figure 2.3. Continuous fiber reinforcements. a) Unidirectional. b) Plain weave fabric c) twill weave fabric. Retrieved from (Cai et al., 2017, p.144).

Although the stiffness of woven fabric drops due to the undulation of its fibers, it can drape and cover the non-flat, curved surfaces much better than unidirectional fabric (Harris, 1998, p.56). Other advantages of woven fabric composites are low effort manufacturability and good impact resistance.

Naik reports that the static load limit to initiate damage is higher for woven fabric composites than cross-ply unidirectional composites (Naik & Nemani, 2001, p.167).

Lastly, according to Pein woven fabric composites have higher weight specific energy absorption capacity during bearing failure than UD composites (as cited in Bergmann &

Heimbs, 2017). In Figure 2.4, Bergmann's pin pull-though test can be seen. As the pin is pulled, only the material in contact with the pin is destroyed. Therefore, the woven composite absorbs impact energy as the pin moves forward. In Figure 2.4, the area under the force-displacement curve represents the absorbed energy.

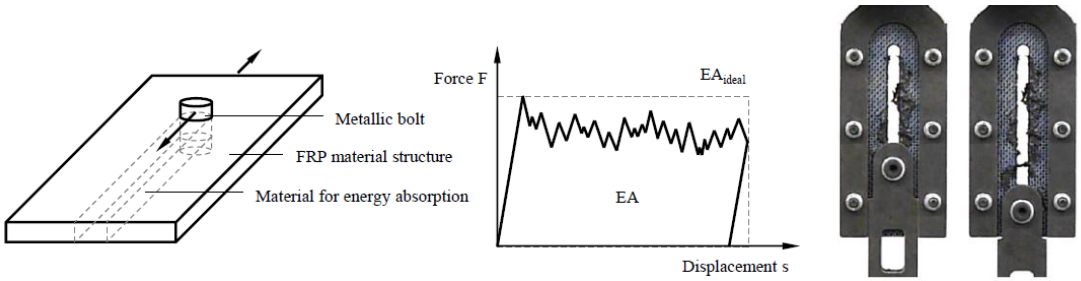

Figure 2.4. Bergmann's pin pull-through test. Reprinted from (Bergmann & Heimbs, 2014, p. 2-4).

2.1.3 Composites in Automotive Applications

According to Kaw (2006, p.39), the weight of the composite parts in an automobile is only 8% of the total weight of the vehicle. In the automotive applications mainly, short E-glass fiber reinforced polymer matrix composites (PMC) are used. The short fiber E-Glass is preferred because of its low cost and suitability for mass production with injection molding and compression molding (Mallick, 2010, p.18). Some thermoplastic PMC automotive parts are: inner door panels, bumper beams and seat backs (Mallick, 2010, p.18). The thermoplastics used at these components are polypropylene (PP), Polyamide-6 and polyamide 6, 6. The common used thermoset PMCs in automotive industry are sheet molding compounds (SMCs). Its structure is random-oriented discontinuous E-Glass fibers inside a polyester or vinyl ester resin. Some SMC automotive parts are door and roof frames, hoods and radiator support (Mallick, 2010, p.18). The advantages of making leaf springs from composite material are unlikeliness of catastrophic failure, ride comfort and longer fatigue life (Kaw, 2006, p.39).

2.2 Failure Modes of Woven Fabric Reinforced Composites

The Failure of FRPs is a highly complex phenomenon since it is a combination of simultaneous cracking, bending and deforming of its building elements (reinforcement and matrix). In addition to the type and volume fraction of the components, the weave pattern of the fibers also plays a very crucial role. On the top of it, drilled and bolted composites show much more complex behavior than non-drilled composites. In this section, the failure modes of woven fabric reinforced composites are covered.

The failure of composites can be basically classified as inter-laminar failure, intra-laminar failure and bearing failure.

2.2.1 Inter- and Intralaminar failures

The inter-laminar failure is detachment of the plies from each other. This failure is also referred to as delamination failure (Figure 2.5). In delamination failure, mainly the matrix falters and the plies of the composite laminate detach from each other, the fibers do not undergo any failure.

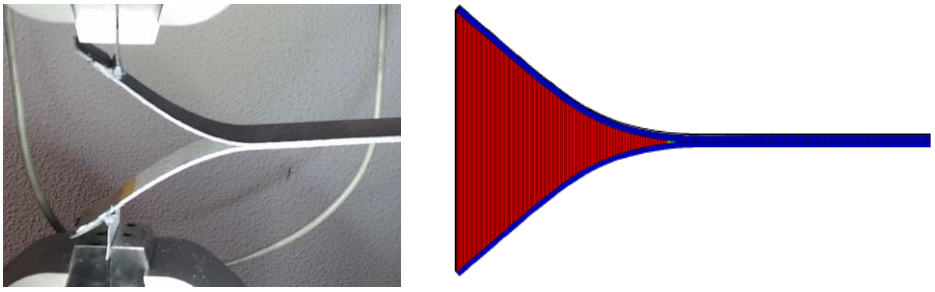

Figure 2.5. Delamination of the composite plies. Retrieved from (Schraa, 2016, p.28).

Intra-laminar failure stands for the cracks that occur within one or multiple plies of the laminate. At UD composites, intra-laminar cracks might tear the ply either between the fibers or perpendicular to fibers by breaking them apart (Figure 2.6). At woven composites, intra-laminar ply failure grows by destroying the fiber tows.

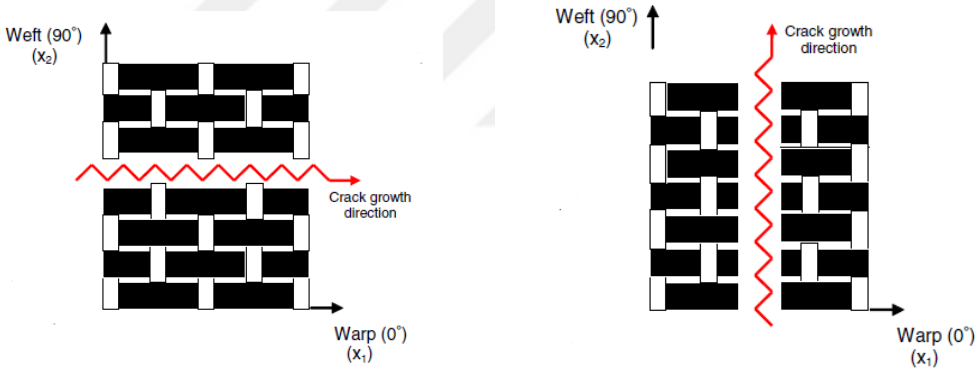

Figure 2.6. Intra-laminar cracks at PWTC. Retrieved from (Donadon et al., 2007, p. 1598).

The failure mechanisms of plain and satin weave composites under compression are kink band formation and delamination. The sets of compressively broken fibers are called kink bands (Figure 2.7). For higher fiber waviness, kink band formation is more likely. In other words, the strength of textile composite drops as the waviness of the fiber tows elevates (Cox & Flanagan, 1997, p.3-5).

(A) 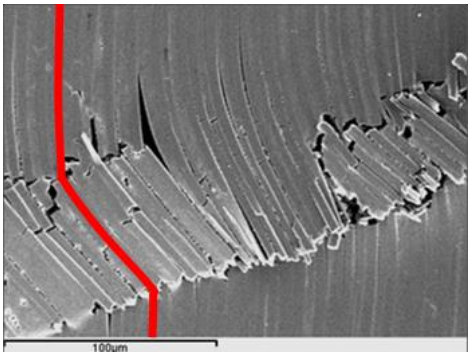

(B) 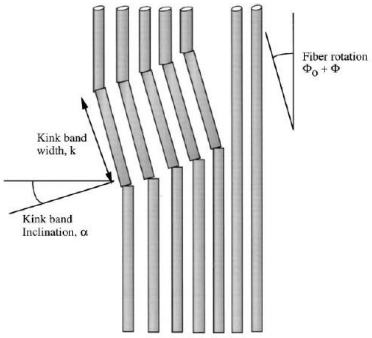

Figure 2.7. Kink bands that occur under compression. (A) Retrieved from Plymouth University teaching support materials (Summerscales, 2017) (B): Retrieved from (Garland et al., 2001, p.2462)

As the fiber architecture of the woven composites include waviness and crimp of fibers in 3D, their failure modes are more complicated than unidirectional composites. The tow waviness (undulations) of woven fabric (Figure 2.8), results in stiffness reduction in in-plane directions and additional failure mechanisms that are not observed at UD composites.

(A) 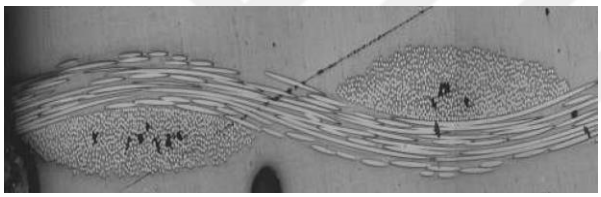

(B) 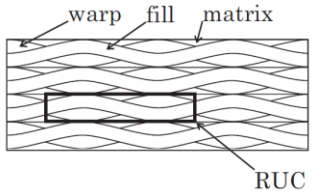

Figure 2.8. Microstructure of a PWTC. The undulation of the fiber tows (A). Repetitive unit cell of a plain weave textile composite (B). Retrieved from (Adumitroaie & Barbero, 2012, p.4).

2.2.2 Bearing at Composites Failure

Drilling, weakens the composites drastically since it violates the continuity of the fibers and creates notch effect. As the main load carrying component is the reinforcement fiber, the damage on the fiber tows results in serious stiffness and strength reduction of the composite. Therefore, the strength of open hole composite coupon (drilled composite) is much lower than non-drilled composites coupon.

Four principle failure modes of fastened composites (filled hole composite by pin or bolt) are net-tension, shear-out, cleavage and bearing failure (Figure 2.9).

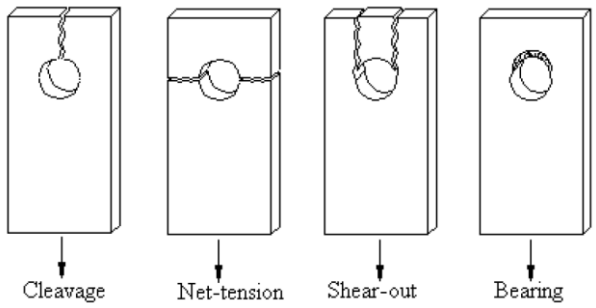

Figure 2.9. Bearing failure modes at drilled and fastened composites. Retrieved from (Pakdil et al., 2011, p.124)

The bolted composites fail at the bearing area by local compressive stresses in front of the bolt (Bergmann & Heimbs, 2017, p.300). According to the Farley and Jones (1992), the failure mechanisms of composite at drilled bearing area are: crushing characteristics by bolt are transverse shearing, laminate bending, brittle fracturing and local buckling (Figure 2.10).

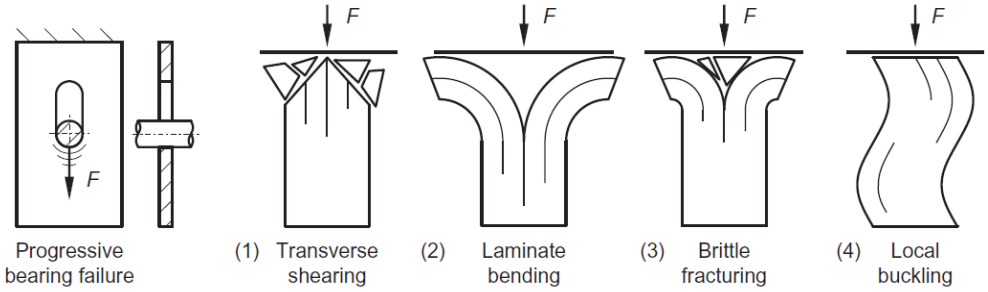

Figure 2.10. Crush characteristics of the composite under pin compression (Bergmann & Heimbs, p.300)

For safety concerns, energy absorber materials are used in passenger cars, trains and airplanes. These absorbers overtake the impact energy so that high forces and accelerations on the passengers are prevented. Composites is a type of energy absorber material.

Under bearing mode failure (Figure 2.9) fastened composite acts as a good impact energy absorber. When the bolt is pulled through the length of the composite, it shows a relatively constant rate of progressive failure. As the bolt pulled through the composite, it crushes the fibers bundles and the matrix sequentially along the way. This allows for absorption of a high amount of energy. Therefore, bearing mode failure of composites can be used as high weight specific energy absorption (SEA) materials for the above-mentioned purposes. Under progressive crushing, woven FRP absorbs more energy than unidirectional FRP according to Kim et al. (2009).

2.2.3 Bearing Response of Composite under Compression by Pin

The material properties of a drilled material are lower than of a non-drilled (unnotched) material of the same kind. The drilled but not fastened specimen is called an open hole (notched) specimen. An open hole specimen fastened with a pin or bolt is called filled hole specimen (Figure 2.11). The response of bearing under compression of a pin or bolt can be called as bearing properties which are fundamentally lower than unnotched specimen configuration.

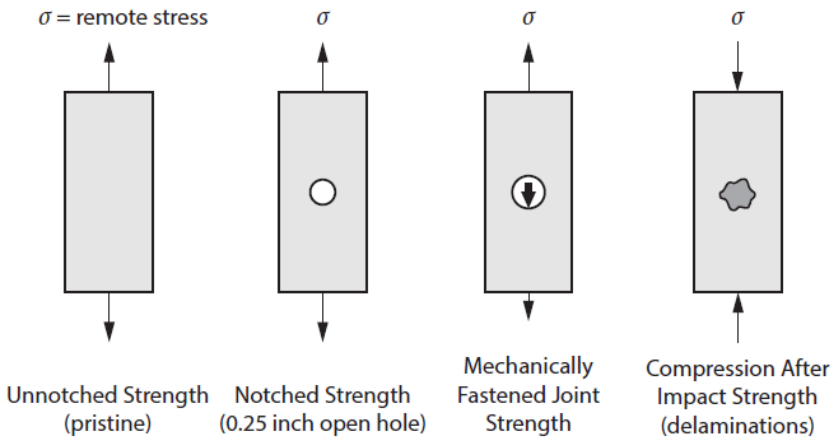

Figure 2.11. Specimen configurations. Reprinted from (Esp, 2017, p.28)

During the pin pull-through tests, the bearing region of the composite is compressed by the pin. As the pin moves forward, it opens its way by crushing the composite. The output of pin pull-through tests is force-displacement plots. The obtained plots are evaluated in terms of three parameters: stiffness, ultimate load bearing capacity of the bearing and bearing strength. In the Figure 2.12, a sample force-displacement curve of pin pull-through test of reference specimen W1 is shown. In this work, the pin pull-through force-displacement curves are investigated for stiffness, bearing strength and ultimate load bearing capacity.

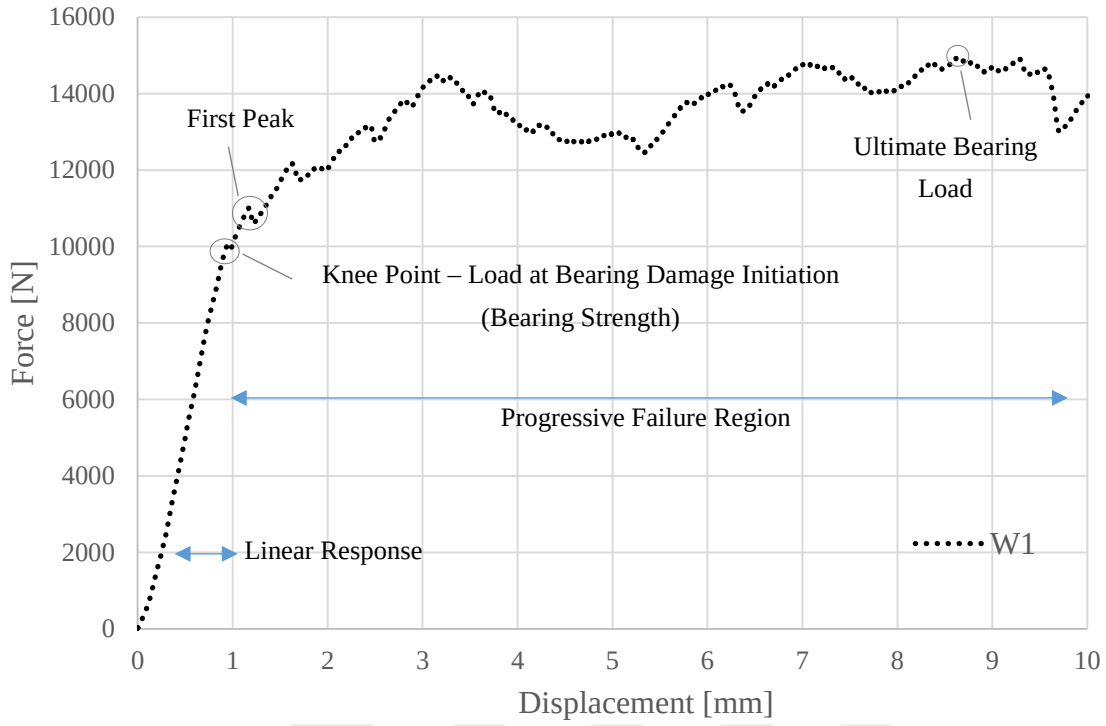

Figure 2.12. The transition from elastic to plastic response of reference specimen W1

The stiffness corresponds to the slope of the linear region of the force-displacement curve. According to Xiao (2015), the bearing strength (or damage initiation) value can be taken at 4%-hole displacement value (p.1024). The designed test system in this work is a customized test concept that represents a specific loading condition of a Mercedes Truck component. Therefore, a standard procedure cannot be followed to determine the bearing strength as Xiao suggests. The first drastic load drop is named as knee point. The knee point is considered as the damage initiation point which is the starting point of the non-linear bearing response. In the figure, the elastic response can be seen up to 1mm hole displacement. After the knee point, the scattered region is the non-elastic response. During the non-elastic response, the composite undergoes permanent damage and its stiffness drops. Despite the stiffness drop, the bearing can still carry load after the failure. The ultimate load capacity of the bearing is observed at the progressive failure region of the curve.

The bearing strength cannot be obtained from force displacement curve. Therefore, it should be calculated to stress-strain plot for calculation of bearing strength and elastic modulus. To determine the effective elastic properties at the bearing area, first the force-displacement curves of reference laminates should be converted to stress-strain curves, and then from the linear region of the obtained stress-strain curve, the elastic constant in pin movement direction should be calculated.

According to Karakuzu et al. (2008, p.4), bearing stress at one of the two parallel pin-loaded holes is

$$\sigma = \frac{F}{2 \,.\, D \,.\, t} \qquad \textit{Equation 2.1}$$

where σ is the bearing stress at each hole, *F* is the applied load, *t* is the thickness of the laminate and *D* is the diameter of the hole. According to Gay et al. (2014, p.140) and Liu et al. (2014, p.967) bearing strain for two parallel pin-loaded holes is

$$\varepsilon = \frac{\delta}{D} \qquad \textit{Equation 2.2}$$

where ε is the bearing strain and δ is the bolt displacement.

2.3 Multi-Material Design and Hybridization

For a robust hybrid structure, the strength of contact surfaces between structural elements is crucial. The strength of interface between hybrid components can be enhanced by modifying the contact surface. Some contact surface modification alternatives are customized contact zone by intrinsic hybridization, surface structuring the joint surface and roughening of the contact surface.

2.3.1 Intrinsic Hybridization

One method to produce multi-material hybrid parts is intrinsic hybridization. Intrinsic hybridization is a production method that the hybrid components are joined to each other during the production of one of its components.

For example, over molding a thermoplastic onto a metal with injection molding process is an intrinsic hybridization. Instead of producing the thermoplastic and metal separately, and then joining the two components in another production step, by intrinsic hybridization method the hybrid component can be produced in one single step. Intrinsic hybridization can also be implemented in resin transfer molding (RTM), integral tube blow molding, rotational molding and automated fiber placement processes. (Koch et al. 2016, p.239). In short, by consolidation of production steps, time and money for production of the hybrid component can be reduced.

Examples for customized contact zones are curved and inclined joining zones (Figure 2.13). Such joining zones improves the joint strength by reducing the stress peaks on the joint interfaces. The hybridization methods can be combined to superimpose their effects (Kießling et al. 2016, p.4).

(A) 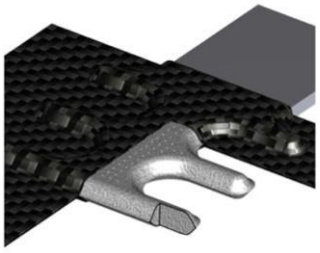 (B)  (C) 

Figure 2.13. Customized contact zones: (A) Inclined contact zone and (B) curved contact zone and, (C) curved and inclined contact zones combined. (A) and (B) retrieved from (Kießling et al. 2016, p.4).

2.3.2 Surface Structuring and Surface Roughness

The customized contact surface between hybrid components (Ch.2.3.1) provides mechanical interlocking in macroscale. To further improve the strength of the contact surface, a method called surface structuring can be used. Surface structuring is a method to enhance the surface adhesion between two surfaces. Surface structures are geometric patterns that are shaped on a contact surface(Ucsnik et al., 2010). The surface structures provides mechanical interlocking by penetrating into to surface of the other contact pair. The surface structures can be pins, grooves or walls. They act as mechanical undercuts and improves the mechanical interlocking between metal and composite

Lucchetta et al. (2011) molded thermoplastic polymer onto an aluminum using injection over-molding process. They showed that the joint strength between the metal and the thermoplastic polymer is higher when metal's surface is rougher.

2.3.3 Injection Molding for Hybridization

The main methods to manufacture plastic products are blow molding, extrusion molding, injection molding and thermoforming. Blow molding produces hollow parts, where extrusion molding is used for making fixed profile parts. In thermoforming, a plastic sheet is pressed in a mold. In injection molding, the plastic is pushed to fill a cavity to shape the plastic part.

Very complex plastic parts can be produced with injection molding. Besides, injection molding is very suitable for serial production. In the long run, injection molding is very suitable to produce low cost plastic parts. More importantly, injection molding process is used widely to make hybrid parts. One of the hybrid component can be placed inside the injection mold cavity, then the plastic can be injected to surround the hybrid component. The mechanical interlocking is formed between hybrid components. Complex hybrid parts can be produced with this method. This hybridization method is exploited by Pohl & Stommel in their metal-polymer hybrid connection (2017). In addition, injection molding is used in making of metal-polymer front end of Ford Focus and Audi A6 Avant (Lanxess Corporation, 2005).

2.3.4 Polymer to Metal Surface Adhesion

To join dissimilar materials to each other, a sticky adhesive material can be applied to the interface. Adhesives is not covered in this chapter since it is not used in this thesis work. Another method is direct surface adhesion between the dissimilar materials. Typically, direct surface adhesion between two dissimilar material (e.g. metal and thermoplastic) is not strong.

The three main alternatives to improve the polymer to metal direct adhesion according to Grujicic et al. (2008, p.363) are micro scale interlocking, pre-coating of the metal and chemical modification of the polymer. However, among above mentioned adhesion promoters only the micro-scale polymer-to-metal mechanical interlocking approach was used. The molten plastic infiltrates into the micro scale-roughness features on the metal insert. This infiltration provides with mechanical interlocking between metal and polymer.

The four process parameters that affect the strength of direct adhesion between polymer and metal are the temperature of the metal insert, linear velocity of the injection screw, thickness of the polymer and packing pressure (Ramani & Moriarty, 1998).

In their investigation Ramani and Moriarty (1998) found that the temperature of the metal inserts to be the most critical process parameter. They suggest the optimum temperature for metal as 210 ^{o} C degree during the plastic to metal over-molding process. Ramani also shows that if the metal is at room temperature during the injection, the plastic freezes before being able to infiltrate into the micro-roughness features of on the surface of the metal.

2.4 Finite Element Modeling at Abaqus Environment

Since experimental testing is often a very cost-intensive procedure, the engineers prefer to solve the mathematical description of the engineering problems. The partial differential equations (PDEs) at the mathematical description of the real-life problems can be solved with analytical or numerical models. Although analytical solutions are very accurate, it is difficult or mostly impossible to solve the PDEs of a problem analytically. On the contrary, the numerical methods offer an effort-accuracy friendly solution for engineering problems, therefore numerical methods are preferred by engineers.

Finite Element Method (FEM) is the most popular numerical method that is used by engineers. In Finite Element Analysis (FEA), the geometry (or the solution space) is discretized in smaller volumes that are also called mesh elements. PDEs are solved for each mesh element. The FEM solution to the PDEs approximates the real solution.

- In this thesis, the commercial FEA software Abaqus is used. It allows for simulation of the composites structures. The composites can be modeled in Abaqus environment in different scales according to the purpose of the analysis. Simulia/Abaqus Documentation suggests the following approaches for FE modeling of the composites (Smith, 2009).
- Microscopic Modeling: Both the reinforcement and matrix are modeled and meshed as individual solid bodies. In this method, reinforcement – matrix interface can be modeled.
- Macroscopic Modeling: The composite lamina is modeled as a single anisotropic solid body.
- Mixed Modeling: The layers of composites are modeled forming the composite laminate. Most common and Abaqus offers standard tools for this method (e.g. Composite layup)
- Sub-modeling: A certain area of an already existing model is modeled in a 'sub-model' in more detail (e.g. modeling stress peaks at the tip of the reinforcement).

2.5 FE Modeling of Plain Weave Textile Composite

Composite materials consist of at least two constituents. To perfectly model a composite structure in FE environment, it is necessary to geometrically model and characterize the material properties of each constituent. In an ideal model micromechanics of the composite should be represented. For this, fibers and the matrix of the composite should be modeled and meshed separately. The contact interaction between the fibers and the matrix should be defined. However, FE modeling of PWTC are often simplified since micromechanical modeling requires high effort to model the geometry of the inter-weaved fiber tows and their interaction with the matrix (Knight, 2008, p.3).

One simplification method which is not used in this thesis, is to model plain and satin weave fabric plies as two unidirectional plies at [0^o/90^o] directions. In this configuration, one woven composite ply is represented with two layer of mesh elements. One layer of mesh elements is modeled as an UD ply which is aligned in the warp direction and the other layer of mesh elements is modeled also as an UD ply which is aligned in the weft direction. Both layers of mesh elements should be assigned to have half of the thickness of the actual woven composite ply (Knight, 2008).

In another simplification method, which is used in this work, every composite layer is represented with one layer of mesh element at thickness. The thickness of mesh elements should have the same thickness as composite plies. The characterized material properties of the composite should be assigned to the mesh elements. In this approach, the mesh elements represent the fibers both in warp and weft directions. Therefore, the corresponding material property of the composite should be assigned to principal directions of the mesh elements. It can be assumed that the properties of the composite are the same in warp and weft directions for further simplification (E1=E2).

3 Design of Composite Specimens

3.1 The Real Case Scenario – Truck Component

The design of the composite specimens was realized according to the connection area of current Cab rear suspension bracket to the chassis. The component was produced from steel and would like to be replaced to composite material within the scope of cost & weight reduction.

The Mercedes Benz-Truck component of interest is a bracket (Figure 3.1) at rear cab suspension unit. This bracket was fastened to the chassis with two M18 bolts.

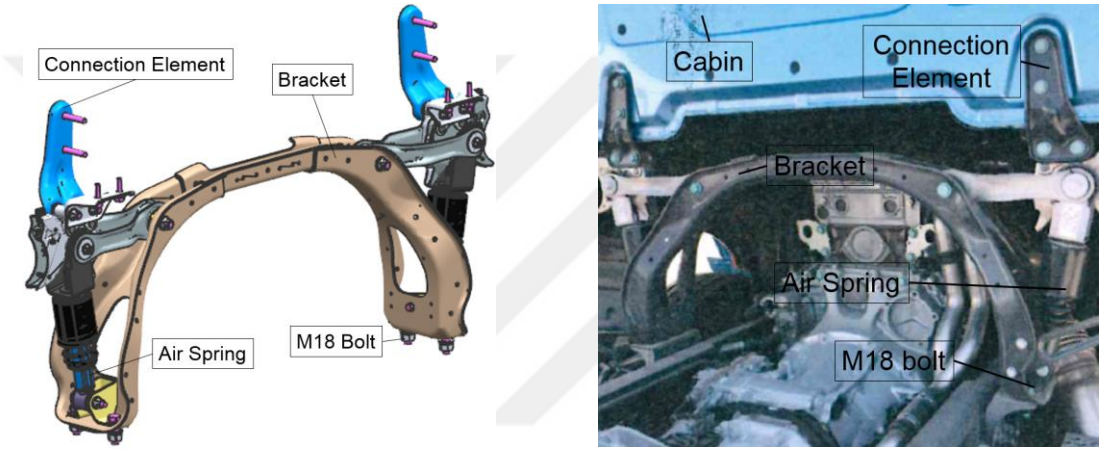

Figure 3.1. The rear cab suspension bracket

The bracket is in U shape, has two flat surfaces at its both ends, these two flat surfaces (Figure 3.1) sits on the chassis. These flat surfaces of the bracket are fastened to chassis with two M18 bolts at each side (Figure 3.2). The bracket is part of the rear cabin suspension unit. The steel bracket and the air springs damp together the impacts on the cabin.

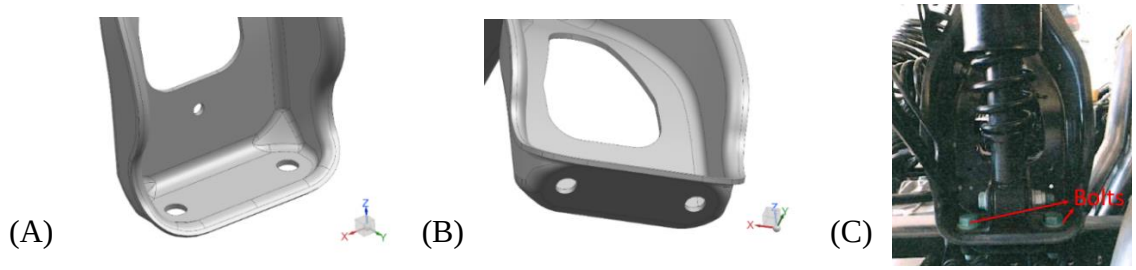

Figure 3.2. The flat surface of the bracket that sits on the chassis (A & B) and bracket is connected to the below connection elements with two M18 bolts (C).

3.2 The Concepts used at the Design of Inserts

Two joining concepts from literature inspired the insert design at this thesis. As shown in Figure 3.3, the first concept is the hybrid connection element of Pohl & Stommel (2017). And the second concept is the fastener inserts that can be placed between the layers of the composite (BigHead® Bonding Fasteners, 2015). In Figure 3.5., implementation of a Bighead® insert in composite can be seen.

The concept of Pohl and Stommel (2017) is based on mechanical interlocking of the joint partners to each other. The joining components are interlocked to each other with the help of inclined contact zones which creates bumps as in the Figure 3.4. In his specimens, he joins a rectangular aluminum sheet and CFRP to each other (Figure 3.3).

Figure 3.3. Hybrid metal-composite connection element with a polymeric material in the interface (Pohl & Stommel, 2017).

There are two problems regarding joining the composites with mechanical fasteners (e.g. bolt). First is that drilling weakens the composite, and second is tapping of composite is not perfectly possible. Bighead® inserts offers remedy for these two issues.

Some type of the Bighead® inserts has a tapped bolt socket (Figure 3.5). The Bighead insert is placed between the layers of the laminate before curing of the composite. By doing so, the tapped bolt socket is placed at the composite. In addition, the reinforcement fibers can be layed around the socket collar during the production of the composite. In short, by using Bighead® inserts, drilling and weakening of the composite can be avoided. Besides, the metal sheet of the BigHead® insert provides with additional contact and reinforcement between fastener and the composite (Figure 3.5).

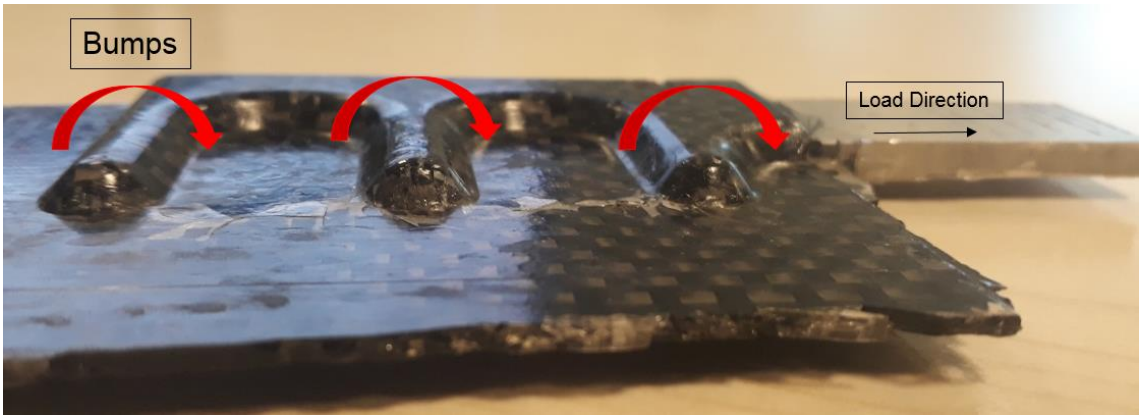

Figure 3.4. Inclined contact surfaces (bumps) (Pohl & Stommel, 2017).

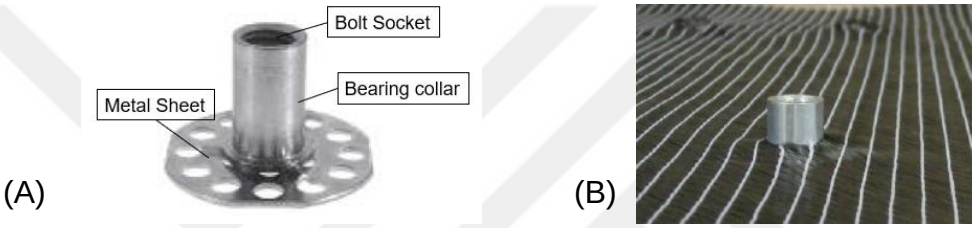

Figure 3.5. A commercial Bighead® Insert (A) with a pre-defined bolt socket and Bighead® insert embedded in CFRP (B). Images retrieved from (BigHead® Bonding Fasteners, 2015).

The above mentioned three concepts (curved contact surface, pre-defined, tapped bolt and directing the fibers around socket collar) were exploited at the inserts of this thesis work (Table 3.1). As can be seen in the following Figure 3.6, in this work the inclined contact surface were inspired from Pohl's design.

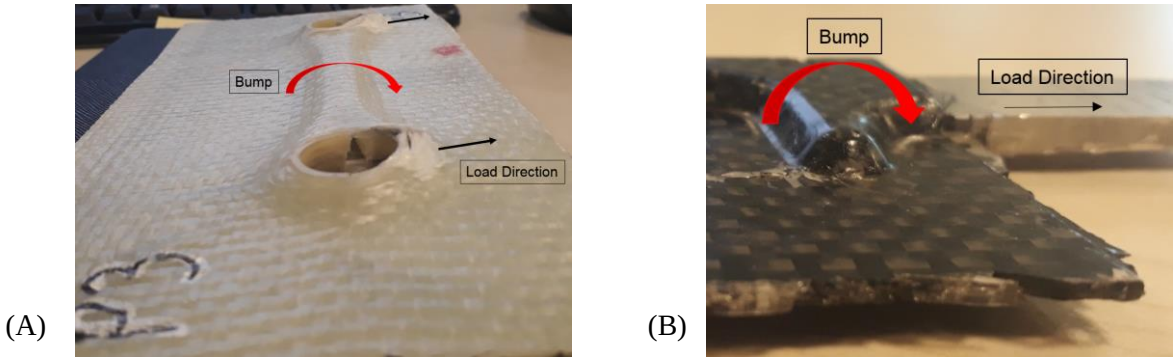

Figure 3.6. Curved contact surface designed at this work (A) and curved contact surface at Pohl & Stommel's design (B).

The inserts of this thesis have bolt sockets (Figure 3.7) similar to BigHead® inserts. However, in this thesis the sockets were not tapped for two reasons. First, the material of the insert (thermoplastic) is not suitable for tapping. Second, tapped hole is not necessary since pinned

connection is used in this work. Pinned joint was used to be able to observe crush of the composite and to avoid the pretension on the composite by tightening of the nut.

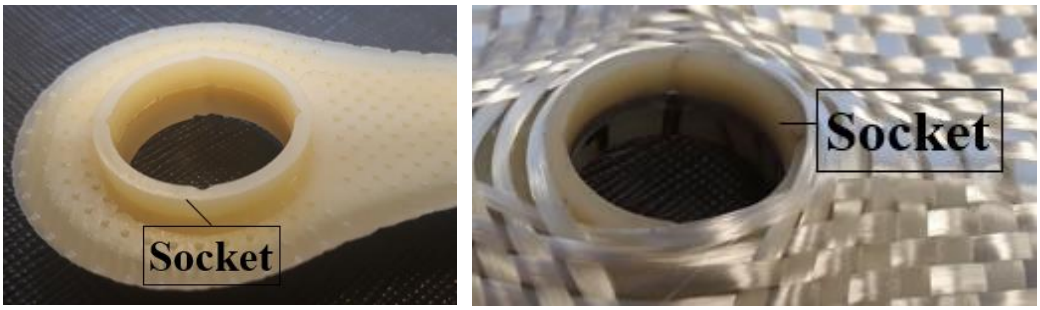

Figure 3.7. The pin socket design of this work

In the scope of this work, three types of inserts were developed. Namely: metal insert, polymer insert and metal-polymer hybrid insert (Figure 3.8, Figure 3.9). The concepts that are used in their design is listed in the Table 3.1.

Table 3.1. *The concepts used at the designed inserts*

Insert Type	Collar	Buried Inside the composite	Curved contact surface
Metal Insert	No	Yes	Yes
Polymer insert	Yes	Yes	Yes
Metal-polymer insert	Yes	Yes	Yes

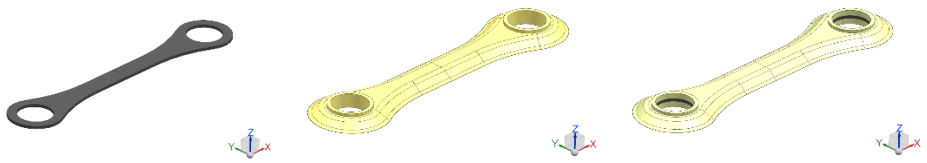

Figure 3.8. The three types of designed inserts. (Left) Metal Insert, (Middle) Polymer Insert, (Right) Metal-Polymer Insert

The metal-polymer hybrid insert consist of two materials, metal core and a thermoplastic material covering the core metal.

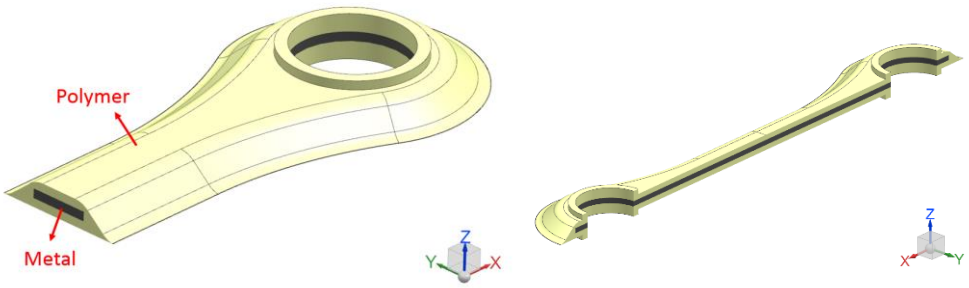

Figure 3.9. Section of the metal-polymer hybrid insert.

3.3 Design of Laminate and Inserts

The main load bearing constituent of an FRP is the reinforcement fiber. If the composite is drilled to create a bolt hole, the continuity of the fibers is violated. The drilled fibers are not able to bear load, therefore drilling weakens the strength and stiffness of the composite. One method to avoid drilling the composite is to create the bolt hole during the production of the composite. To avoid drilling, inserts with bolt hole socket (as in Bighead® concept) can be used (Figure 3.7). The fibers can be layed around the socket collar so that the continuity of the fibers is not violated. In addition, the insert provides with a socket to fasten the bolt. The inserts in this thesis were designed accordingly.

All the designed inserts consist of two bearing holes on the both sides and a rod connecting the two bearings. The connection rod transfers the load to the middle of the insert from the bearings. In other words, the load at the bearings is reduced by spreading the total load along the insert.

3.4 The Concepts used at the Design of Inserts

3.4.1 Metal Insert

The thickness of the metal was chosen to be 1.5mm. According to pull-out experiments on Bighead® inserts, the thickness variation of the insert plate from 1mm to 2mm provided 54% improvement of load bearing capacity whereas variation from 1mm to 3mm provided only 58% improvement in load bearing capacity (Gebhardt et al. 2015, p. 513). For thicker insert plates delamination failure risk increases, therefore the load bearing capacity does not increase linearly. Thus, 1.5mm insert thickness seem to be a good compromise between strength and weight. In addition, Gebhardt et al. (2015, p.512) showed that thicker plate leads to crack initiations at carbon fiber due to steeper bend angle of carbon fabric.

The metal insert has two sockets for M18 pin or bolt, but it does not have a collar to direct the fiber. Metal insert is a sheet part, which has constant thickness at all points. Therefore, the socket is in plane with other areas of the metal insert.

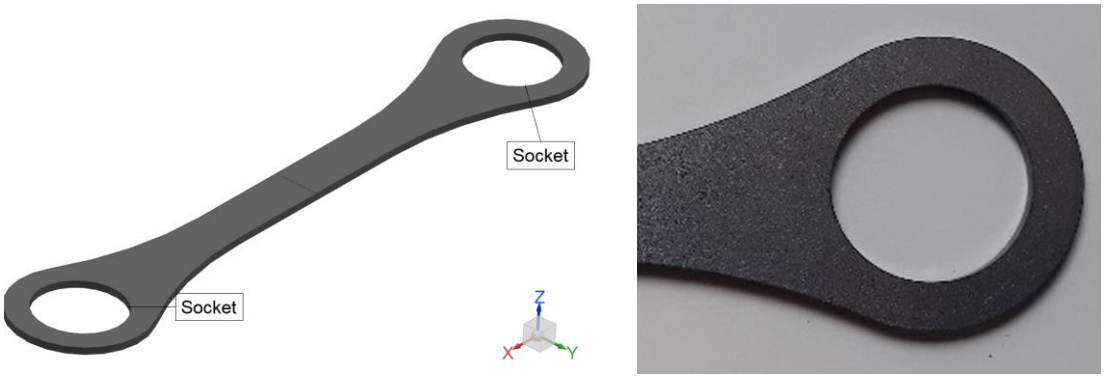

Figure 3.10. The sheet metal insert with plain bearing socket

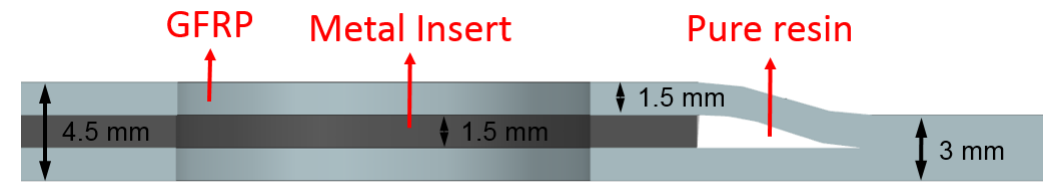

a

Figure 3.11. The cross-section dimensions of the composite laminate with metal insert

Figure 3.12. The cross-section of the composite laminate with metal insert

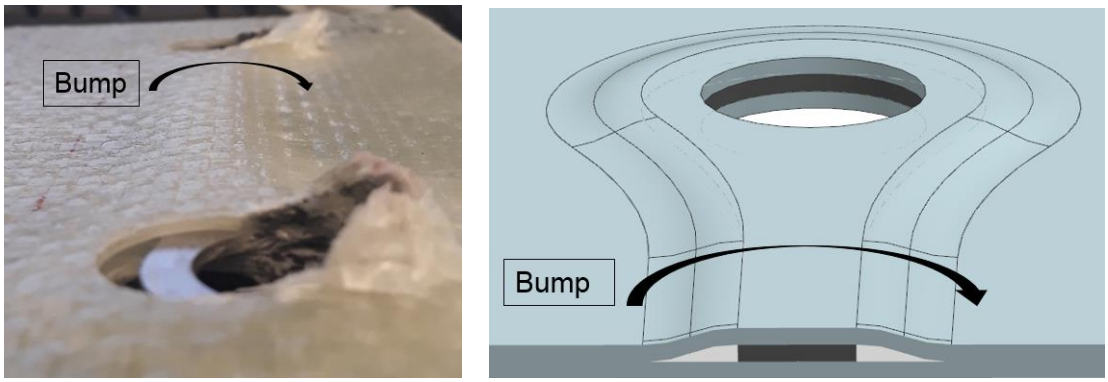

Figure 3.13. The bump at the metal inserted specimen

3.4.2 Polymer Insert

The polymer insert has two untapped sockets for M18 pin or bolt. The polymer insert is not a sheet part, it has non-constant thickness. Besides, its socket has collar. The purpose of the collar is to create a guide to direct the fibers around it. So that during the production of the composite laminate, the fibers can be simply widened (Figure 3.13). Hence direct contact between rod and GFRP is avoided by this way.

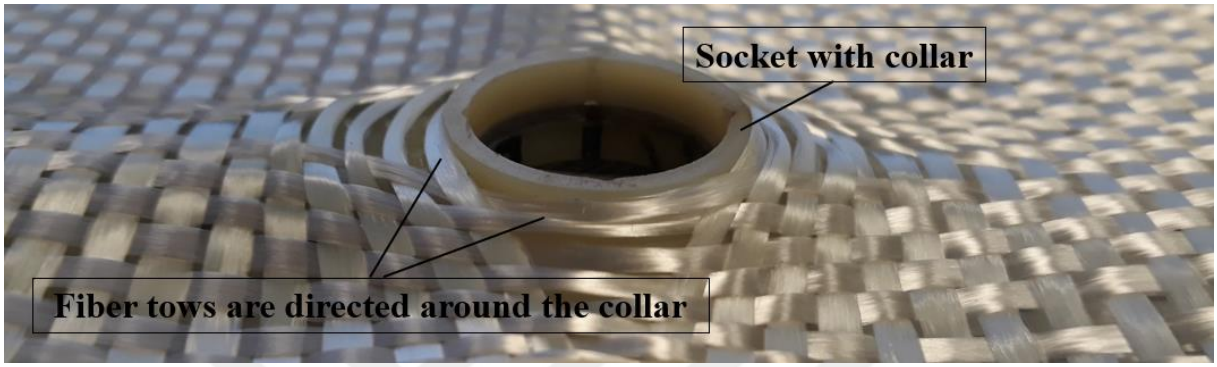

Figure 3.14. Tows of glass fibers are directed around the collar

As can be seen in the Figure 3.14, the fibers diverge from each other a socket collar region. This disrupts the distance between the glass fiber tows of the plain fabric and creates triangular unidirectional fiber regions (Figure 3.14).

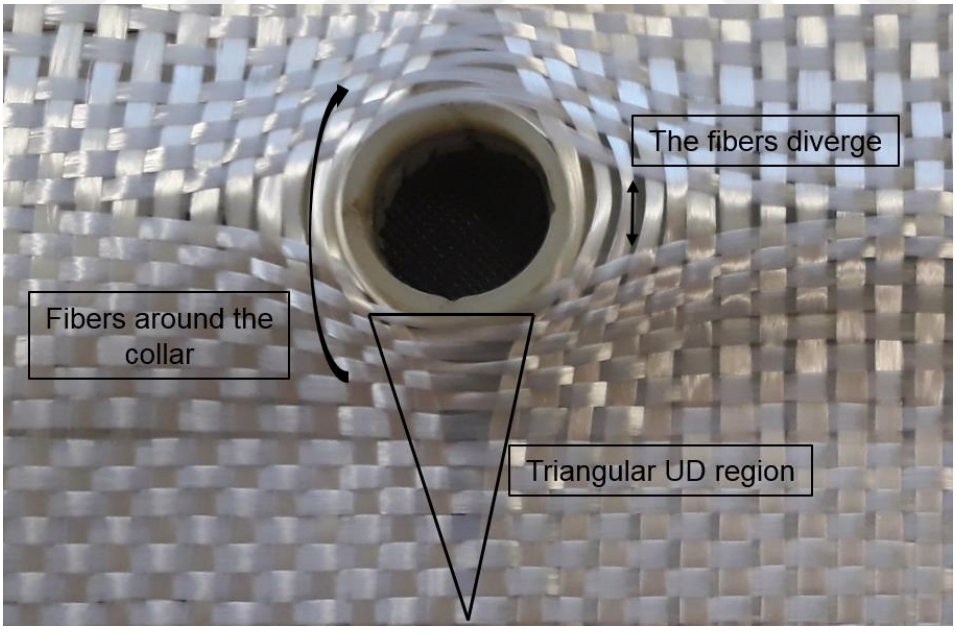

Figure 3.15. Change of distance between fiber tows due to collar

The top and bottom surfaces of the insert collar was designed to be at the same plane. The reason of this design is to avoid out of plane geometry protrusions form the surface of the

laminate. This should be ensured because the bracket surfaces sit on the chassis, so that bottom of the bracket should be flat.

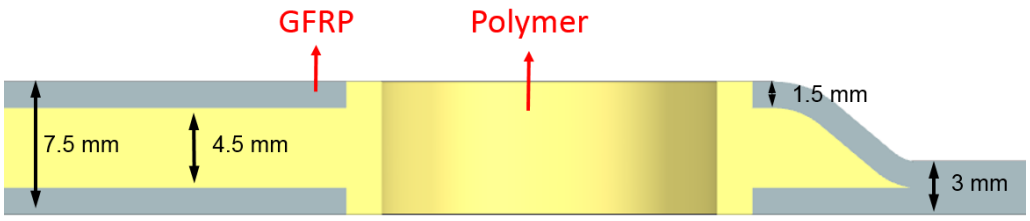

Figure 3.16. Cross sectional dimensions of the composite laminate with metal-polymer insert

Figure 3.17. Cross-section of the composite laminate with polymer insert

The contact surface between the polymer and FRP can be designed in a way that it provides mechanical interlocking between polymer and FRP as already studied by Pohl & Stommel. In their study, an inclined contact surface increases the interlocking between GFRP and polymer Pohl & Stommel, 2017, p.4). The same inclined contact zone concept is implemented in this thesis work. As in Figure 3.18, the contact between embedded polymer insert and the composite is also inclined which creates a so-called bump. This inclined zone carries loads in perpendicular direction to its bump.

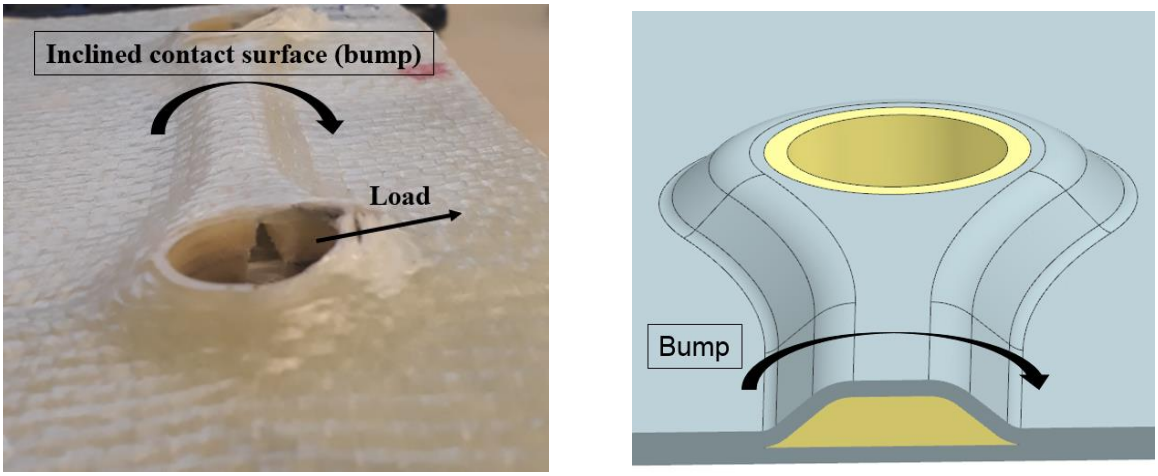

Figure 3.18. The inclined contact zone at the polymer inserted specimen

3.4.3 Metal-Polymer Insert

The metal inserts that was explained in the chapter 3.3.1 was used at the metal-polymer hybrid inserts. The idea of covering the metal with a polymeric material is to avoid the direct contact between the edges of metal and GFRP, so that the sharp edges of metal would not damage the fibers. Besides that, the curvature angle of fibers should not be sharp. Otherwise, fibers would break, and their load bearing capacity would diminish. To smoothly direct the fibers, the side of the polymer was designed as in the Figure 3.18. However, this design brings a serious problem. The edges of the metal insert are very sharp. These sharp edges might lead to delamination of the composite.

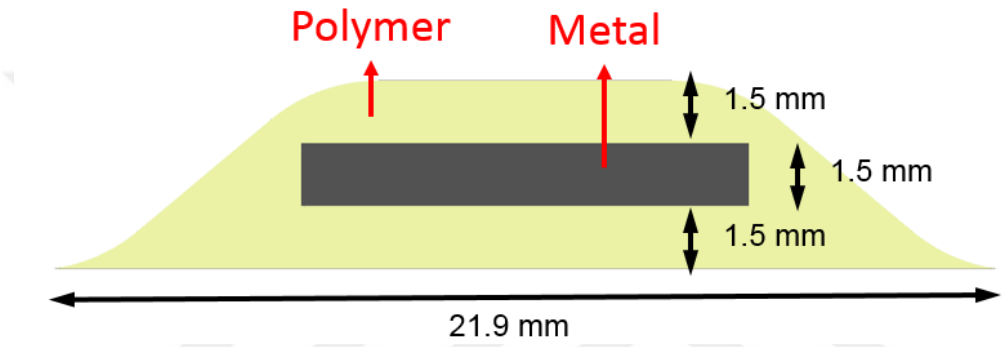

Figure 3.19. *Dimensions of the metal-polymer insert*

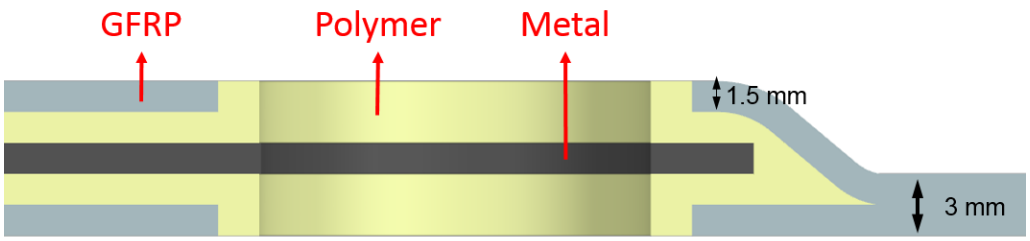

Figure 3.20. Cross-section dimensions of the composite laminate with metal-polymer insert

Figure 3.21. The cross-section of the composite laminate with metal-polymer insert

The total thickness of the specimen is 7.5mm at the insert area (Figure 3.19).

The polymeric material was injected around the metal insert using ‘Arburg Allrounder 270 S 400 – 100’ injection molding machine at the machine hall of LKT (Lehrstuhl für Kunststofftechnik) of TU Dortmund.

The sharp edges (Figure 3.22) of the polymer might be disadvantageous because it might intensify the delamination by cutting and splitting the matrix between the composite plies.

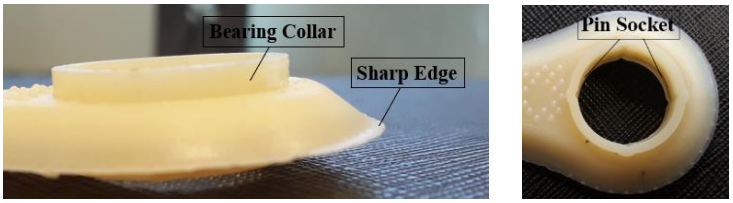

Figure 3.22. Sharp edges of the polymer and metal-polymer inserts.

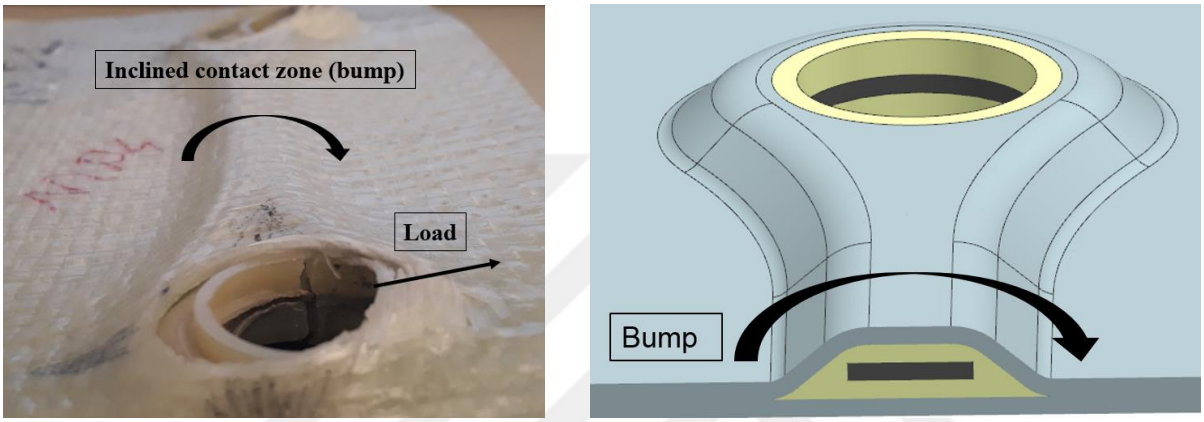

Figure 3.23. The inclined contact zone at the metal-polymer inserted specimen

3.5 Laminate Design

The composite specimens that are designed in this thesis represents the flat surfaces of the bracket as can be seen in the (Figure 3.23). Therefore, the diameter of the holes (19mm) and the distance between the holes (125mm) is predetermined (Figure 3.24).

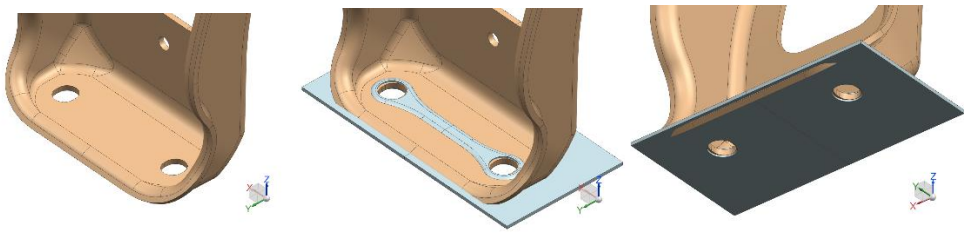

Figure 3.24. Flat surface of the cab rear suspension bracket and the designed specimen

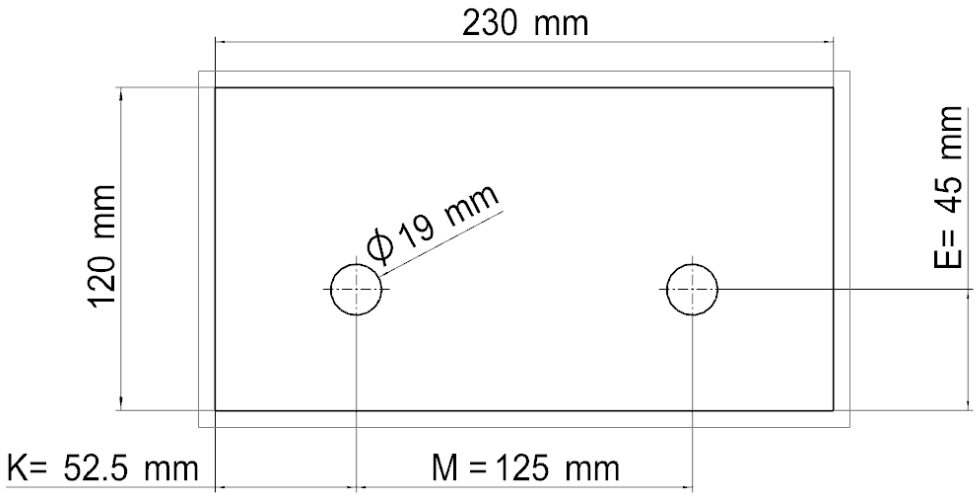

Figure 3.25. Dimensions of the composite specimen

As reinforcement material glass fiber is chosen due to its cost and durability advantage. As a rule-of-thumb, elongation at failure for carbon and E-glass is 1.5% and 4.9% subsequently (Mallick, 2010, p.17). Glass material was chosen because its cost is lower, and it is more elastic than carbon. Since the truck component is a part of suspension unit, it deforms recurrently under road conditions, so the composite bracket should be able to deform without failure up to a certain extent.

As the form of fiber, bi-directional (0^o, 90^o) plain woven fabric was used (Figure 3.25). Every ply was stacked at same orientation which is 0, 90^o with respect to the edges of the lamina. In total, 10 layers of glass fabrics were stacked. The thickness of each plain weave glass fabric ply is 0.3 mm. Therefore, the thickness of composite laminates is in total 3mm.

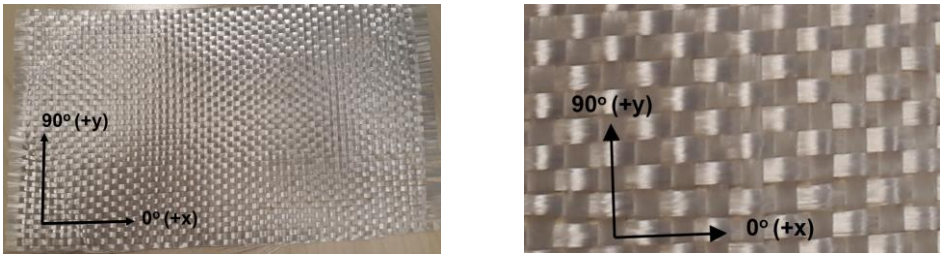

Figure 3.26. E-glass plain weave fabric

In total four types of specimens were designed: the reference specimen, specimen with metal insert, specimen with polymer insert and specimen with metal-polymer insert (Table 3.2). All types of inserts create a bump at the top surface of the laminate. This bump provides extra interlocking between the composite and the inserts.

Table 3.2. *The four types of designed specimens*

Abbreviation	Insert	Holes
W	No	Drilled
M	Metal Insert	Drilled
P	Polymer Insert	Not drilled
MP	Metal-Polymer Insert	Not drilled

4 Production of Inserts and Specimens

In the production of designed inserts and the composite laminates, cost-friendly and suitable methods for serial production were pursued. As in the future steps of this research, the inserts are desired to be used in a real world automotive applications, cost and serial production suitability are important concerns.

As a general overview, the used production methods are laser cutting, injection molding and hand lamination. The metal insert was produced by laser cutting process. The polymer insert was produced by plastic injection molding process. And the composite laminates were produced by hand lamination process. The produced three types of inserts can be seen in the Figure 4.1.

Figure 4.1. Pictures of produced inserts. (Top) Metal insert, (middle) polymer insert, (Bottom) Metal-polymer hybrid material insert

Two FRP production processes are Hand lamination and resin transfer molding. Hand lamination is the most manual FRP production method. The placement of the fibers, application of the resin, and the placement of the un-cured FRP in a vacuum bag performed manually by hand. On the other hand, resin transfer molding machine automates the injection and the curing

of the resin, only leaves the placement of the fibers to the operator. In fact, the placement of the fibers in the mold can be automated with an automated fiber placement (AFP) machine.

4.1 Production of Metal Inserts with Laser Cutting

For this thesis work, 1.5mm thick metal inserts are produced with laser cutting process. The metal inserts were cut from steel sheet plates using Trumpf LASERCELL TLC 1005 machine at IUL (Institute für Umformtechnik- und Leichtbau) of TU Dortmund (Figure 4.2). The edges of the produced inserts are not sharp which is advantageous since the edges of the metal insert would not create severe notch effect on the FRP.

(A)  (B) 

Figure 4.2. (A) Laser Cutting Machine, Retrieved from Kistner Machine Tools (2001, p.11) and (B) production defect during laser cutting

The only disadvantage of laser cutting is local over molten spot defect which is shown in Figure 4.2. The laser nozzle stays without moving at its starting position for too long, therefore extra material was removed from the steel at a certain spot.

4.2 Production of Polymer Insert with Injection Molding

Plastic injection molding process was used for production of polymer insert and metal-polymer insert. In addition to its applicability to serial production, another advantage of injection molding is its ability to produce complex geometries. Considering the complex geometry of the designed polymer insert, injection molding might be the only method to produce the plastic insert and cover the metal insert with polymer. The Arburg 270 S 400-100 machine (Figure 4.3) was used for injection of the polymer around the metal insert.

Figure 4.3. Injection Molding Machine - Arburg 270 S. Retrieved from (Arburg GmbH, 2015).

The injection tool was machined with CNC process. Aluminum mold plates were chosen because the machinability of aluminum is high. The mold plates can be seen in Figure 4.4.

Figure 4.4. Injection molding tools (Mold plates)

The maximum stroke volume of the Arburg 270 S is 49 cm^3 (Arburg GmbH, 2015). This volume corresponds to the amount of polymer that the injection machine can inject from the nozzle at one cycle. The total volume of polymer volume of the cavity and the sprue is 11 cm^3. Although the stroke volume capacity of the machine is far more than the polymer's volume, only one cavity was machined on the die to ensure the filling of the small features (the thin edges) of the polymer's geometry.

Sprue gate was used to inject the polymer into cavity. As a rule of thumb, the sprue gate should have circular cross section. It is suggested to place the sprue gate at the thickest section of the

molded part (Menges et al., 2001, p.205,206). The diameter of the sprue is suggested to be 1 mm larger than the section thickness (s_{max}) (7.5 mm for our part) as in the formula (Menges et al., 2001, p.205, 206):

$$d > s_{max} + 1\,mm \qquad \textit{Equation 4.1}$$

where s_{max} is the maximum section thickness and the d is the sprue diameter. The thickest section (s_{max}) of our designed plastic part is 7.5 mm. Therefore, the sprue diameter was chosen to be 9mm (>7.5mm + 1mm) according to Equation 4.1 with half millimeter extra.

The only disadvantage of the sprue gate is at post-processing. The removal of the produced part from the injection tool is troublesome. In the production of the inserts that are designed in this work, the sprue was often stuck in the sprue bushing, therefore it had to be pulled out with the help of a gripper.

In this work, pin shaped surface structures were placed on the surface of polymer insert (Figure 4.5). These pins create a mechanical interlocking in milimeter scale between polymer and FRP by penetrating into the matrix of the FRP. The same injection tools were used to produce both the polymer insert and the metal-polymer insert. The process steps were explained in the following two sections.

(A) 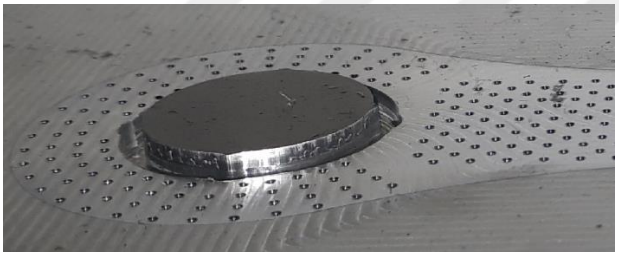 (B) 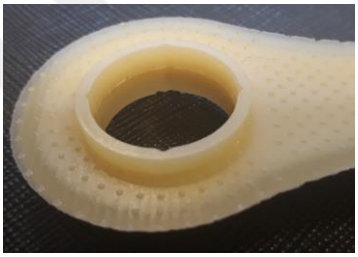

Figure 4.5. (A) Surface structure cavities on the mold plate and (B) the pin shaped surface structures on the polymer insert

4.2.1 Production Steps of Polymer Insert

The polymeric material is Vestamid HT plus M1033 – Polyamid (PA) 66 with 33% glass fiber content of its volume. The recommended melt temperature of Vestamid HT plus PA66 - M1033 during injection molding is 315 ^{o}C and the recommended tool temperature interval is 140-180 ^{o}C (Kuhmann, 2012, p.12). The mold temperature was chosen to be biggest value which is 180 ^{o}C to prevent freezing of the polymer before filling all the small features i.e. the tip of the polymer.

First, according to the Vestamid HT Plus Processing Datasheet for injection molding, the polymer granules were heated for 4 hours in the hopper to drop the moisture content below 0.06% by weight (Kuhmann, 2012, p.2).

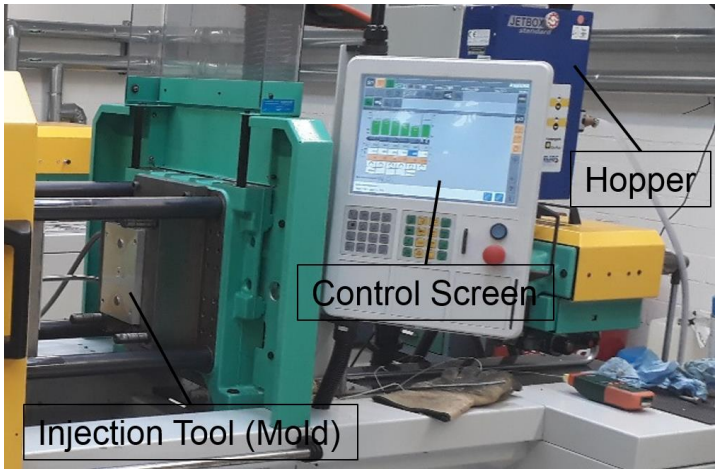

Figure 4.6. Plastic Injection machine

Then, up to 200 ^{o}C heated mold plates were closed. The polymeric material was injected from nozzle to the cavity. After the injection and the packing, the molds open and the part is removed from the cavity manually.

4.2.2 Production Steps of Metal-Polymer Insert

The same drying, injection, packing and removal processes were performed as in the production of the polymer insert. The only difference of metal-polymer insert is the placement of the metal inserts to the cavity before closing the mold and injection of the thermoplastic.

Before the placement in the mold cavity, the metal inserts were cleaned with a cleaning agent in an Ultrasonic Vibration machine (Figure 4.7) to remove the residual materials (e.g. dust, dirt, and burr) on the metal surface. The cleaned metal inserts were heated up to 200 ^{o}C in an oven and then placed in the cavity at the injection tool (Figure 4.8). After that, the molds are closed, and polymer is injected.

(A) 

(B) 

Figure 4.7. (A) Ultrasonic Vibration Machine and (B) Cleaning Agent.

To be able to place the metal insert in the mid plane of the cavity, support pins were machined on the injection tool (Figure 4.9). These pins hold the metal from top and bottom so that the

metal insert is positioned in the desired location. When the metal insert is placed, the remaining volume between metal insert and the injection tool is the cavity for polymeric material.

(A) 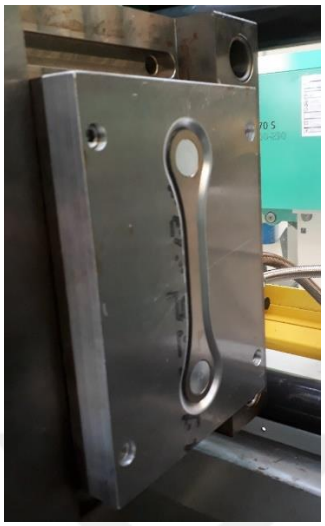 (B) 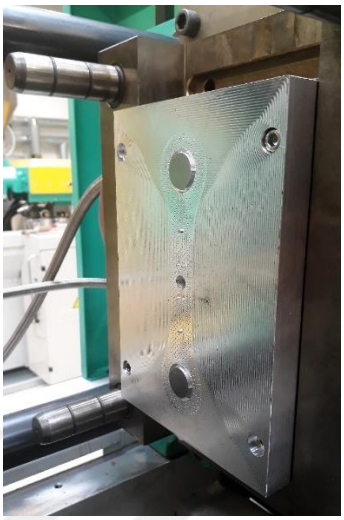

Figure 4.8. Mold cavities inserted in the machine. (A) first mold cavity with metal insert placed and (B) second mold cavity

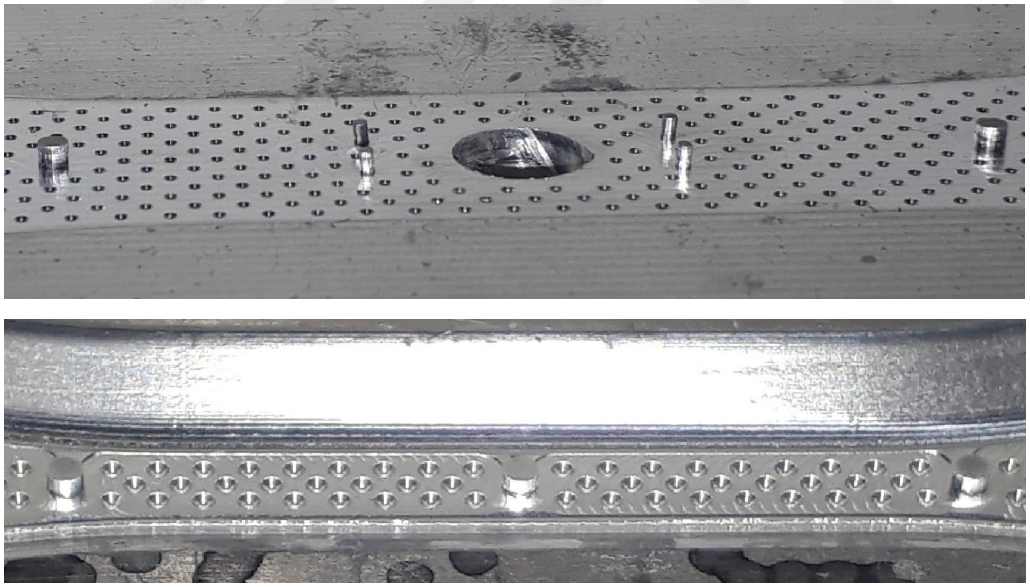

Figure 4.9. Support pins to hold the metal in the middle of the cavity

4.2.3 Surface Contact between the Components of Metal-Polymer Insert

The binding mechanism between the metal insert and the over-molded polymer is only direct adhesion. No adhesives were used to glue the polymer and metal to each other. Use of adhesives is avoided because it might cause sticking of the metal insert on the injection molding tool.

As mentioned in Ch.2.3.1, for a strong adhesion between polymer and metal, the metal should be heated prior to the injection molding process. Therefore, in this thesis work the metal inserts were pre-heated in an oven up to 200 ° C prior to the injection molding as mentioned in Section 4.2.2.

After the completion of the injection and the mold opens, the polymer is still ductile. Therefore, the metal-polymer insert was bent occasionally due to its ductility during the removal from the cavity. This bending broke off the adhesion between metal and plastic. In the Figure 4.10, the darker colored areas represent good adhesion between metal and plastic and lighter colored areas represent the areas where the adhesion was broken off and there is a slight gap between metal and polymer. The poor adhesion between metal and polymer might decreases the specimen durability. The effect of adhesion between polymer and metal on insert durability should be investigated.

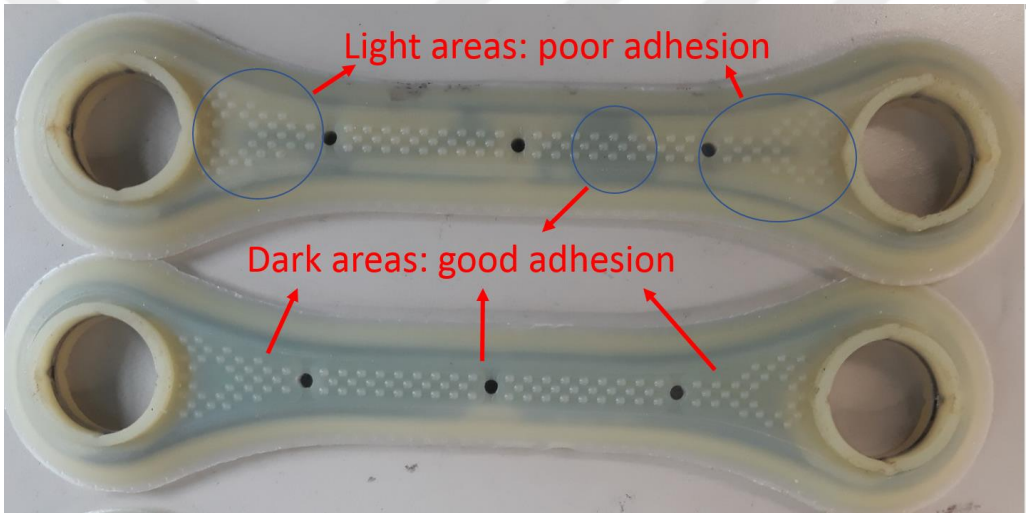

Figure 4.10. Good and poor surface-to-surface adhesion between polymer and metal

4.2.4 Defects during the Injection Molding

Three different defects that occurred during the injection molding are cracks on the polymer, poor filling of the cavity and diesel effect. Some polymer inserts cracked around the sprue region during the removal from the mold. The cracks can be seen in the Figure 4.11. These cracked inserts are scrap.

(A)  (B) 

Figure 4.11. (A) Cracks on the polymer and (B) diesel defect on the polymer bearing

The diesel effect is burning of the trapped air inside the cavity. The air burns under high pressure. The chemical composition of the polymer contributes to the burning reaction. The air was trapped at a certain location in the mold cavity under high pressure. The air burned with a sudden burst and left the burn marks that can be seen in Figure 4.11.

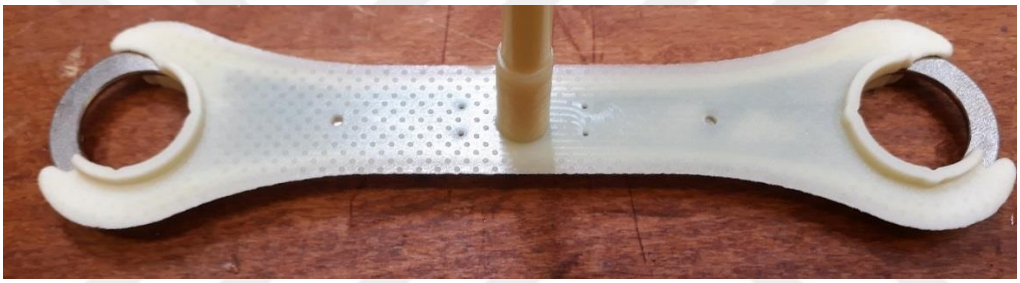

Figure 4.12. Poor filling of the cavity at injection molding process

4.3 Production of Composite Laminates by Hand Lamination

All the four types of laminates were produced with Hand Lamination. The reinforcement, resin and the number of layers is same for all the four types. The fabric material is HP-P401E plain woven glass fabric (Table 4.1) from the manufacturer HP-Textiles GmbH. It is appropriate to be used with epoxy or polyester resin.

Table 4.1: *Properties of the glass woven fabric at the Product Catalog (HP-Textiles, 2017), p.50)*

Brand	HP-Textiles
Type	HP-P401
Weight per unit area	400 g/m^2
Number of tows per length (warp x weft)	3,3 x 2,3 /cm
Weave style	Plain

As matrix material, Biresin CR170 Resin with Biresin CH170-3 Hardener were used. This epoxy resin system is suitable for automotive applications due to its high thermal performance

(up to 180 C^{o} degree) (Sika Deutschland GmbH, 2017). According to the datasheet, the Biresin should be cured at least at 70 C^{o} for 2 hours. Its glass transition temperature can be elevated up to 170 C^{o} by increasing the cure temperature (Sika Deutschland GmbH, 2017). In other words, its maximum service temperature can be adjusted for different by changing its curing temperature.

First the glass fabric roll was cut in the desired dimensions (230 mm x 120 mm) (Figure 4.13). The fabric plies were stacked on a flat surface on top of each other. After placement of every fabric ply, resin was poured on the glass fabric. Between the 5th and 6th plies, the inserts were placed in the desired position. After the 10th ply is placed, the un-cured laminate is placed in a vacuum bag. With a compressor, the trapped air inside the vacuum bag is removed. Removing the trapped air is very important, since air voids weakens the material properties of the composite. As last step the composite laminate was cured at an oven at 70 C^{o} for two hours.

(A)  (B) 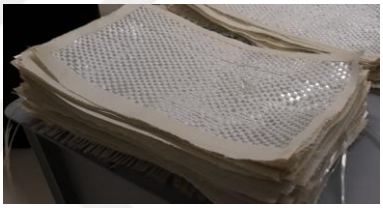

Figure 4.13: (A) Woven Fabric Roll and (B) Fabric Plies

The usage of vacuum bag is very important step of a Hand Lamination process. The main two purposes of vacuum bagging are removing the trapped air and removing the excess resin from the reinforcement-resin mixture. It is important to remove the trapped air between the fabric plies since the trapped air leads to delamination of the laminate. And the excess resin is removed so that the laminate can have the desired dimensions. In addition, the specific strength of the laminate is increased during vacuum bagging by compacting it with pressure.

The fiber volume fraction of the composite specimens is 0.52. One sample from each type of specimen can be seen in Figure 4.14, Figure 4.15 and Figure 4.16.

(A) 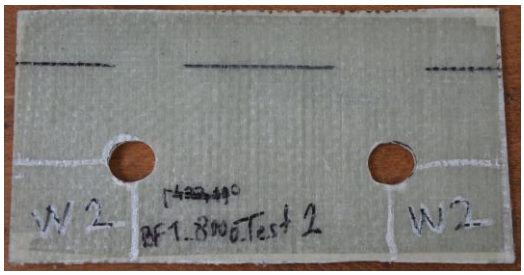

(B) 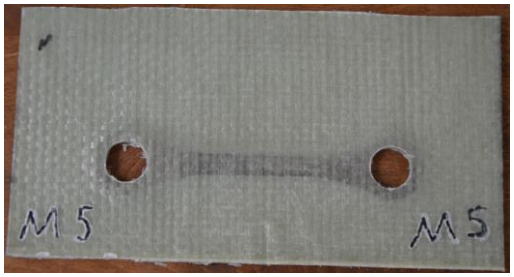

Figure 4.14: Drilled inserts: (A) Reference laminate and (B) Metal inserted laminate

(A) 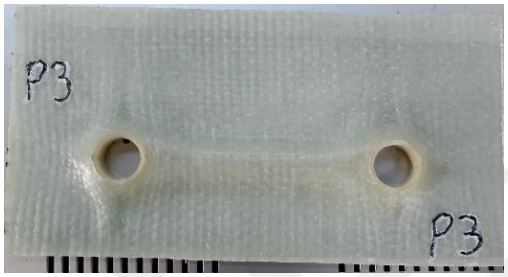

(B) 

Figure 4.15. Non-Drilled, Polymer inserted Laminate. (A) Top view and (B) bottom view

(A) 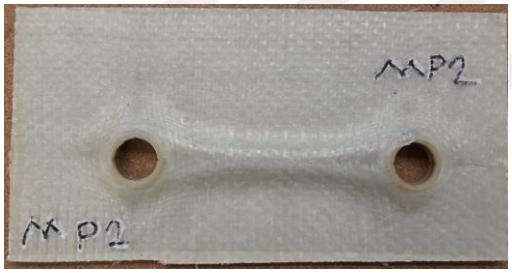

(B) 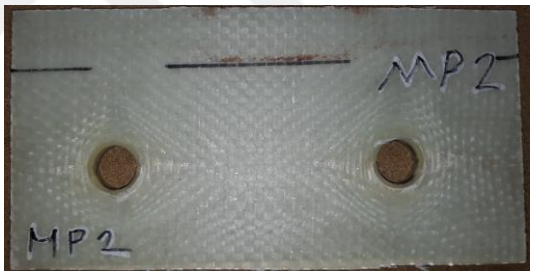

Figure 4.16. Non-drilled, metal-polymer inserted laminate. (A) Top view and (B) bottom view

5 Experiments

The main two purposes of conducting experiments are to observe the failure modes at the bearing area and to compare the durability of the bearing region under real-life loading conditions.

It was expected that the placement of the inserts at the bearing area would improve the bearing strength. To observe the effect of inserts, the inserted laminates were compared with reference specimens. The first type of specimens are reference specimens which have no insert. They are drilled composite laminates. Second type of specimens are supported with metal insert at bearing area. Similarly, to the first type, the second type is also drilled. On the contrary, the 3rd and 4th type of specimens are not drilled, instead the bearing hole were created during the laminate layup. At their bearing area, 3rd and 4th type of specimens also has inserts to support the bearing. These two types of inserts (polymer and metal polymer insert) help the shaping of the bearing hole during the stacking of the composite plies.

5.1 Loading Condition and Clamping Device

The rear cab suspension bracket unit is mainly under compressive loading in –z direction, as the bracket is positioned under the driver cabin. However, under some lateral loading conditions, the loads in +-y direction become critical. Therefore, the fastener region of the rear cab suspension bracket undergoes loadings y direction (Figure 5.2). As the flat surfaces of the bracket is fastened with bolts, the in-plane loads apply pressure on the bearing area. The designed experiment setup aims to represent the pressure on the bearing area (Figure 5.3).

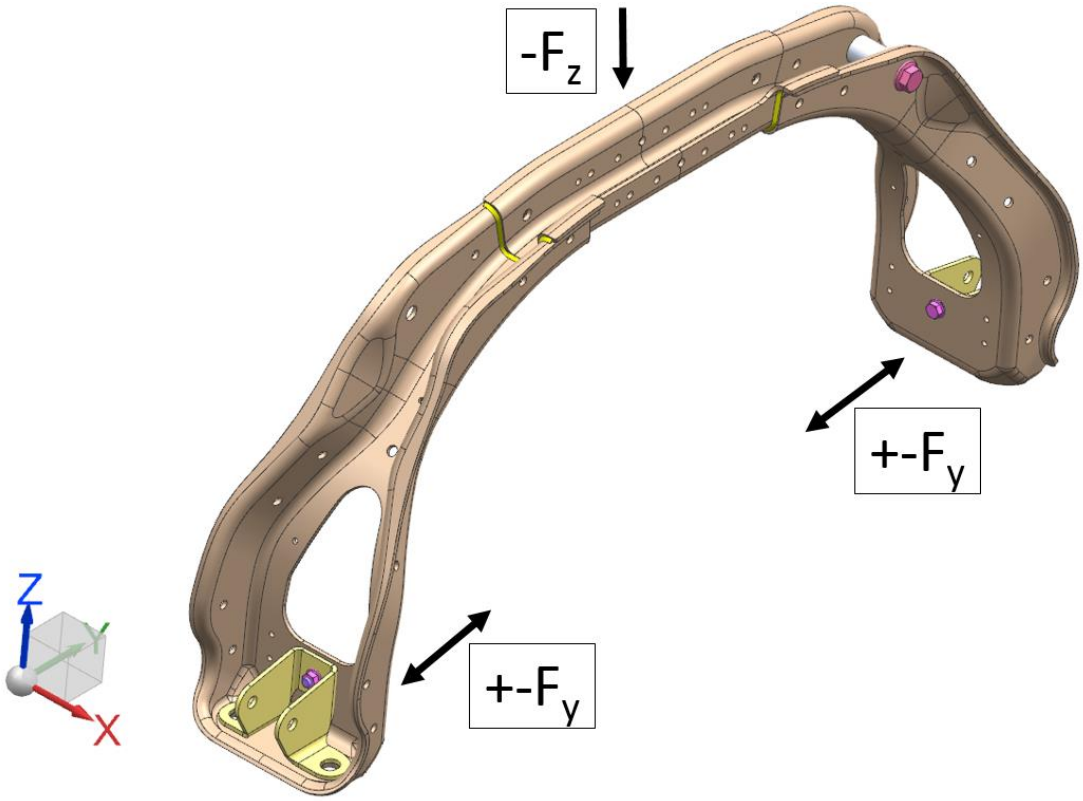

Figure 5.1. Loads on the bracket

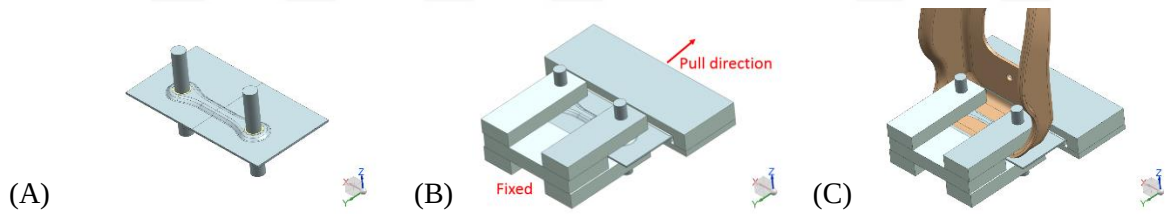

Figure 5.2 . *(A) Specimen with pins, (B) specimen with clamps and (C) clamping device located at the bracket*

(A) 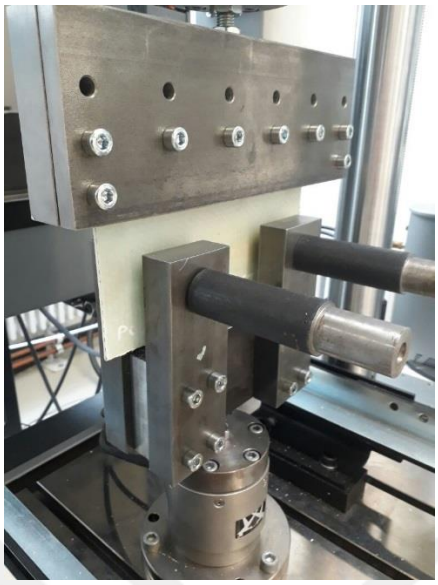 (B) 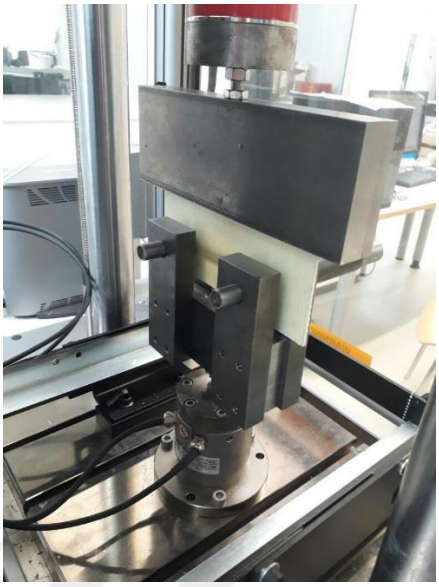

Figure 5.3. Experiment ready setup. (A) front view and (B) back view.

In this experimental setup, the pinned joint was used despite the fact that the Mercedes Truck rear cab suspension bracket is fastened with bolts and nuts. In the pinned joint, only two steel, threadless pin go through the holes. The pinned joint does not have any pre-tension force as it was not tightened with bolts. On the other hand, a bolted joint is tightened with bolts from both sides of the hole, therefore pre-tension forces exist.

There are three reasons for using pinned joint instead of bolted joint. First, the failure mode remains the same for pinned and bolted joints. According to experimental comparison by Pakdil et al. (2011), same failure mode at the bearing area of composite was observed for pinned and bolted joint. Therefore, the pinned joint that is used in this work is expected to reflect the failure mode of the bolted joint at the bracket. Secondly, the nuts at the bolted joint would hinder the visual inspection of the failure of fibers at the bearing area. And last, the loading was desired to be isolated only with in plane pressure exerted by the pins. Therefore the pre-tension forces of tightening of the nut is avoided.

5.2 Quasi-Static Pin-Pull through Test

The machine used for quasi-static pin pull-through experiments are Zwick 100kN device. It can apply up to 100kN force. The tests were performed at 2mm/min displacement rate until 10 mm pin displacement (Figure 5.5). For every specimen type, three tests were performed.

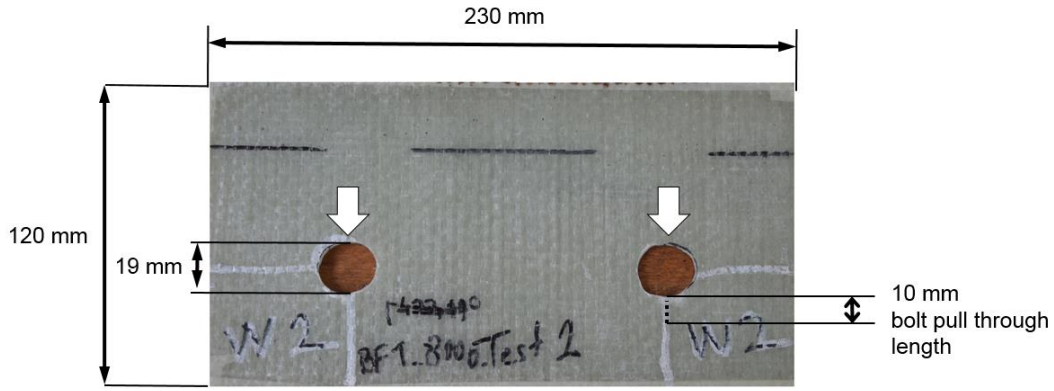

Figure 5.4. Dimensions of the specimens and pin pull-through direction

The purpose of the quasi-static tests is to observe the failure modes of the specimens at high loads and strains. In this work, the pin pull-through tests showed that the pins crush the bearing area of the composite progressively as it is pulled through the laminate. It is observed that the fiber bundles break in sequence after one another. During this sequential failure, the composite can absorb impact energy at every progression of the failure. The high specific energy absorption potential of composites is mentioned also in literature (Jacob et al., 2002).

The failure mode at all 4 types of specimens is bearing mode failure (Figure 5.6 & Figure 5.8). As mentioned in the Ch. 2, the bearing mode failure is local crush of the composite at the vicinity of the bolt area (Figure 5.6). Thus, the failure modes of inserted specimens are the same as reference specimens.

The bearing damage is more severe at reference specimens in comparison to other specimen types. The bearing damage at reference specimens starts in average at 10.10kN (Table 5.1), whereas metal inserted specimen at 11.23kN (Table 5.3), polymer inserted specimen at 17.66kN (Table 5.4) and metal-polymer inserted at 16.43kN (Table 5.5). It can be interpreted that all inserts were able reinforced the bearing area. That means the inserts hindered the damage by crushing up to a certain extent. This improvement at the bearing performance can be explained by the transmission of the total load from the bearings to the bumps at the middle region of the specimens (Figure 5.6). As the load is distributed to a wider area, the stress concentrations at the bearing reduced. Thus, the inserted bearings were able to endure up to higher forces than the reference specimens. However, the distribution of the load on wide insert leads to another failure mode which is delamination.

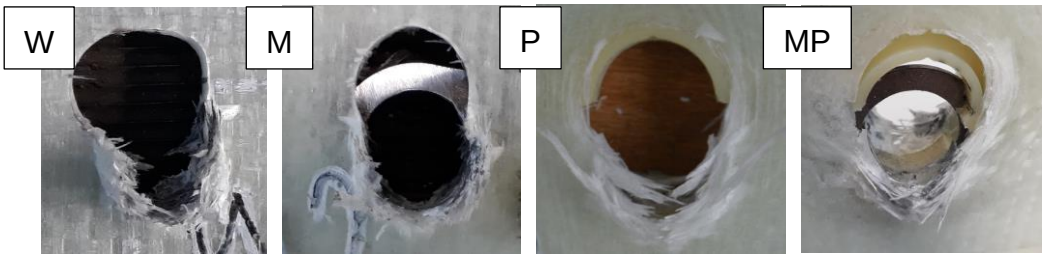

Figure 5.5. Bearing mode failure of four types of specimens

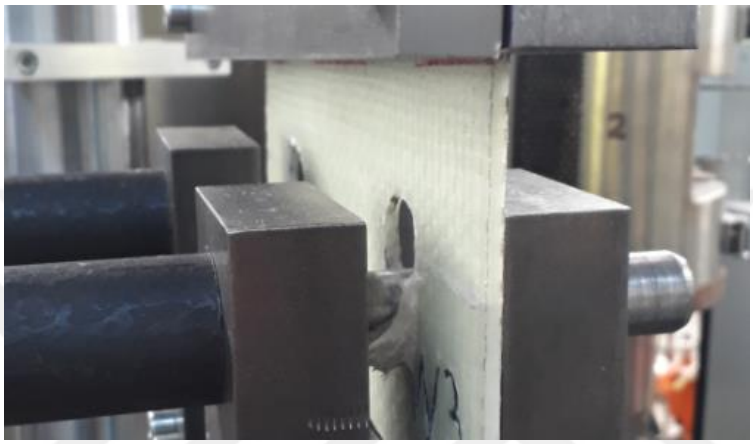

Figure 5.6. The crush of the composite around the hole as the pin moves through*

As mentioned in Ch. 2.2.2, the failure modes at bearing are cleavage mode, net-tension mode, shear out mode and bearing mode failures (Figure 2.9). The structural integrity of the composite is highly lost at cleavage, net-tension and shear out failure modes. Widespread cracks or rupture are observed on the composite specimen under these three failure modes. On the other hand, bearing mode failure (Figure 5.8) is not a complete rupture of the composite. Therefore, even the composite undergoes bearing mode failure, it can still endure loads. In this aspect, local bearing mode failure is more advantageous than cleavage, net-tension and shear out failure modes.

(A) 

(B) 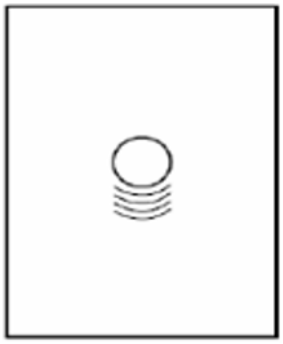

Figure 5.7. (A) Bearing crush at this work. (B) Schematic representation of bearing failure. Image Retrieved from (Pakdil et al., 2011).

5.2.1 Failure at Reference (W) Specimens

The reference specimens were abbreviated as 'W'. The force displacement plots of the reference specimens can be seen in the Figure 5.10. It is observed that after the elastic deformation, the bearings start to crush and fail progressively (Figure 5.9). The scattered region at the force-displacement curve represents the progressive failure region.

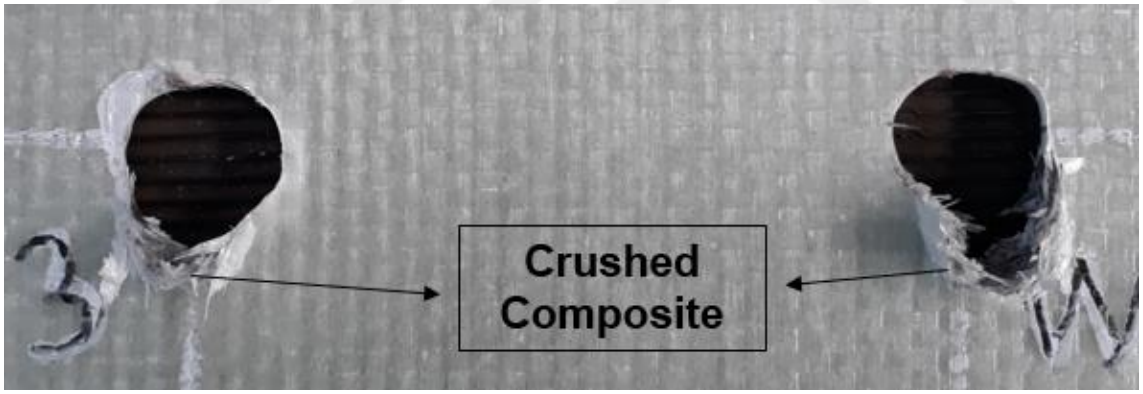

Figure 5.8. Failure at reference specimens

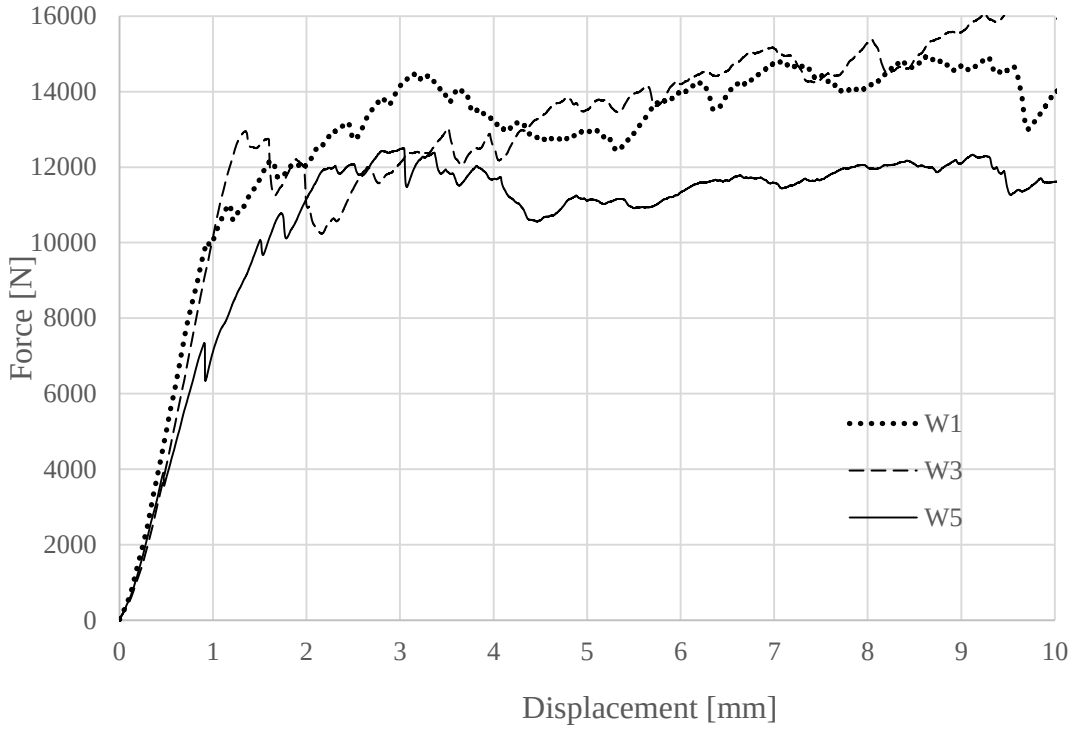

Figure 5.9. Force - hole displacement plots of the reference specimens

It can be observed at the Figure 5.10 that the stiffness values of the reference specimens vary from each other. Such stiffness variations at experiments can also be found in the literature. In his experiments, Vangrimde & Boukhili observe variations in the bearing stiffness values (2012). He reports that the experimental bearing stiffness values variates from each other up to 16.1%. In this work, the experimental stiffness variation was found to be 12.7%.

Table 5.1. *Bearing Response of reference (no insert) specimens*

Specimen Type	Stiffness [kN/mm]	Ultimate Bearing Load [kN]	Bearing Load at damage onset [kN]	Bearing Strength [MPa]
W1	12.1	14.94	10.02	87.96
W3	11.9	16.28	12.94	113.58
W5	9.6	12.50	7.43	64.40
Standard Deviation	1.4	1.9	2.80	24.6
Coefficient of Variation	12.7%	13.1%	27.7%	27.7%
Average	11.2	14.57	10.10	88.65

Vangrimde & Boukhili (2012) suggests that the variations in the bolt-hole clearance is the cause of the stiffness variations. Similarly, the pin-hole clearance variance is one of the reasons of the stiffness variations in this work. The other reasons for the variation of the experimental stiffness results at this work are the elastic deformation of the clamping device, the small sliding of the specimens between the fixture clamps and the elastic deformation of the non-bearing composite regions.

5.2.2 Material Property Calculation of Reference Specimens

In the pin pull-through tests, the bearing properties (bearing stiffness and ultimate bearing load) of reference filled-hole composite specimens are determined in Ch.5.2.1. In addition to those three parameters, the effective bearing elastic moduli and bearing strength are calculated from stress-strain plots of reference specimens (Appendix 3). The calculated effective bearing elastic moduli and bearing strength values are used in the finite element simulations in Ch.6.

In calculation of elastic moduli, the approach in Ch.2.2.3 was used. The force – displacement plot of reference specimens was converted to bearing stress – strain plots using the formulas (Equation 2.1 & Equation 2.2). The stress-strain plot calculation can be seen in Appendix 2. The slopes of the elastic regions of stress-strain plots stand for the effective bearing elastic modulus for each reference specimen. The calculated elastic moduli values can be seen in the Table 5.2. The calculations elastic moduli values can be seen in the Appendix 3.

Table 5.2. *Calculated elastic modulus and bearing strength values (Appendix 3)*

Specimen name	Bearing Strength [MPa]	Elastic Modulus (MPa)
W1	87.96	1993.26
W3	113.58	2026.78
W5	64.40	1566.17
Average	**88.65**	**1862.07**

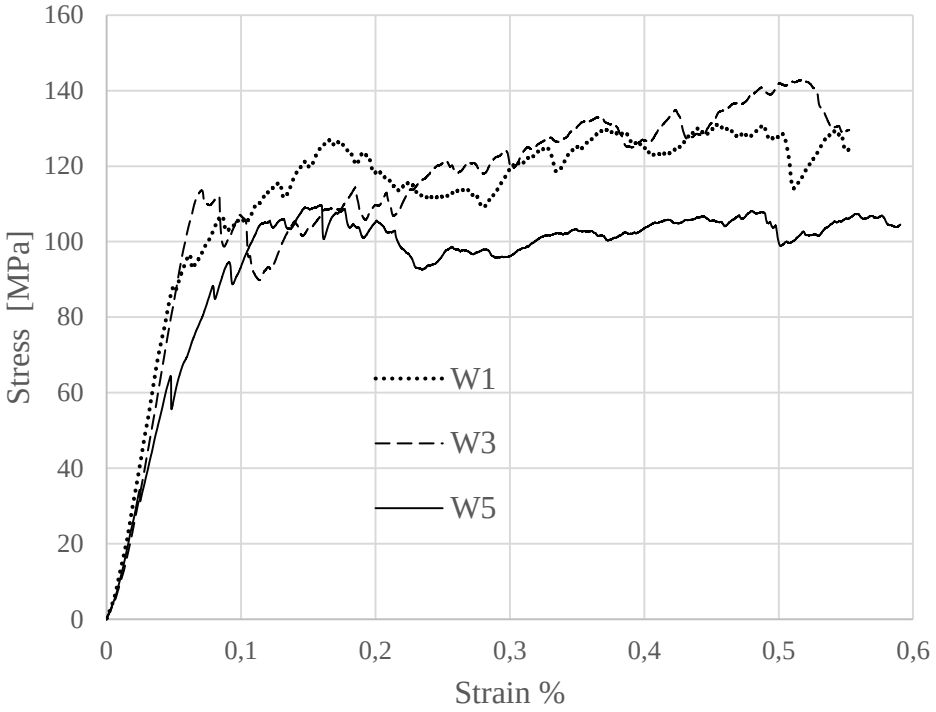

Figure 5.10. The stress – strain plots of reference specimens

5.2.3 Failure at Metal Inserted Specimens

There are four main characteristics of failure of metal inserted specimens. They are the crush of the composite due to compression by the pin, the slide of the metal insert between the composite layers, the bending of the metal insert and the delamination of the composite due to slide of the metal insert.

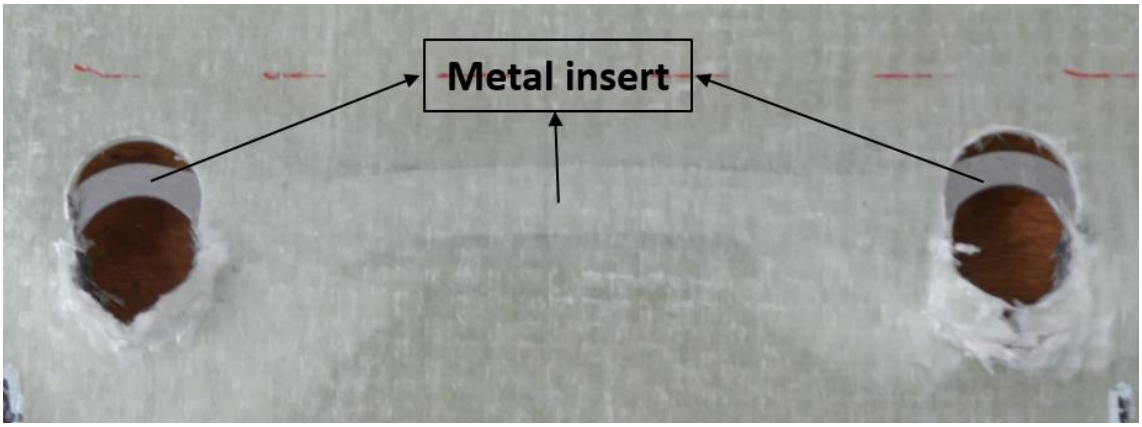

Figure 5.11. Failure at metal inserted specimens (M)

The bearing regions of metal inserted specimens are damaged by the compression of the pin similarly to the reference specimens. In the first contact of the pin, the pin compresses the

composite. The composite resists the movement of the pin until the fibers start to form kink bands. The formation of the kink bands leads to stiffness knock-down. The weakened composite is crushed by the pin. The fibers and the matrix of the composite are pushed in out-of-plane direction by the moving pins.

As the pins move, they pull the metal insert from the bearing region (Figure 5.14). The metal insert slides between the 5^{th} and 6^{th} plies of the composite in the pin's movement direction. The slide of the metal and the crush of the composite occurs simultaneously. The slide of the metal between the composite layers results in local delamination. The delamination can be visually observed. The white colored areas on the specimen are the delaminated regions (Figure 5.14).

As mentioned in the Ch.3.4.1, the contact zone between metal insert and composite was deliberately made inclined to constrain the metal insert. In experiment, it is seen that this intention come true. The metal insert is constrained by the composite along the inclined contact zone in the pin's movement direction. When this constraint is coupled with the pull force that pins exerts on metal's bearing area, the metal insert plastically deforms and bends. The bending of the metal insert can be seen in the Figure 5.14 and Figure 5.15. The metal insert does not break despite it bends.

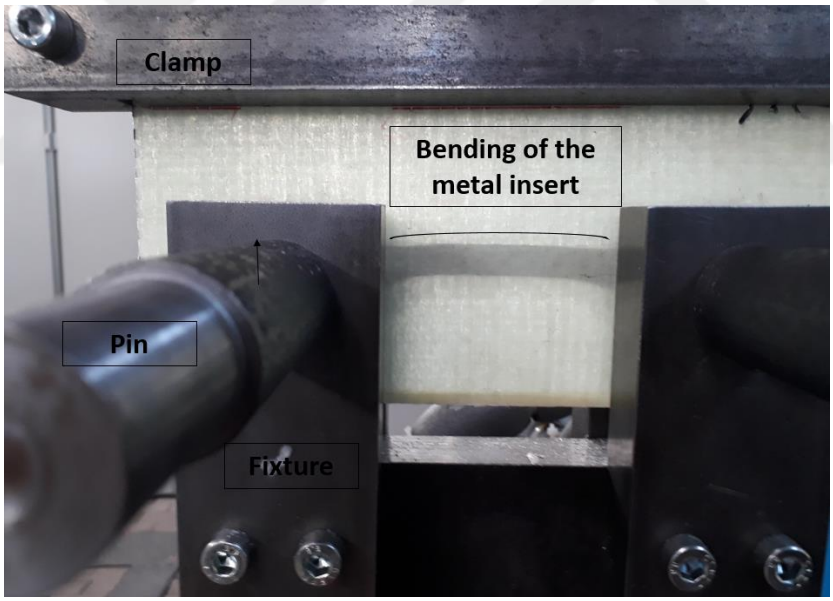

Figure 5.12. Bending of metal insert

Table 5.3. *Bearing Response of the metal inserted (M) specimens*

Specimen Type	Stiffness [kN/mm]	Ultimate Bearing Load [kN]	Bearing Load at damage onset [kN]	Bearing Strength [MPa]
M2	11.42	19.98	10.04	88.10
M3	13.01	22.28	14.64	128.5
W4	11.11	20.91	9.00	79.02
Standard Deviation	1.01	1.15	3.00	26.33
Coefficient of Variation	8.5%	5.4%	26.7%	26.7%
Average	**11.85**	**21.06**	**11.23**	**98.54**

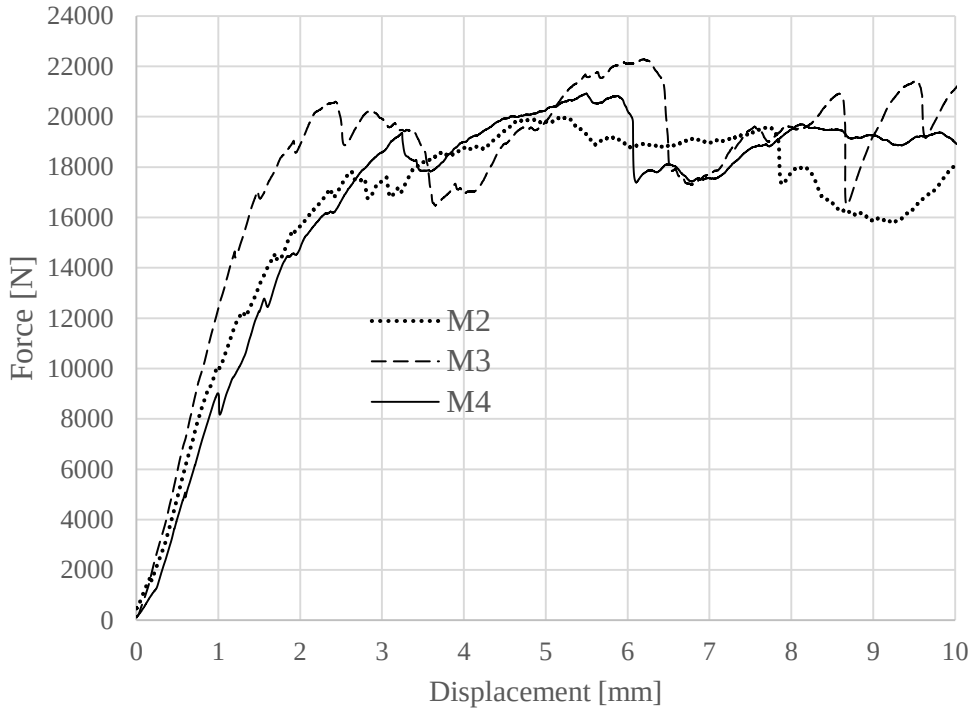

Figure 5.13. Force - hole displacement plots of the metal inserted specimens

5.2.4 Failure at Polymer Inserted Laminate

The main characteristic of polymer inserted specimens is brittle failure of the polymer insert, the crush of the composite due to compression by the pin and the delamination of the composite layers.

In this specimen configuration, the pins have contact only with polymer insert. In the beginning of the experiment, the pins do not touch composite at all. The applied load by the pins on the bearing were endured together by the polymer insert and the composite. The elastic region that can be seen in the plot is the coupled response of polymer insert and composite.

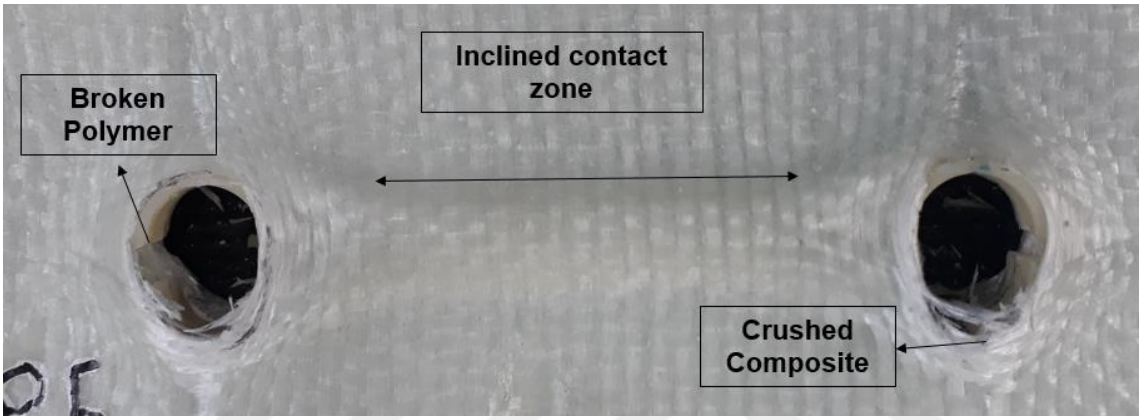

Figure 5.14. The failure at polymer inserted specimens (P)

The exerted force on the bearing was distributed by the polymer insert to the inclined contact zone between polymer insert and the composite. This load distribution reduces stress concentration at the bearing area. Despite the load distribution, the polymer inserts are broken around its bearing collar in average 17.66 kN load. The failure of the polymer is a brittle fracture. Therefore, suddenly, all the load must be endured by the composite. From the results of reference specimens, it is known that the bearing fails in average at 10.10kN load. Considering that, composite cannot endure 17.66 kN load alone. As expected, soon after the brittle failure of the polymer insert, the composite undergoes a sudden drastic failure and crushed by the pin.

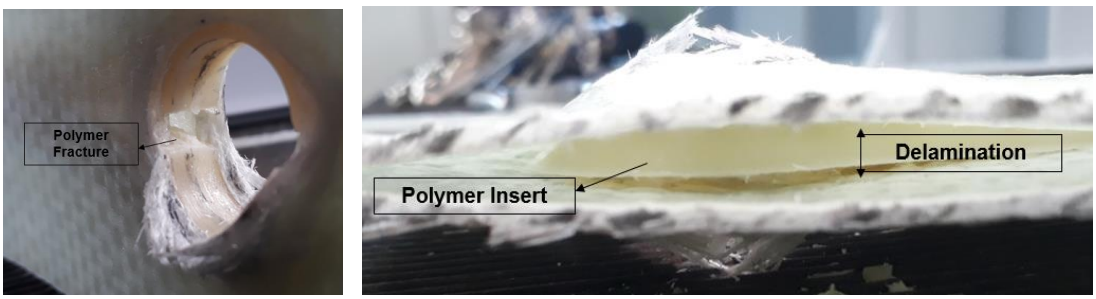

Figure 5.15. (Left) Brittle fracture of the polymer, (Right) Delamination due to the polymer insert

In the plot, the first peak is the brittle fracture of the polymer and the consecutive sudden force drop is the failure of the composite. The same pattern was observed at both three specimens.

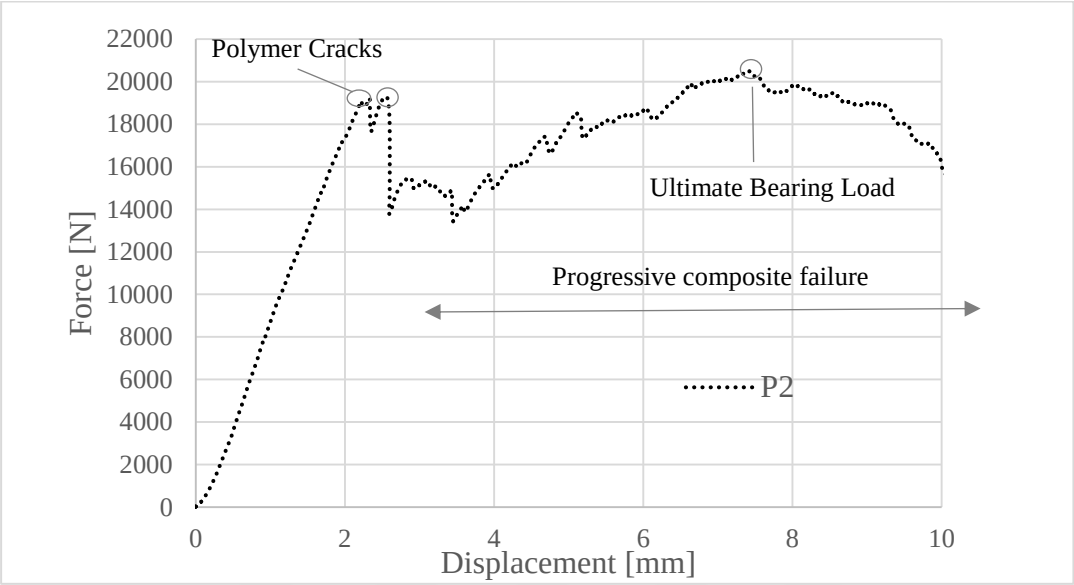

Figure 5.16. The transition of specimen P2 from elastic to plastic region

In more detail, until its brittle failure, the P type insert protects the bearing are of the laminate by transferring the energy to its length. No drastic composite failure occurs during the elastic deformation of the specimen. Than the thermoplastic breaks at its bearing collar. After its failure, polymer insert can no longer transfer energy and protect the bearing of the laminate. The pins push the broken part of the polymer insert in y-direction. As polymer slides between the 5th and 6th plies, it breaks the contact between the composite layers. Thus, the composite delaminates (Figure 5.18 & Figure 5.20).

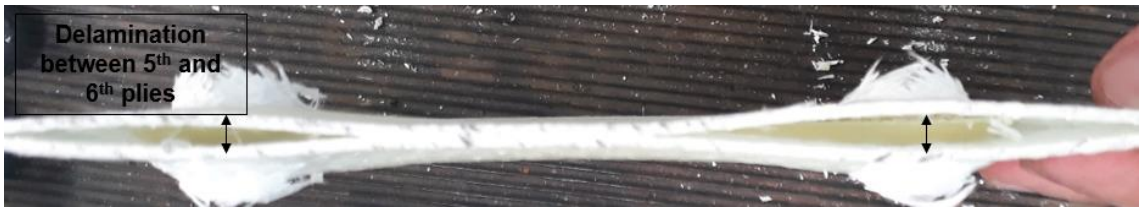

Figure 5.17. Delamination at polymer inserted specimens

Table 5.4. *Bearing Response of the polymer inserted (P) specimens*

Specimen Type	Stiffness [kN/mm]	Ultimate Bearing Load [kN]	Bearing Load at damage onset [kN]	Bearing Strength [MPa]
P2	9.35	20.49	19.06	167.26
P3	10.55	18.19	18.19	159.62
P5	9.30	18.17	15.72	137.94
Standard Deviation	0.70	13.31	1.73	15.20
Coefficient of Variation	7.2%	7.0%	9.8%	9.8%
Average	**9.73**	**18.95**	**17.66**	**154.94**

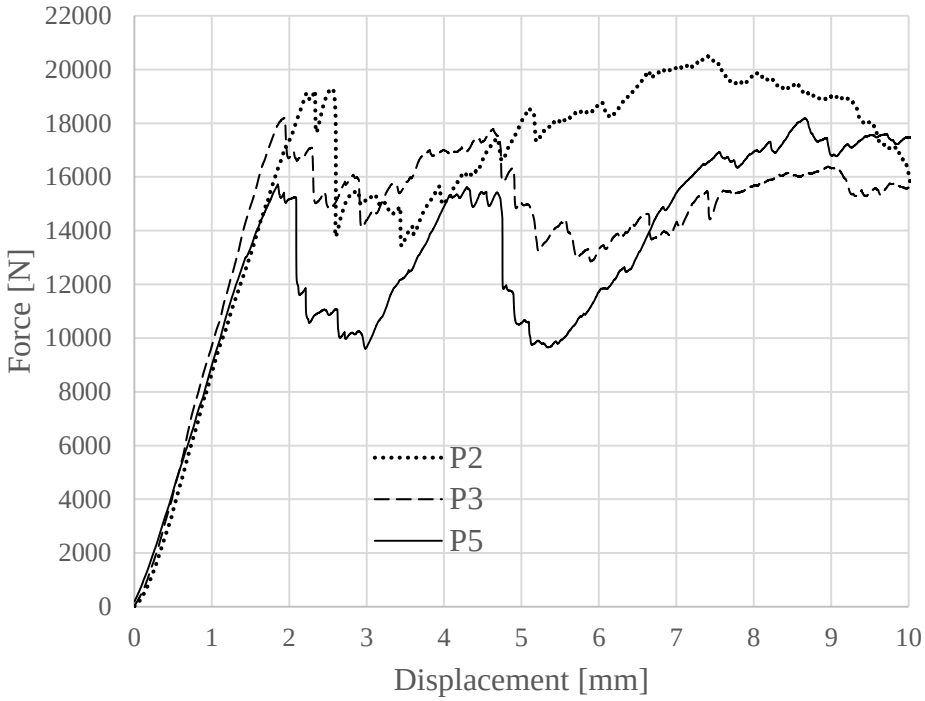

Figure 5.18. Force - hole displacement plots of the polymer inserted specimens

5.2.5 Failure at Metal-Polymer Inserted Laminate

The main characteristic of metal-polymer inserted specimens (MP) are delamination, brittle failure of the polymer inserts, bending of the metal and sliding of the metal-polymer insert, the bearing on the damage due to compression by the pin. All these failure modes were also observed at M and P type specimens. Therefore, failure modes of other specimen types were combined in MP type specimens.

However, all the above-mentioned failure modes are not observed in every MP specimen. Delamination failure was observed at every MP specimen due to slide of the metal-polymer insert between composite layers. The bearing damage was also observed every MP specimen. The polymer was broken at specimens MP3 and MP5. Without exception, bending of the metal follows the breakage of the polymer, that is, metal bends at specimens MP3 and MP5. The polymer failure and metal bending were not observed in specimen type MP4. In short, the failure of metal-polymer inserted specimens consists of a certain randomness.

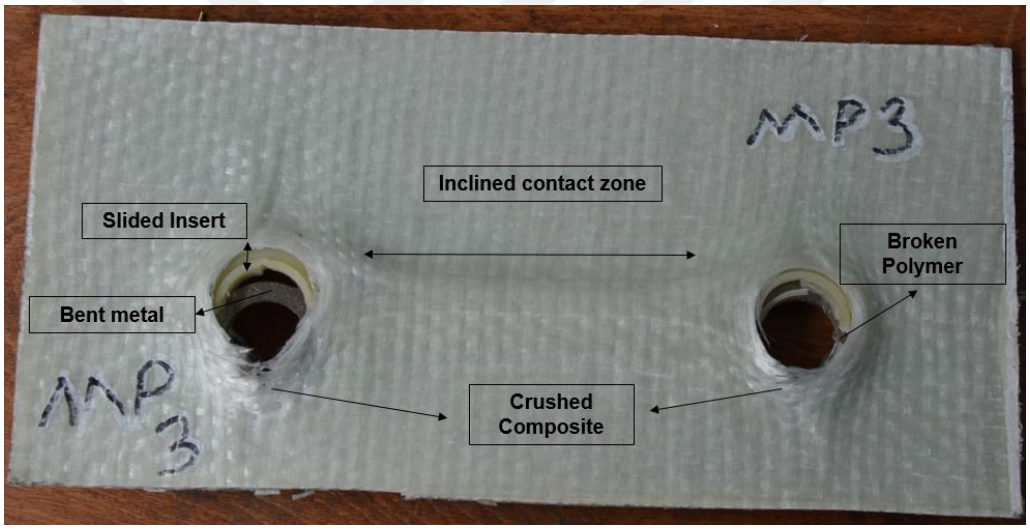

Figure 5.19. Failure at specimen MP3

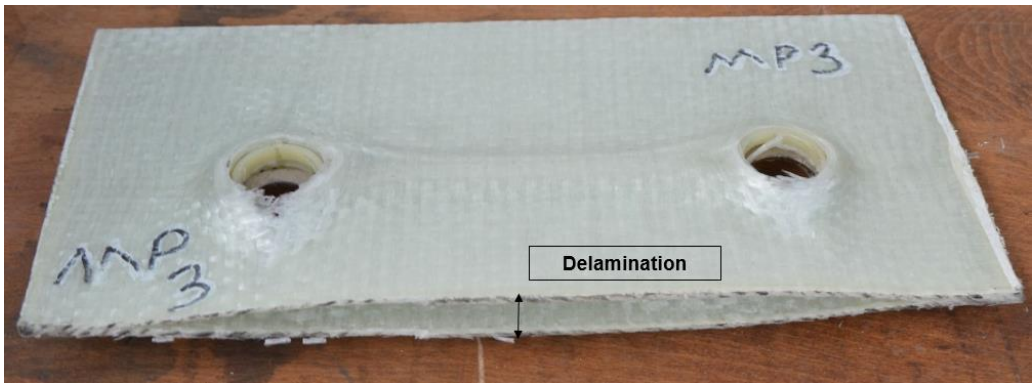

Figure 5.20. Delamination failure at specimen MP3

The specimen MP3 fail in two steps. First, the thermoplastic component of the insert breaks, where metal still bears load. In the second step, metal undergoes ductile deformation in which metal component of the insert bends. In parallel to metal bending, the composite is crushed by the pin compression. During its ductile deformation, the metal component still transfers the deformation energy to the middle part of the insert. Therefore, the insert slides parallel to the bottom edge. Because of the slide of the insert, a wide and drastic delamination occurs along the bottom edge.

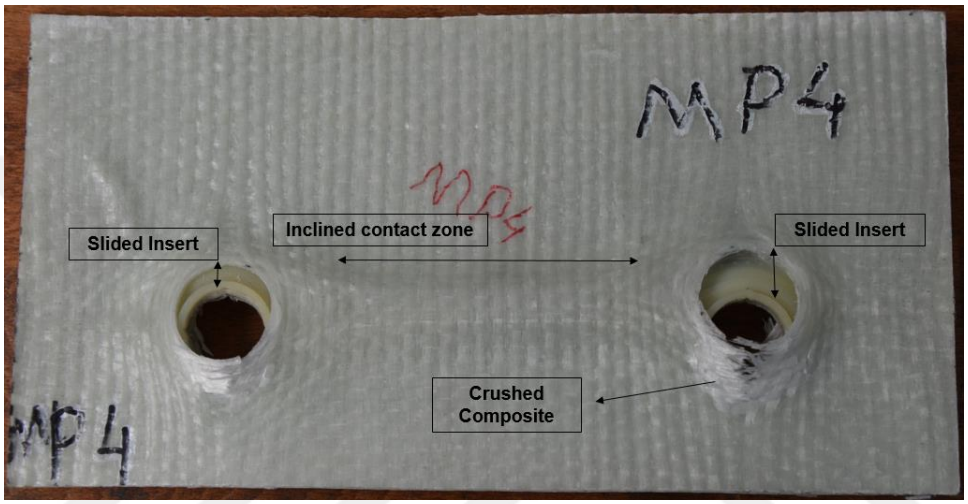

Figure 5.21. Failure at specimen MP4

Figure 5.22. Delamination failure at specimen MP4

The specimen MP4 does not undergo polymer failure and metal bending. The metal-polymer insert slides between the composite layers. This leads to delamination all along the bottom edge. In addition, the bearing regions crush due to compression by the pins. The bearing strength values of specimens MP3 and MP4 are very close to each other, namely 122.78MPa and 129.86 MPa with only 5.7% error.

Figure 5.23. Delamination failure at specimen MP5

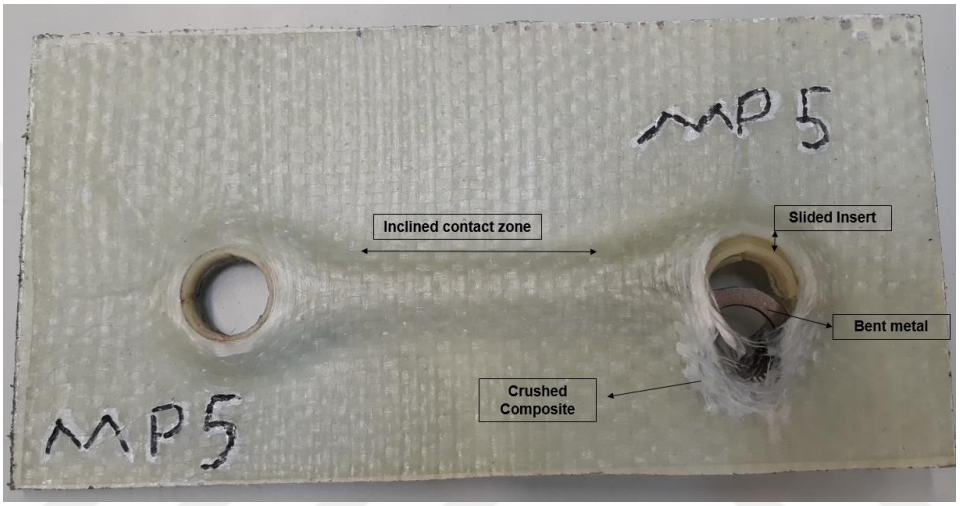

Figure 5.24. Failure at specimen MP5

Only the bearing at the right-hand side failed at MP5 specimen. The bearing at the left-hand side remains undamaged. This asymmetric damage occurred because the specimen slide from the clamps and only one bearing was compresses by the pin. Normally, asymmetric deformation is not desired. However, it enabled us to interpret the following conclusions. The delamination at MP5 only observed at the damaged bearing side (Right hand side) where insert slide. Delamination did not occur at the undamaged bearing side (Left hand side) where insert did not slide. It proves that the sliding of the insert between composite layers leads to delamination failure (Figure 5.27).

Table 5.5. *Bearing Response of the metal-polymer inserted (MP) specimens*

Specimen Type	Stiffness [kN/mm]	Ultimate Bearing Load [kN]	Bearing Load at damage onset [kN]	Bearing Strength [MPa]
MP3	8.13	17.97	13.99	122.78
MP4	8.44	20.47	14.80	129.86
MP5	9.18	21.42	20.50	179.91
Standard Deviation	0.54	1.77	3.54	31.13
Coefficient of Variation	6.3%	8.9%	31.1%	31.1%
Average	8.58	19.95	16.43	144.18

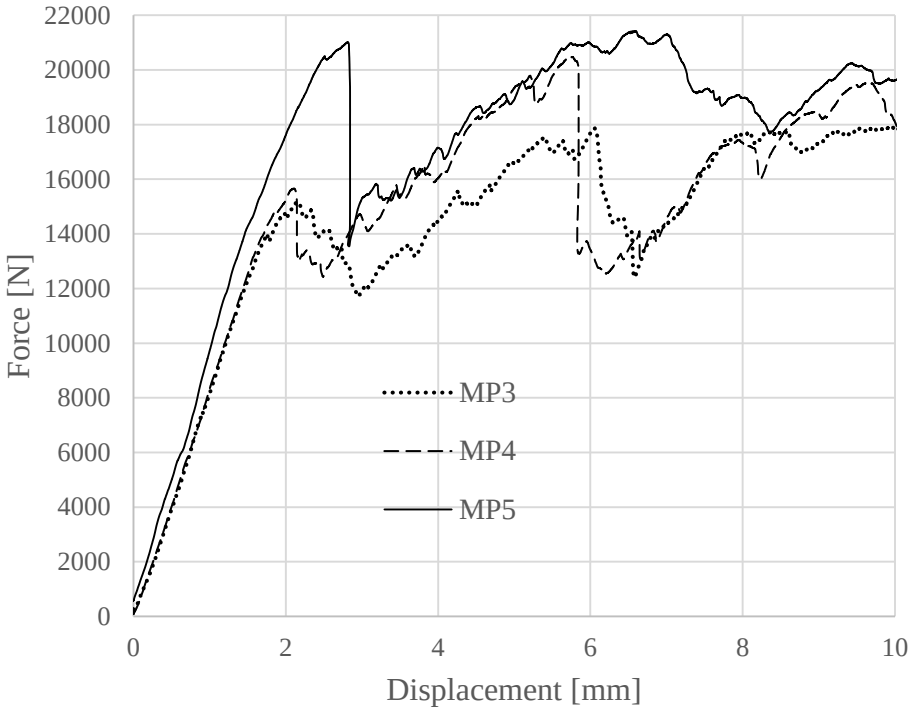

Figure 5.25. Force - hole displacement plots of the metal-polymer inserted specimens

As mentioned, specimen MP5 experienced asymmetric failure due to improper clamping. The force-displacement plots support the situation. The curve of MP5 diverges from the specimens MP3 and MP4. A very consistent force-displacement curve is observed between MP3 and MP4 type specimens. The specimen MP4 which was not subject of polymer failure reached a higher

ultimate bearing load than specimen MP3 (Figure 5.28). Although, specimen MP5 reaches to much higher bearing strength and ultimate bearing load values (179.91 MPa & 21.42 kN) (Table 5.5), the values are unreliable since clamping was improper.

5.3 Results and Discussion of the Experiments

Figure 5.29 compares the average elastic regions of the four types of specimens. The stiffness knock-down at reference specimen (W) occurs at the lowest bearing displacements. On the other hand, the metal inserted specimen (M) is observed to be the most resistant to the stiffness knockdown due to bearing displacement. The polymer (P) and metal-polymer inserted specimens show similar stiffness knock-down response. They (P & MP) are more resistant to stiffness knock-down than reference specimen (W), however less resistant than metal inserted specimen (M).

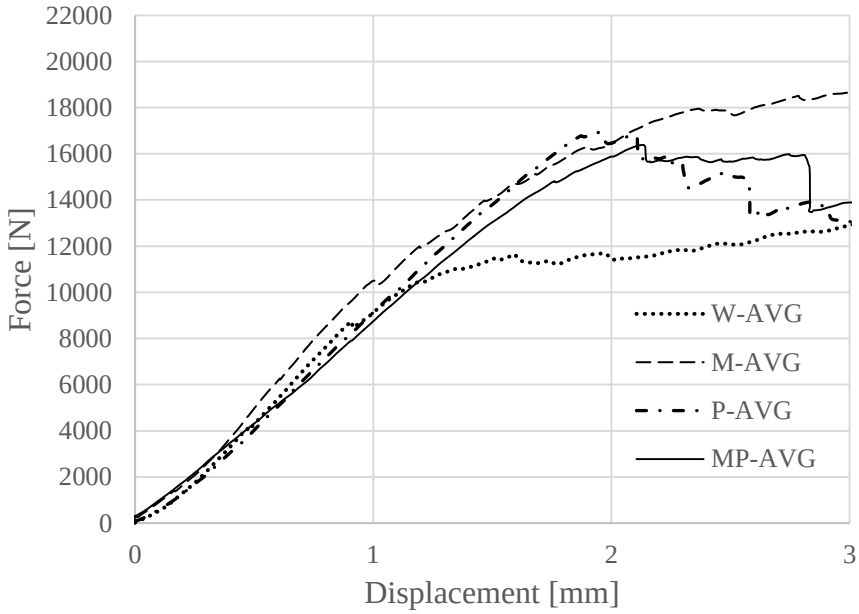

Figure 5.26. Elastic region comparison of four types of specimens

The placement of polymer and metal-polymer inserts improves the bearing strength and the ultimate load bearing capacity of the composite. However, they have negative impact on the stiffness. On the other hand, the placement of the metal inserts improves all three material properties with respect to reference specimen (Table 5.7). Therefore, the metal insert seems to be superior to other two insert types when only positive contributions are compared. But selection of an appropriate insert also depends on the quantity of the contribution of the insert to the material property and the choice of critical material property at the specific loading condition.

When quantitative values of the properties are compared, it is observed that polymer and metal-polymer inserts improve the bearing strength by 74.7% and 62.6% in sequence. The metal insert

improves the bearing strength of the composite only by 11.1%. Polymer and metal-polymer inserts have much better contribution to bearing strength than metal insert. Thus, it is suggested to use a non-drilled composite which can be produced with the help of polymer and metal-polymer insert designs.

The polymer and metal-polymer inserted specimens are non-drilled, and they have good bearing strength. Whereas the metal inserted specimens are drilled, and they have low bearing strength relatively. This result supports the idea that the drilling has a drastic effect on the bearing strength of the composite.

Table 5.6. *Comparison of inserted specimens with reference specimen*

Specimen Type	**Stiffness [kN/mm]**	**Ultimate Bearing Load [kN]**	**Bearing Load at damage onset [kN]**	**Bearing Strength [MPa]**
No Insert specimen (reference)	11.2	14.57	10.10	88.65
Metal Inserted Specimen	11.85 (+5.8%)*	21.06 (+44%)*	11.23 (+11.1%)	98.54 (+11.1%)*
Polymer Inserted Specimen	9.73 (-13.1%)*	18.95 (+30%)*	17.66 (+74.7%)	154.94 (+74.7%)*
Metal-Polymer Inserted Specimen	8.58 (-23.3%)*	19.95 (+36.9%)*	16.43 (+62.6%)	144.18 (+62.6%)*

*Percent variation with respect to the Reference (W) Values

The delamination failure of MP type is more severe than the delamination observed in the P type. The edge of P type delaminates only partially in the projection of the holes on the edge (Figure 5.30), whereas a full delamination is observed in the edge of MP type (Figure 5.31).

The placement of the insert changes the failure mode from bearing mode to delamination mode. The thickness of both P and MP inserts are 4.5mm, therefore, this is not an effective factor on delamination. The effect of metal component in the MP type is the reason of the difference in the delamination amounts of P and MP type. First, the amount of delamination is less at P type insert, because it becomes ineffective at an earlier hole displacement than MP insert does. Therefore, total amount of energy transferred to delamination failure is lower at P type, as a result P type delaminates less than MP type. Second, the position of delamination is different because the thermoplastic of P type is only pushed by pins at the bearing areas. This causes delamination only at the line of bearing holes. On the other hand, polymeric component of MP

type is pushed by the metal at all over its length, therefore the delamination occurs at all the length of MP type laminate.

(A)

(B)

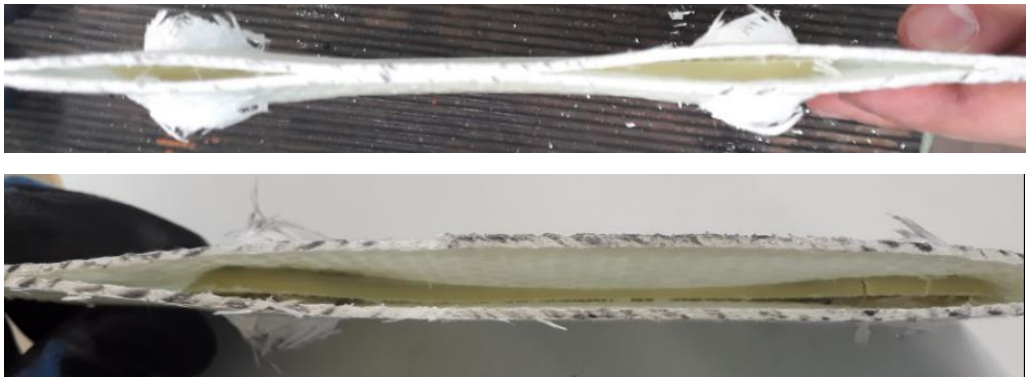

Figure 5.27. Delamination at (A) polymer inserted specimen and (B) metal-polymer inserted specimen

6 FE Analysis of Pin Pull-Through Test

In this chapter, the finite element analysis (FEA) of reference specimen (Ch.6.2) and metal inserted specimen (Ch.6.3) by commercial FEA software Abaqus are explained. The remaining two specimen types were not modeled and analyzed with FEA.

In this work, each woven composite ply was represented with one single mesh element layer as mentioned in Ch.2.5. Every mesh element layer is 0.3mm thick which is the actual thickness of the composite plies. In total, there are 10 mesh elements in the thickness each representing one ply. Each layer of mesh element was assigned with the woven composite material property. It is assumed that the properties of the composite are the same in warp and weft directions (E1=E2).

6.1 Material Properties

Abaqus environment requires a set of material parameters. The required parameters are elastic constants, damage initiation properties and damage propagation properties. Since the properties of the composite is critical around the drilled hole region (bearing), the effective properties at bearing should be calculated. The pin pull-through test provides us with bearing strength and bearing elastic modulus properties. The damage propagation properties which are intra-laminar fracture toughness values can be determined by compact tension and compact compression tests. However, compact tension and compression tests were not performed in this thesis work.

In this work, as mentioned above, full scale material characterization tests were not performed on the composite specimens. The elastic moduli and the failure strength properties in warp and weft directions (E_{warp} and E_{weft}) were determined from the pin pull-through tests of the reference specimens. In fact, elastic moduli in warp and weft directions are not equal ($E_{warp} \neq E_{weft}$) because the number of fiber tows per length in warp and weft directions are 3.3/cm and 2.3/cm consecutively. However, elastic moduli in warp and weft directions were assumed to be same for simplification.

To determine the bearing elastic modulus and bearing strength properties, first the force-displacement plots of reference specimens were converted into bearing stress-strain plots. The bearing elastic modulus was calculated from the slope of the linear-elastic part of the bearing stress-strain plot in Ch. 5.2.2 (Table 5.2 & Figure 5.13). The stress-strain calculation can be seen in the Appendix (Ch.10.2). Similarly, the bearing strength of the reference specimens were determined from the stress-strain plots. The first drastic drop in the bearing stress in the stress-strain plot corresponds to the bearing strength. The effective bearing strengths and young's modulus of the reference specimens were averaged. The averaged values were used as the material properties at the simulations. The other material properties (V_{xy}, V_{yz}, V_{xz}, G_{xy}, G_{yz}, G_{xz}) that are necessary for FE analysis were taken from literature.

Table 6.1. *Material Properties of glass/epoxy laminate*

Parameter	**Unit**	**Value**	**Description**
$E_{x=warp=x}$	[MPa]	1862 (1)	Elastic modulus at first principle direction
$E_{y=weft}$	[MPa]	1862 (1)	Elastic modulus at second principle direction
$E_{z=out-of-plane}$	[MPa]	1011 (5)	Elastic modulus at third principle direction
V_{xy}, V_{yz}, V_{xz}	[-]	0.096 (2)	Poisson ratios
G_{xy}, G_{yz}, G_{xz}	[MPa]	473 (2)	Shear Modulus
X_t	[MPa]	245.01 (6)	Tensile strength at x (longitudinal) direction
X_c	[MPa]	88.65 (1)	Compressive strength at x (longitudinal) direction
Y_t	[MPa]	245 (6)	Tensile strength at y (transverse) direction
Y_c	[MPa]	88.65 (1)	Compressive strength at y (transverse) direction
S_{xy}	[MPa]	56.19 (3)	Shear Strength at x-y plane
GIc	[kJ/m^2]	45 (4)	Intra-laminar tensile fiber fracture energy
GIIc	[kJ/m^2]	40 (4)	Intra-laminar compressive fiber fracture energy

(1) Pin pull-through tests on reference inserts (See Table 5.2), (2) Data from Kadhim. (2010, p.6022), (3) Data retrieved from (Cai et al., 2017, p.148), (4) Data from Kaddour (as cited in Lee, 2015, p.56), (5) Estimated from pin pull-through tests of this thesis work, (6) Tensile coupon test by Pohl

6.2 FE Analysis of Reference Specimens

6.2.1 FE Model

In total four types of specimens (W, M, P, MP) were tested. Among those four types, only the reference specimen (W) and metal inserted specimen (W) were modeled in the FE environment.

The FE model of reference specimen consists of 3 parts: the laminate and two pins (Figure 6.1). The 3D geometries of the parts of the clamping system was not included in the model for simplification purposes. The computation time is reduced because less mesh elements and less contact definitions were used with this simplification.

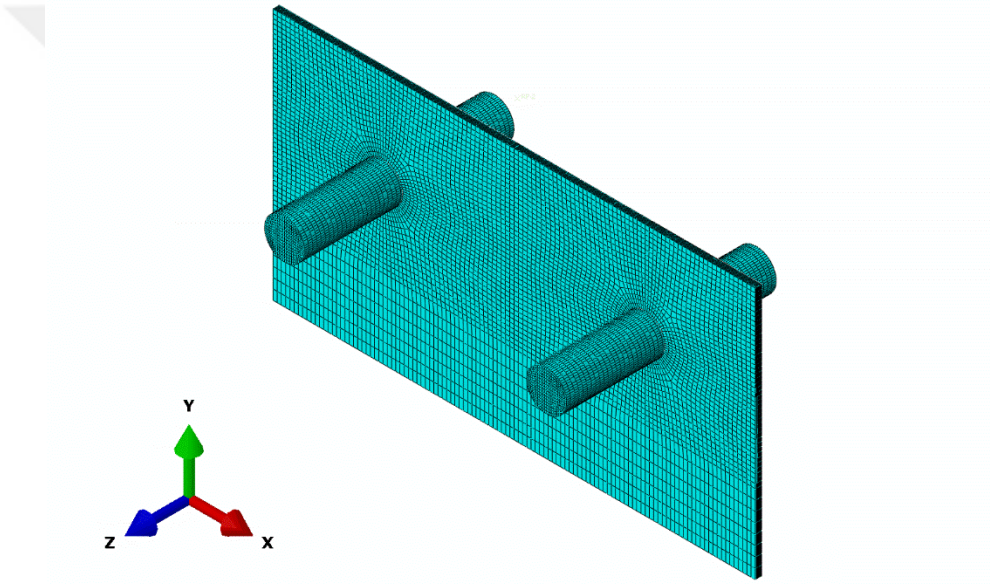

Figure 6.1. Pin pull-through assembly of reference specimen in with two pins and composite

The mesh element type of pins is 3D hexahedral solid element of C3D8R type. The mesh element type of the laminate part is SC8R continuum shell elements. In total 10 layers of mesh elements were used in the thickness of the laminate (z – direction). Each element layer represents one ply of the composite laminate. In the model, there are 103,955 nodes and 91,480 mesh elements. 56,680 of them are SC8R and 34,800 of them are C3D8R.

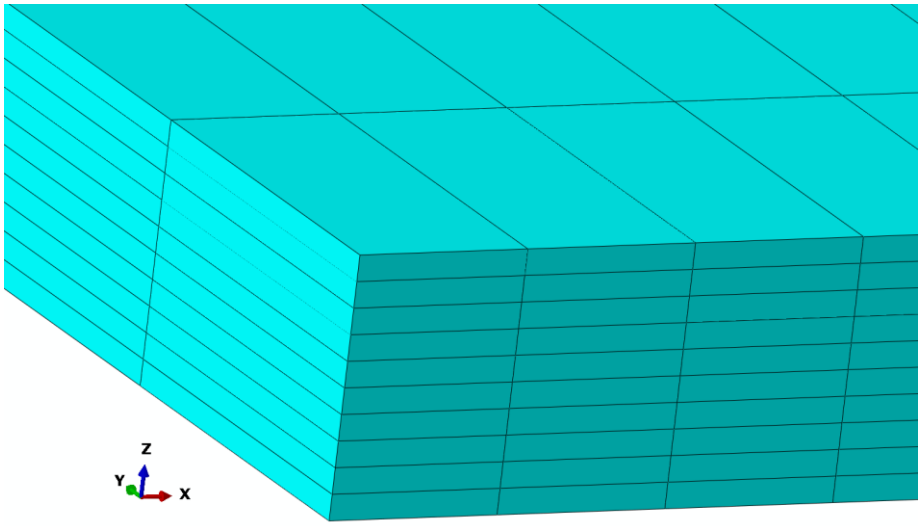

Figure 6.2. Each ply is represented with one layer of mesh element in the thickness (z-direction)

The main deformation occurs at the mesh elements around the bearing. For an accurate calculation, the first four row of mesh elements are finer (the smallest edge 0.8mm). The global edge size of the other mesh elements is approximately 2mm. Therefore, the mesh at around the hole was refined for better accuracy (Figure 6.3).

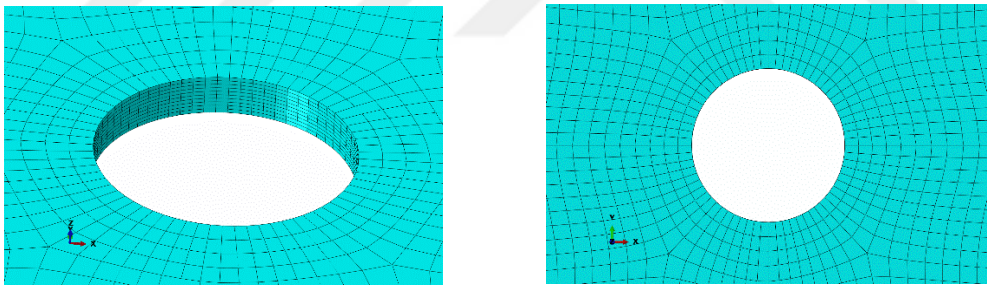

Figure 6.3. Fine mesh around the hole

At the hole-pin interface there is no gap between composite mesh elements and the rod mesh elements for an accurate contact interaction. An accurate contact interaction reduces the computation time and eases the convergence.

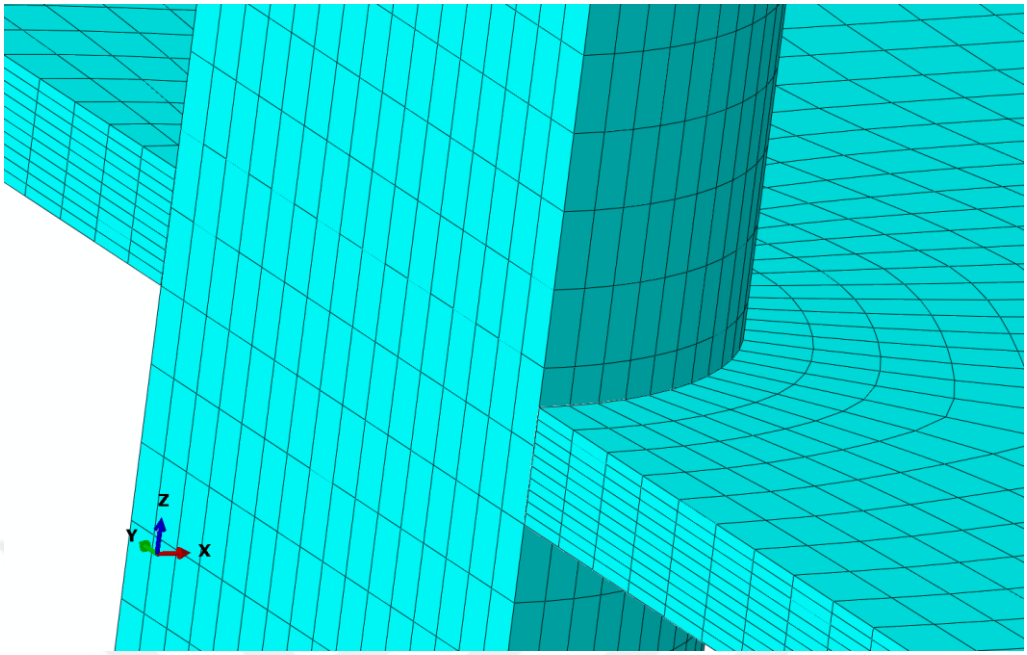

Figure 6.4. Pin-composite interface – cross section view

At the bearing (Figure 6.4), contact definition between the pins and the inner surface of the hole on the laminate is defined as surface-to-node contact formulation. 10mm displacement in +y direction was applied to a rigid body element. All the nodes of the pins are connected to the rigid body element with kinematic coupling interaction (Figure 6.5). The kinematic coupling transfers all the degree of freedoms of the rigid body element to the nodes of the pins. Therefore, the pins also move in 10 mm displacement.

As a rule-of-thumb, the contact surface with the bigger mesh elements should be assigned as master, and contact pair with smaller mesh elements as slave surface. As can be seen from the Figure 6.4, the pins which have bigger mesh elements are assigned to be master surfaces.

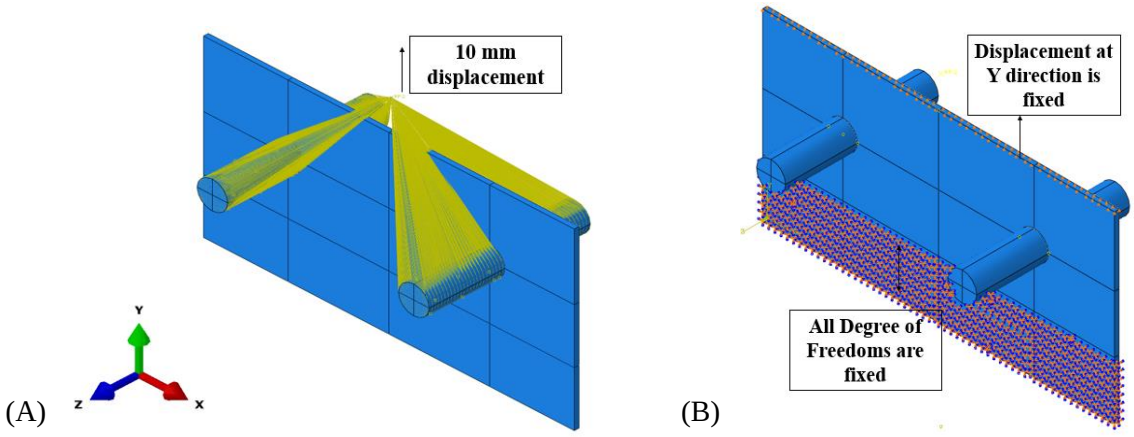

Figure 6.5. (B) Kinematic coupling between rigid body node and pins and (B) encastre boundary condition at the bottom 30mm of the laminate

To capture the movement of the pins, a rigid body node was created in the mid-plane of the laminate. The rigid body node was pulled 10mm in +y direction with displacement boundary condition. All the nodes of the pin geometries were linked to the rigid body node with kinematic coupling (Figure 82). The same 10mm displacement is transferred to the pins thanks to the kinematic coupling. The displacement boundary condition results in more gradual failure rate than force boundary condition.

The first 10 rows of composite mesh elements at –y direction was constraint with encastre boundary condition which limits the motion at every degree of freedom (Figure 82). This encastre boundary condition represents the clamping of the laminate. In addition, displacement of the top edge of the composite in +y direction was limited in y direction.

6.2.2 Comparison of FE Results and Experiments

Table 6.2. *Comparison of properties obtained at tests and simulations*

Specimen Type	Stiffness [kN/mm]	Ultimate Bearing Load [kN]	Bearing Strength [MPa]
Reference (W) (Average)	11.2	14.57	88.65
Simulation	11.8	12.6	110.9
Error	5%	13.5%	25%

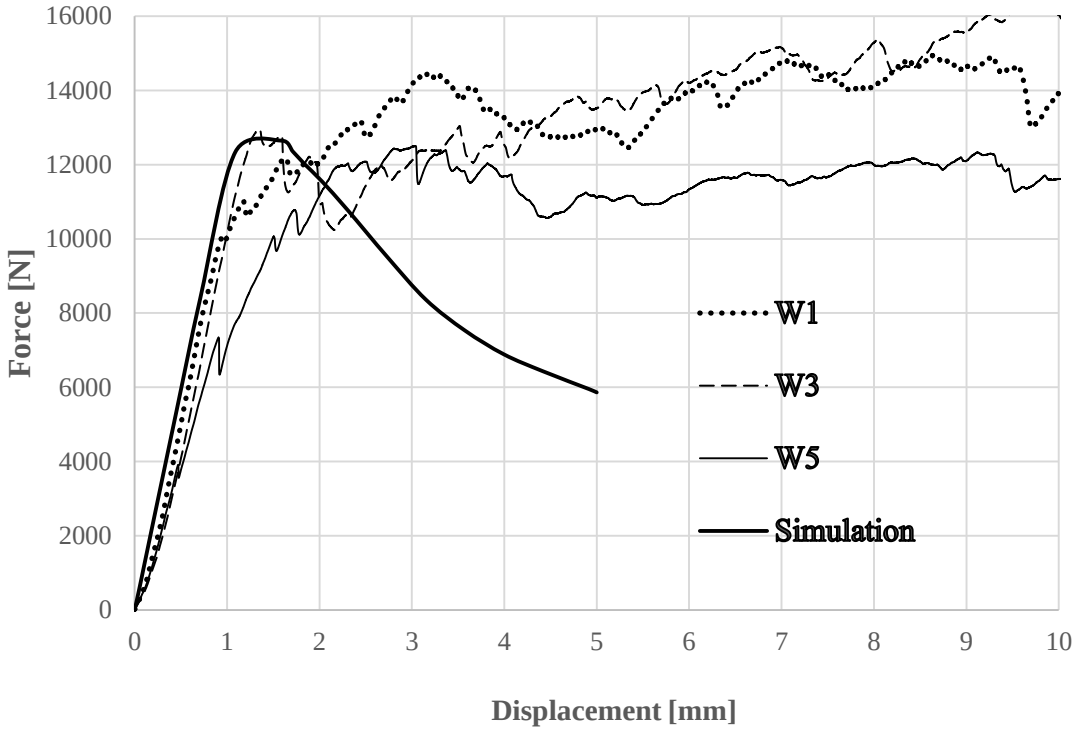

Figure 6.6. Force-Displacement Curve Comparison of simulation and experiments

The stiffness error between tests and simulations is only 5%. There is good correlation between simulation and experiment for elastic response of the composite. The correlation of force-displacement curves can be seen in the Figure 86. It can be interpreted that the simplified FE model is able to properly represent the elastic deformation at the pin pull-through test. In addition, the use of characterized material constants contribute to the accuracy of the simulation (Ch. 6.1.1).

The bearing strength error between test and simulation results is 25 %. It is observed that the simplified FE model is able to represent the elastic response better than the damaged response.

The progressive failure of the composite was not represented in the simulation. In the tests, the force displacement curve at the damaged area has sudden force drops and elevations. However, the stiffnesses of the mesh elements in the simulation continously drops after the damage initiation, therefore force-displacement curve of simulation shows a decline (Figure 86). There are two reasons for this bad correlation after damage initiation. Firstly, the damage propogation properties (intra-laminar fracture toughness) of glass/epoxy specimens at the thesis work are not characterized. The fracture values of another glass/epoxy specimen from literature were used in the simulation. To accuractely simulate the damage propagation, the fracture toughness values should be characterized. Secondly, the microstructure of the composite is not represented in the FE model. In the test, when a fiber tow fails the force value shows a sudden drop. The force value elevates again when the next undamaged fiber tow resists the displacement of the

pin. In the simulation, the mesh elements that has direct contact with the pin undergo a continuous stiffness degredation which is not the reality.

Abaqus offers an element deletion option which can be used to improve the FE model. In this option, the mesh elements that satisfy a specific damage condition is removed from the model. This element deletion option would represent the sudden failure of the fibre tows. When an element is deleted, the force at that increment of the simulation would suddenly drop (as in the experiment) since the removed element cannot resist the movement of the pin.

Figure 6.7. The tearing of the fibers due to fiber tension (right) out-of-plane bending of the fibers

During elastic deformation, only compressive stresses are observed at the bearing area (Figure 88).

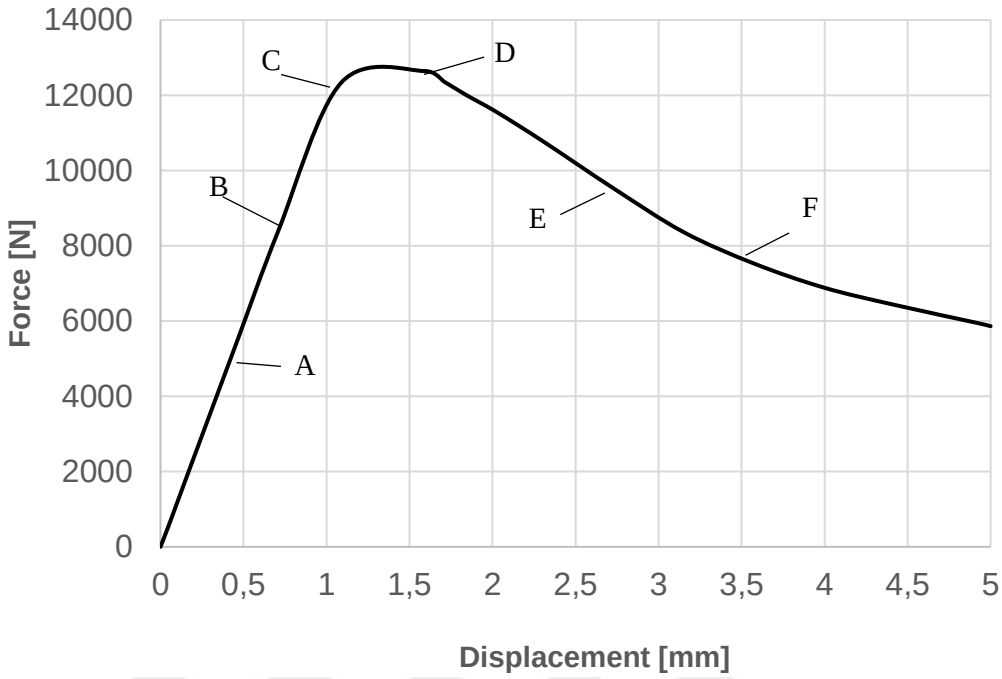

Figure 6.8. Instances from the F-X plot

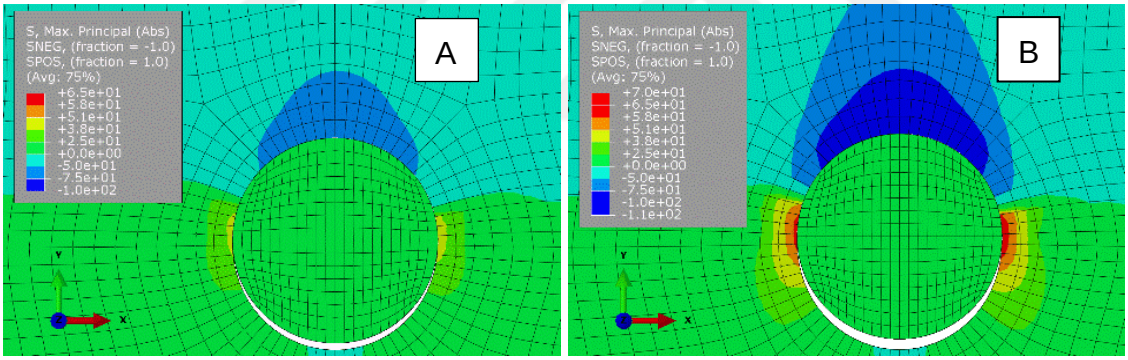

Figure 6.9. Absolute Principal Stresses at elastic region points (A) and (B) point C. Blue colors represent compression. Green and red represent tension.

As can be seen in Figure 88, during elastic deformation there is mainly compressive stresses. After the damage initiation, the stiffness of the mesh elements starts to degrade. Tensile stresses emerge at the top periphery of the pin-composite interface due to the stiffness degradation. The positive principal stresses (tensile stress) can be seen in Figure 87 and 88 in red, yellow and green colors. The light blue, blue and dark blue colors represent the negative principal stresses (compressive stress).

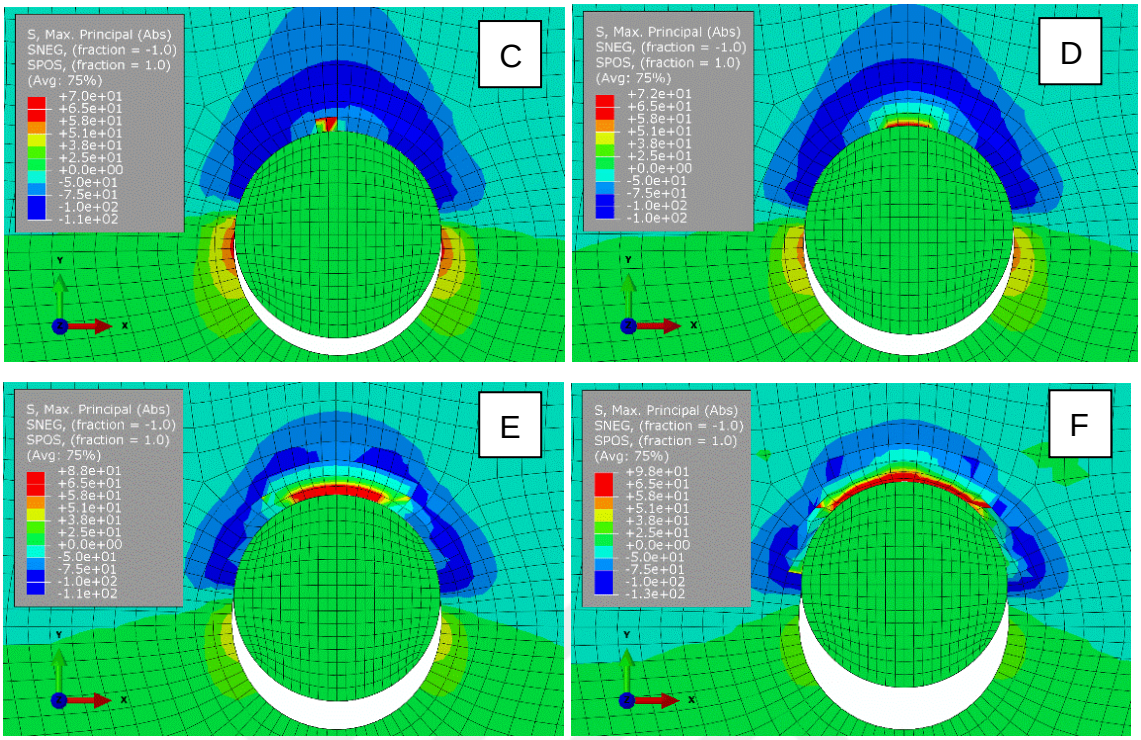

Figure 6.10. After the damage initiation, tensile stresses in x-direction emerges.

6.3 FE Analysis of Metal Inserted Model

6.3.1 FE Model

From the reference specimen's FE model, metal inserted specimen's FE model has one extra part which is the metal insert that is placed between 5th and 6th mesh elements of the laminate. All of the surfaces of the metal is in contact with pins or the composite laminate. Therefore, the FE model of metal inserted specimen consists of many contact definitions.

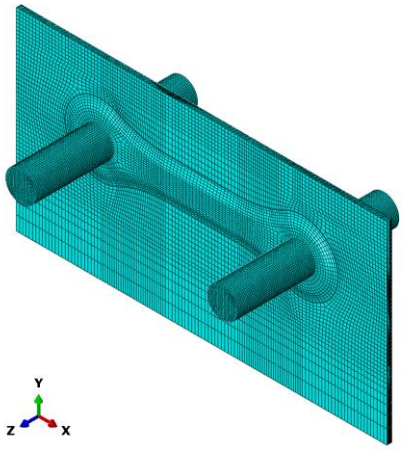

Figure 6.11. The assembly of M Laminate

In the model, there are 182,948 nodes and 153,766 mesh elements in total. 4364 hexahedral COH3D8 elements which are assigned to the pure resin solid body and the zero thickness cohesive surfaces on the top and bottom of the metal insert. 80800 continuum shell C3D8R type elements are assigned to the composite specimen. 67,100 hexahedral solid SC8R type elements are assigned to the pin geometries. And lastly, 1502 hexahedral solid C3D8 type elements are assigned to the metal insert.

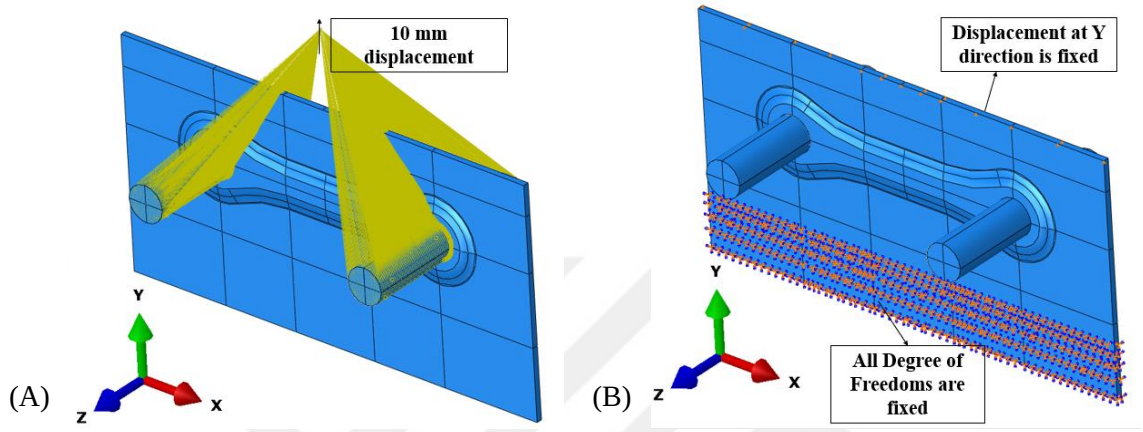

Figure 6.12. (A) Kinematic coupling between rigid body node and pins and (B) Encastre boundary condition at the bottom 30mm of the laminate

The metal – pin interface is modeled with a surface-to-surface contact definition. The pin surfaces are selected as master surface and the metal's bearing surface are selected as slave surface.

The 5 layers of composite plies that was laid on the metal insert smoothly curves down to meet the bottom 5 composite plies. This creates a gap between composite laminate and the metal all the way around the edge of the metal (Figure 6.13). The gap that occurred after laying the glass fabric is filled with epoxy resin during the hand lamination process.

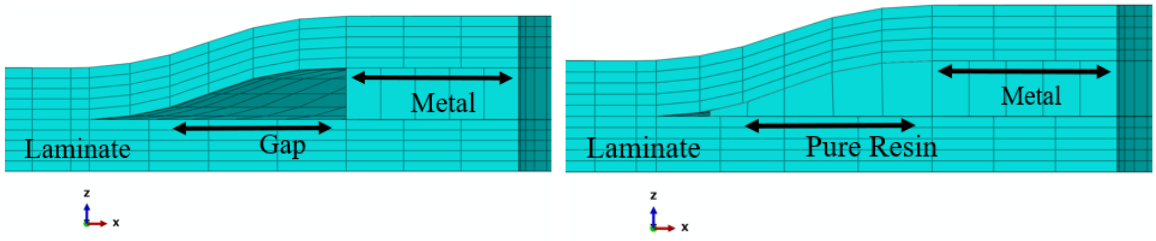

Figure 6.13. Pure resin body fills the gap between metal insert and composite laminate

(A) 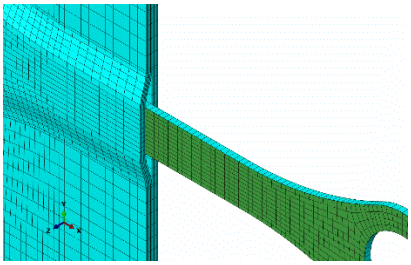 (B) 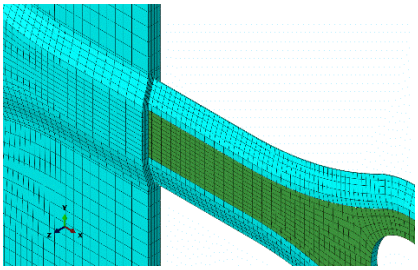

Figure 6.14. (A) Pure resin body is hidden and (B) Pure resin body is visible

The gap was modeled with an individual solid body in the FE model. The individual solid body represents the pure resin that is between the metal insert and composite. The pure resin body in the FE model covers all the way around the edge of the metal insert (Figure 6.13, Figure 6.14). The pure resin solid body assigned with COH3D8.

Table 6.3. *Material properties of cohesive elements*

Parameter	**Unit**	**Value**	**Description**
E_x	[MPa]	2650 (1)	Elastic modulus at first principle direction
E_y	[MPa]	2650 (1)	Elastic modulus at second principle direction
E_z	[MPa]	2650 (1)	Elastic modulus at second principle direction
G_{IC}	[kJ/m2]	1.2 (2)	Elastic modulus at third principle direction
G_{IIC}	[kJ/m2]	1.9 (2)	Poisson ratios
G_{IIIC}	[kJ/m2]	1.9 (2)	Shear Modulus

(1) Taken from Product Data Sheet for Biresin® CR170 (Sika Deutschland GmbH, 2017), (2) Taken from (Schraa, 2016, p.28)

The epoxy resin fills all the volume inside the glass fabric and, the gap between metal insert and composite interface. Therefore, the bonding behavior between the metal and composite laminate is provided by the epoxy resin. Epoxy resin can be modeled in Abaqus/CAE with cohesive mesh elements. Kießling et al. (2016, p.2) suggests modelling the metal-composite interface with zero-thickness surface mesh elements that are assigned with cohesive material property.

To actualize zero thickness cohesive response, first an offset mesh surface was created at 0 mm distance from the bottom and top surfaces of the metal. The two offset mesh surfaces are tied to the original metal mesh elements. COH3D8 elements were assigned to the zero thickness

surface mesh elements. The nodes of the cohesive elements are connected to the composite laminate nodes with tie contact. Tie contact glues two surfaces or node sets to each other.

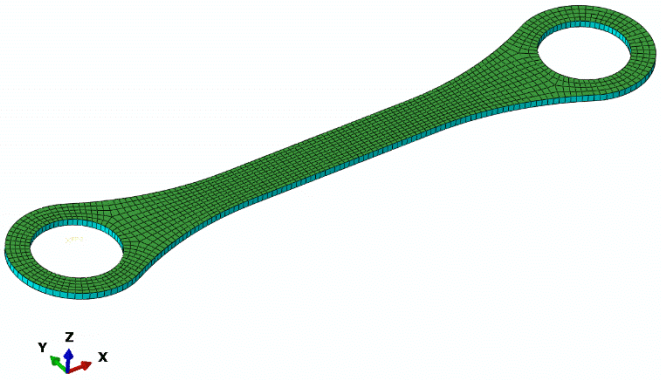

Figure 6.15. *The green surface represents the cohesive zero thickness mesh surface*

6.3.2 Comparison of FE Results and Experiments

The FE model of metal inserted specimen represents the main failure behavior. In the experiment, it is observed that the metal insert slides between the laminate. It was successfully shown in the FE simulation result (Figure 6.17 & Figure 6.18). In the experiment, the metal insert bends to make an arc shape. Such arc shape is also shown in the results of the FE analysis (Figure 6.17 & Figure 6.19). However, the local delamination that is observed in the tests of metal inserted laminate cannot be shown in the FE analysis results. The FE model was not aimed to show the delamination. As a further step, a layer of mesh elements with cohesive material behavior can be placed between the 5th and 6th layers. This improvement would be a method to represent the delamination.

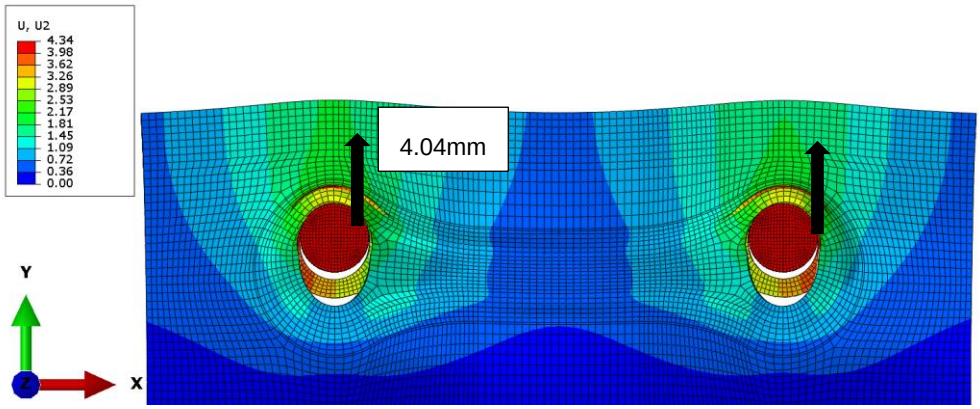

Figure 6.16. Pins pull the metal insert and compress the composite

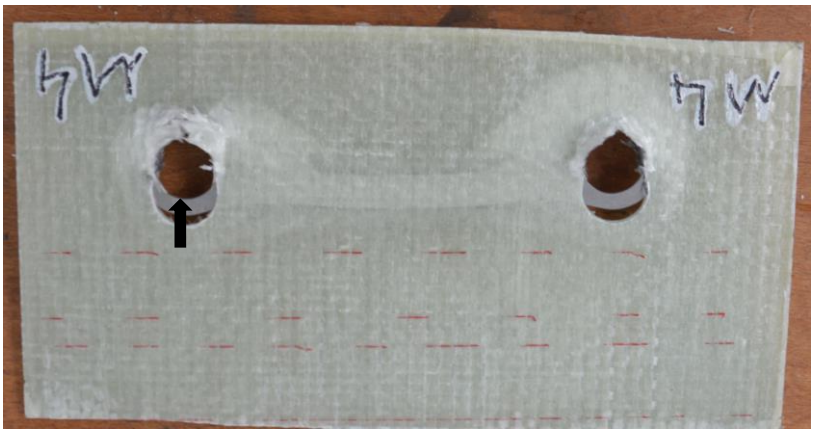

Figure 6.17. Slide and bending of the metal insert at experiment

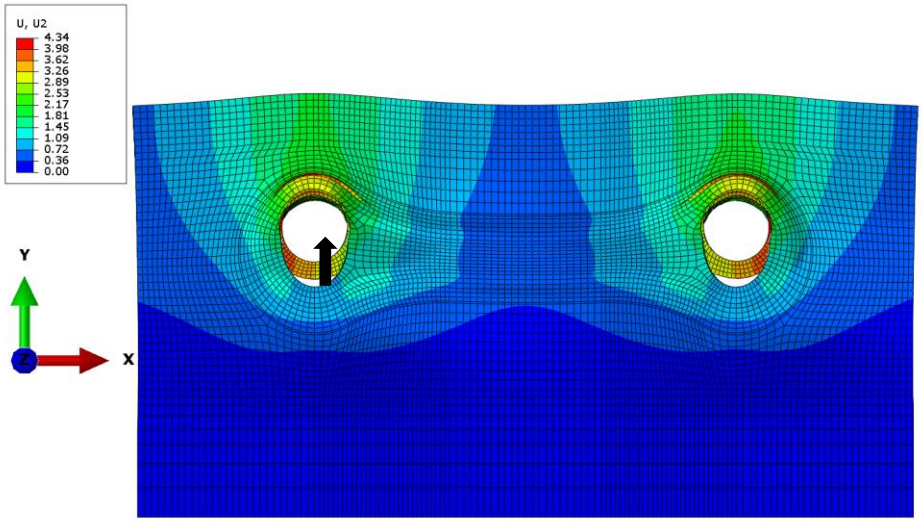

Figure 6.18. Slide of the metal insert at simulation

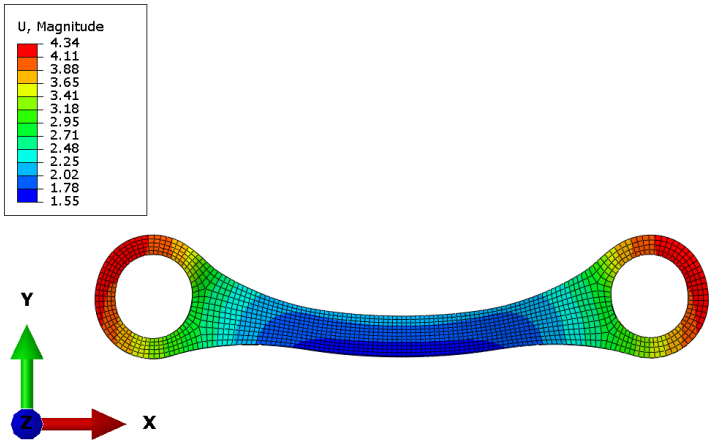

Figure 6.19. Bending of the metal insert at simulation

In simulation, total slide distance at the middle of the metal insert is 1.55mm and 4.34 mm at metal bearing areas for 4.04 mm pin displacement (Figure 6.19).

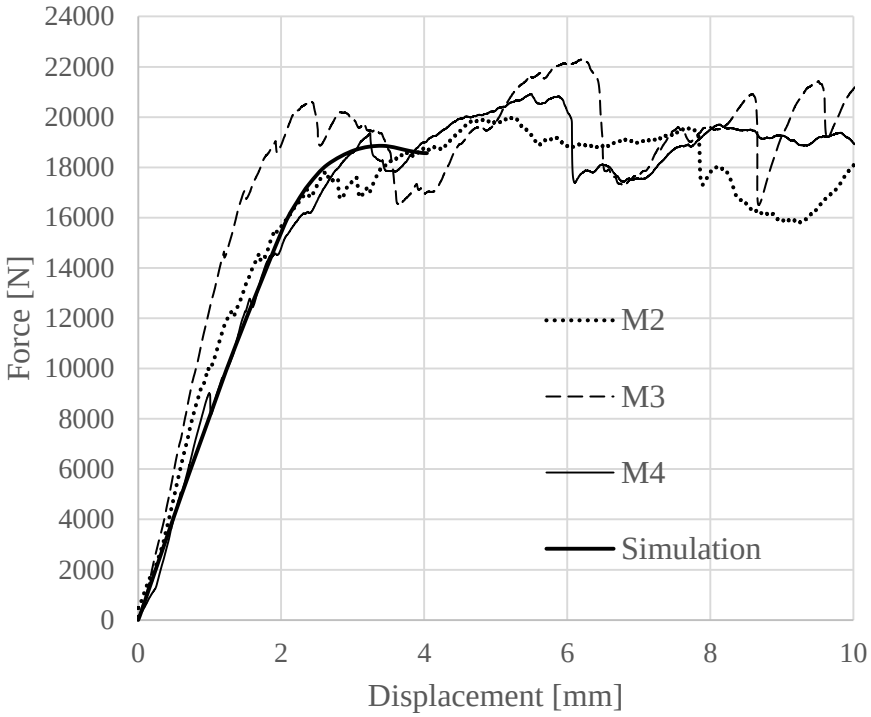

Figure 6.20. Force-Displacement Curve Comparison of simulation and experiments

Although the FE model of metal inserted specimen represents the characteristics of the failure fundamentally, experimental and simulation parameter values has quite big error from each other. T stiffness values obtained in the simulation is 39.2% lower than the experimental stiffness (Table 6.4). There are two reasons for this stiffness error. First, there are many contacts between metal insert and the composite. Contact formulations is a source of error in FE analysis. Second, there is an overclosure in one contact pair. When the contact surfaces penetrate each other, their resistance to pin's movement becomes less effective. Therefore, lower stiffness value is observed.

Table 6.4. *Comparison of properties obtained at tests and simulations of metal inserted specimen*

Specimen Type	Stiffness [kN/mm]	Ultimate Bearing Load [kN]	Bearing Strength [MPa]
Metal Inserted (M) (Average)	11.85	21.06	98.54
Simulation	7.2	18.8	152.0
Error	%39.2	10.7%	54%

7 Summary and Conclusion

The composite structures have taken their place in many forms as one of the major materials in automotive and aerospace industry in the last quarter of the 20th century. The use of bolted joints to fasten FRPs might be problematic since composites are weakened drastically when they are drilled. This work attempts to use inserts to reinforce the plain weave textile composite (PWTC) at drilled joint regions. The inserts are embedded between the layers of glass/epoxy PWTC specimens by intrinsic hybridization method. With the help of the designed inserts, the hole can be formed during composite lamination. Thus, the drilling process can be avoided. Moreover, with the help of the inclined contact zone between composite and insert, the inserted bearing is expected to carry higher forces than non-inserted bearing. To observe the failure modes and the durability of inserted PWTC, a pin pull-through experiment setup was designed, and then, the bearing durability of inserted PWTC specimens is compared with reference no-insert PWTC specimens. Lastly, the pin pull-through test was modeled in commercial Abaqus FEA software environment. The FE analysis was performed with Abaqus/Standard finite element solver.

Firstly, this thesis proposes to use inserts to reinforce the bearing area. For this purpose, three different inserts were designed for a rear cab suspension bracket of a Mercedes Benz Truck. Four types of PWTC specimens were produced among which three of them are inserted and one of the type has no insert.

With quasi-static experiments the failure modes of the composite specimens were observed. The following conclusions were drawn according to the experiment results.

- The strength of all the inserted laminates found to be higher than the reference laminate. Despite that improvement, use of inserts brings a certain disadvantage: delamination. In other words, use of inserts causes delamination which is not observed in reference specimens.
- It is observed that the main failure mode at all specimen types is bearing mode failure (Figure 2.9). This failure mode is local crush of the composite around the hole under compression by the pin.
- In addition to bearing failure, all the inserted specimens undergo delamination failure. The delamination at metal inserted specimens is not significant. However, polymer inserted, and metal-polymer inserted specimens undergo very significant delamination. Their 5th and 6th plies delaminate from each other totally. At the most drastic case the plies of metal-polymer inserted specimen delaminated 3mm from each other.
- Metal insert which is 1.5mm thick, causes less delamination than polymer and metal polymer inserts which are 4.5mm thick. Therefore, it can be concluded that as the thickness of the insert increases, the risk of delamination also increases.
- The failure modes of polymer inserted, and metal-polymer inserted laminates are a mixture of bearing mode failure and delamination mode failure.

- The quasi-static pin pull-through tests were investigated in terms of three parameters: stiffness, bearing strength and ultimate bearing load. It is observed that placement of inserts at the bearing region always improve the ultimate bearing load capacity and bearing strength. However, placement of polymer and metal-polymer inserts reduced the stiffness at the bearing.
- Metal inserted specimens have improvement 5.8% in stiffness, 44% in ultimate bearing load capacity and 11.1% in bearing strength with respect to reference specimens.
- Polymer inserted specimens have improvement 30% in ultimate bearing load capacity and 74.7% in bearing strength with respect to reference specimens. However, stiffness dropped for 13.1%.
- Metal-polymer inserted specimens have improvement 36.9% in ultimate bearing load capacity and 62.6% in bearing strength with respect to reference specimens. However, stiffness dropped for 23.3%.
- The improvements at ultimate load bearing capacity show that the force on the bearing is distributed to the inclined contact zones at all three types of inserted specimens. This proves that the inclined zone reinforces the bearing as expected.
- The drilled specimens have significantly lower bearing strength values than non-drilled specimens. This proves that the bearing socket improves the bearing strength as expected. The non-drilled specimens endured higher loads because the continuity of their reinforcement fibers is not violated, and they did not have notch effect due to drilling.
- In the experiments, it is observed that even though the composite is crushed, it can still bear load. The failure is a progressive, local fiber and matrix failure. This kind of failure has an advantage since it is not a sudden ultimate failure of the material. Therefore, under this type of failure mode, multiple impacts can be absorbed by the composite. This impact energy absorption capability of composites was already studied by Bergmann and Heimbs (2017) at their pin-pull through tests.

Beside the experiments, pin pull-through tests of reference and metal inserted specimens were modeled in Abaqus environment. Both models represent the fundamental traits of the experiments.

The FEA results of metal inserted specimens and reference specimens show the fundamental elastic behavior that was observed in the experiments. From the FE analysis, following conclusions are drawn:

- The simulation results of reference specimens have 5% stiffness error, 13.5% ultimate load bearing capacity error and 25% bearing strength error from the experiment results.
- The simulations result of metal inserted specimens have 39.2% stiffness error, 10.7% ultimate load bearing capacity error and 54% for bearing strength error.

- The elastic response of specimens is represented at simulations relatively good. However, the non-elastic response and progressive failure of composite specimens are not properly represented in simulations.
- During the crush of the bearing region, the fiber tows breaks due to tensile stresses and pushed in out-of-plane direction by the pin. This deformation behavior was show in both FE models.
- In the FEA result of metal inserted specimen, main deformation characteristics are properly shown, which are bending of the metal and the slide of the metal between the composite layers.

Consequently, there were three main aims of this work. The first aim was to reinforce the bearing region with inserts by exploiting inclined contact zone between insert and composite. The pin pull-through results show that the inclined contact zone functions as expected. The applied load is distributed along the inclined contact zone; therefore, the bearing can endure higher loads. The second aim was to come up with a design solution that prevents the need of drilling the composite. It was expected that if the composite is not drilled, the bearing strength would be higher since stress concentrations that are caused by drilling does not exist at the bearing region. With the intrinsic hybridization method that was used in this thesis, the hole is formed during the production of the composite. Therefore, the composite is not drilled. It is observed that the polymer inserted specimens and metal-polymer inserted specimens that are not drilled have significantly higher bearing strength values than drilled specimens (Ch.5). Thus, the intrinsic hybridization method in which the bearing hole is formed during the production of composite improves the bearing strength as expected. The last aim was to model the deformation of inserted composites at FE environment. Although the progressive failure of the composite cannot be shown in simulations, the fundamental elastic deformation mechanisms of two specimen types are shown in the simulation results.

8 Discussion and Next Steps

The actual component of the Mercedes Benz Truck is fastened to chassis with two M18 bolts and nuts from both sides. In our experiment, pin loading condition was used although the rear cab suspension bracket is fastened with bolted joint. There are three reasons for selection of pinned joint. First, it was aimed to observe the composite failure only under compression by the pin. Therefore, the bolted joint which has pre-tension forces due to tightening of the nuts is not used. Second, it was aimed to let the fiber tows move freely in the out-of-plane direction during failure. This allows to visually inspect the failure of the fiber tows under pin compression. The visual inspection would be difficult at bolted joint, since the fastened nuts would block the view angle. Third, it is reported by Pakdil et al. (2011) that the failure mode remains almost always the same at pinned and bolted composite specimens. Thus, the pin pull-through tests at this work represents the fundamental deformation traits of the bolted joint region of rear cab suspension bracket of Mercedes Benz Truck. However, for a more comprehensive investigation on the failure of cab rear suspension bracket, bolted joint pull-through tests should be performed. The results of pin-pull through tests of this work and bolt pull-through tests should be compared as a further step. In addition, fatigue life cycle tests should be performed as the bracket would undergo cyclic loading under rough road service condition conditions.

The crushed bearing area of composite and out-of-plane deformation of the fibers can be seen in Figure 8.1. The fibers moved freely during failure in the direction of the stress. The direction of failed fiber tows represents the tensile stresses which caused the out-of-plane deformation. Moreover, in Figure 8.1, tearing line of the composite which is in the movement direction of the pin can be observed. Despite this result gives a brief idea of failure under pin compression, for a more detailed observation, the crush of the composite should be viewed with a camera or thermography.

(A)

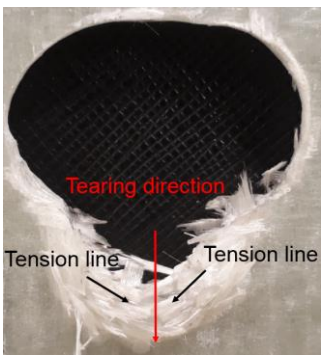

(B)

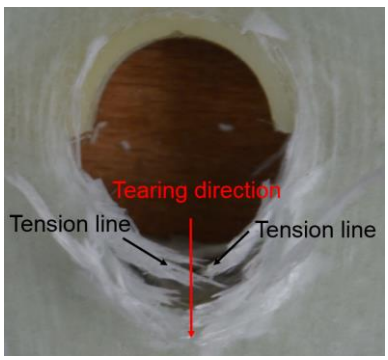

Figure 8.1. Out-of-plane deformation of fibers during the tearing in the pin displacement direction. (A) reference specimen and (B) polymer inserted specimen

In simulation models, the intra-laminar fracture toughness values were taken from literature. The real fracture toughness values of our PWTC specimens are unknown since necessary material characterization tests (Compact tension, compact compression) were not performed. In a more accurate simulation result, a full characterization of the composite material is necessary.

The commercial Abaqus Standard Solver has a Hashin Failure Criterion (Hashin & Rotem, 1973) based built-in material model. The Hashin models the failure of unidirectional composites. For modeling the failure of woven composite material, constitutive models for fabric reinforced composites should be implemented with user defined sub-routines to Abaqus. For instance, in his work Johnson (2001) models the deformation of fabric reinforced composite under impact and crash loads with Abaqus/Explicit solver and with Ladeveze's constitutive material model. The model of Johnson, is available for Abaqus users as a user-material sub-routine with name ABQ-PLY_FABRIC. Bergmann et al. (2017) uses Abaqus/Explicit solver with user subroutine ABQ_PLY_FABRIC to capture the bearing failure progression of his CFRP specimens. It is observed that the Ladeveze based material model and Abaqus/Explicit solver represents also the pin pull-through test quite well (Bergmann & Heimbs, 2017, p.). The sudden force drops and increases of Bergmann's pin pull through tests are shown in the results of his FE analysis. In addition, it is mentioned in the literature that the Abaqus/Explicit solver is more accurate than Abaqus/Standard solver in simulation of quasi-static tests such as pin pull-through tests, because the Abaqus/Explicit solver is more efficient for large deformation problems such as pin pull through tests (Smith, 2009).

The use of lightweight materials in heavy duty vehicles is not as common as in passenger cars. In passenger cars, the lightweight structures are used in many sub-systems of the vehicle. On the contrary, the usage of lightweight structures in heavy duty vehicles is limited mainly in cabin components. Truck manufacturers still prefer mainly metal components over lightweight materials due to durability concerns. In short, the use of lightweight materials is a dilemma for heavy duty vehicle manufacturers such as Mercedes Benz Trucks. However, the energy absorption capability of composites can be exploited by implementing it as suspension unit of a truck which undergoes fatigue loading.

9 References

Kaw, A. K. (2006). *Mechanics of composite materials*. London: CRC

Kießling, R., Ihlemann, J., Pohl, M., Stommel, M., Dammann, C., Mahnken, R., & Kästner, M. (2016). On the Design, Characterization and Simulation of Hybrid Metal-Composite Interfaces. *Applied Composite Materials, 24*(1), 251-269. doi:10.1007/s10443-016-9526-z

Pohl, M., Stommel, M. (2016, June). Designing a Metal-CFRP-Hybrid by Using a Structured Polymeric Component on the Interface. Paper presented at the European Conference on Composite Materials, Munich, Germany

Gebhardt, J., Pottmeyer, F., Fleischer, J., & Weidenmann, K. (2015). Characterization of Metal Inserts Embedded in Carbon Fiber Reinforced Plastics. *Materials Science Forum, 825-826*, 506-513. doi:10.4028/www.scientific.net/msf.825-826.506

Smith, M. (2009). *ABAQUS/Standard User's Manual, Version 6.9*. Providence, RI: Simulia

Lee, H. (2015). *Damage Modelling For Composite Structures* (Unpublished master's thesis). University of Manchester. Retrieved from https://www.research.manchester.ac.uk/portal

Ghlaim, K. H. (2010). Woven Factor for the Mechanical Properties of Woven Composite Materials. Journal of Engineering, 16 6012-6027. Retrieved from https://www.iasj.net/

Kistner Machine Tools (2001). 6 Axes Universal Laser Machining Center. Trumpf Lasercell TLC 1005 Datasheet. Retrieved from http://www.maschinen-kistner.de/

Grujicic, M., Sellappan, V., Omar, M., Seyr, N., Obieglo, A., Erdmann, M., & Holzleitner, J. (2008). An overview of the polymer-to-metal direct-adhesion hybrid technologies for load-bearing automotive components. *Journal of Materials Processing Technology, 197*(1-3), 363-373. doi:10.1016/j.jmatprotec.2007.06.058

Mallick, P. K. (2010). *Materials, Design and Manufacturing for Lightweight Vehicles*. Retrieved from https://books.google.com.tr/books?id=LIdwAgAAQBAJ&printsec=frontcover&source=gbs_ge_summary_r&cad=0#v=onepage&q=doi&f=false

Bergmann, T., & Heimbs, S. (2017). Progressive bearing failure of composites for crash energy absorption. *Dynamic Response and Failure of Composite Materials and Structures*, 299-334. doi:10.1016/b978-0-08-100887-4.00010-x

Cox, B. N., & Flanagan, G. (1997). *Handbook of analytical methods for textile composites*. Washington, D.C.: National Aeronautics and Space Administration. Retrieved from https://ntrs.nasa.gov/

Esp, B. (2017). *Practical Analysis of Aircraft Composites* (pp. 1-103). Grand Oak Publishing. Excerpted from http://www.espcomposites.com/index.html

Xiao, Y., & Ishikawa, T. (2005). Bearing strength and failure behavior of bolted composite joints (Part I: Experimental investigation). *Composites Science and Technology,* 1022-1031. Retrieved from www.sciencedirect.com

Jacob, G. C., Simunovic, S., & Starbuck, J. M. (2002). Energy absorption in polymer composites. *Journal of Composite Materials*

Ucsnik, S., Scheerer, M., & Zaremba, S. (2010). Intralaminar toughness characterization of unbalanced hybrid plain weave laminates. Experimental investigation of a novel hybrid. *Composites Part A: Applied Science and Manufacturing,* 394-374

Kuhmann, K., Schulz, G. (2012). *Evonik Industries, Processing Vestamid HT Plus in Injection.* Retrieved from http://www.vestamid.com/

Arburg GmbH + Co KG Kuhmann. (2015). *Allrounder 270 S - Facts and Figures.* Retrieved from https://www.arburg.com/en/

Bighead® Bonding Fasteners. (2015). *Standard bighead List.* Retrieved from https://www.bighead.co.uk/

Donadon, M. V., Falzon, B. G., Iannucci, L., & Hodgkinson, J. M. (2007). Intralaminar toughness characterization of unbalanced hybrid plain weave laminates. *Composites Part A: Applied Science and Manufacturing, 38*(6), 1597-1611. doi:10.1016/j.compositesa.2006.12.003

Bergmann, T., & Heimbs, S. (2014, June). Investigation of a Composite Tensile Energy Absorption Element under Static and Dynamic Loading. Paper presented at *ECCM16_ 16th European Conference on Composite Materials,* Seville, Spain. Retrieved from https://www.researchgate.net/

Schraa, L. (2016). Simulation des Schädigungsverhaltens von CFK-Proben bei zyklischen Lasten unter der Einwirkung von Laminierfehlern (Unpublished master's thesis). TU Dortmund University

Garland, B. D., Beyerlein, I. J., & Schadler, L. S. (2001). The development of compression damage zones in fibrous composites. Composites Science and Technology, 61(16), 2461-2480. doi:10.1016/s0266-3538(01)00176-2

Summerscales, J. (2017, October 30). Composites Design and Manufacture (Plymouth University teaching support materials). Retrieved January 25, 2018, from https://www.fose1.plymouth.ac.uk/sme/MATS347/MATS347A4%20fracture.htm

Gay, D. (2105). Composite materials: design and applications. Boca Raton: CRC Press

Sika Deutschland GmbH. (2017). *Product Data Sheet for Biresin® CR170 with CH170-3 Hardener.* Retrieved from https://sikaaxson.sika.com/en/group.html

HP-Textiles GmbH. (2017). *Produktkatalog.* Retrieved from http://www.hp-textiles.de/service/video-download-portal/katalog/

Vangrimde, B., & Boukhili, R. (2002). Analysis of the bearing response test for polymer matrix composite laminates: bearing stiffness measurement and simulation. *Composite Structures, 56*(4), 359-3[3174. doi:10.1016/s0263-8223(02)00020-x

Knight, N. (2008). Factors Influencing Progressive Failure Analysis Predictions for Laminated Composite Structures. *49th AIAA/ASME/ASCE/AHS/ASC Structures, Structural Dynamics, and Materials Conference
 16th AIAA/ASME/AHS Adaptive Structures Conference
 10t*. doi:10.2514/6.2008-2108

Ramani, K., & Moriarty, B. (1998). Thermoplastic bonding to metals via injection molding for macro-composite manufacture. *Polymer Engineering & Science, 38*(5), 870-877. doi:10.1002/pen.10253

Menges, G., Michaeli, W., & Mohren, P. (2001). How to Make Injection Molds. *How to Make Injection Molds*. doi:10.3139/9783446401808.fm

Kim, J. S., Yoon, H. J., Lee, H. S., & Kwon, T. S. (2009, June). Energy Absorption Characterization of Composite Tubes. Paper presented at *INTERNATIONAL COMMITTEE ON COMPOSITE MATERIALS*, Edinburgh, UK. Retrieved from http://www.iccm-central.org/

Farley, G. L., & Jones, R. M. (1992). Crushing characteristics of continuous fibre-reinforced composite tubes. *Journal of Composite Materials, 26*(1), 37-50. doi:10.1016/0010-4361(92)90341-q

Hashin, Z., & Rotem, A. (1973). A Fatigue Failure Criterion for Fiber Reinforced Materials. *Journal of Composite Materials*, 7-448. doi:10.21236/ad0760146

Harris, B. (1999). *Engineering composite materials*. London: IOM Communications

Adumitroaie, A., & Barbero, E. J. (2012). Stiffness and Strength Prediction for Plain Weave Textile Reinforced Composites. *Mechanics of Advanced Materials and Structures, 19*(1-3), 169-183. doi:10.1080/15376494.2011.572245

Campbell, F. C. (2010). *Structural composite materials*. Materials Park, OH: ASM International

Lucchetta, G., Marinello, F., & Bariani, P. (2011). Aluminum sheet surface roughness correlation with adhesion in polymer metal hybrid overmolding. *CIRP Annals, 60*(1), 559-562. doi:10.1016/j.cirp.2011.03.073

Naik, N., & Nemani, B. (2001). Initiation of damage in composite plates under transverse central static loading. *Composite Structures, 52*(2), 167-172. doi:10.1016/s0263-8223(00)00164-1

Cai, D., Zhou, G., Wang, X., Li, C., & Deng, J. (2017). Experimental investigation on mechanical properties of unidirectional and woven fabric glass/epoxy composites under off-axis tensile loading. *Polymer Testing, 58*, 142-152. doi:10.1016/j.polymertesting.2016.12.023

Karakuzu, R., Taylak, N., Içten, B. M., & Aktaş, M. (2008). Effects of geometric parameters on failure behavior in laminated composite plates with two parallel pin-loaded holes. *Composite Structures, 85*(1), 1-9. doi:10.1016/j.compstruct.2007.10.003

Liu, Y., Zwingmann, B., & Schlaich, M. (2014). Nonlinear Progressive Damage Analysis of Notched or Bolted Fibre-Reinforced Polymer (FRP) Laminates Based on a Three-Dimensional Strain Failure Criterion. *Polymers - Open Access Polymer Science Journal, 6*(4), 949-976. doi:10.3390/polym6040949

Pakdil, M., Sen, F., & Cakan, A. (2011). Failure Behavior of Two Parallel Pinned/Bolted Composite Joints. *Journal of Mechanics, 27*(01), 121-127. doi:10.1017/jmech.2011.13

Johnson, A. (2001). Modelling fabric reinforced composites under impact loads. *Composites Part A: Applied Science and Manufacturing, 32*(9), 1197-1206. doi:10.1016/s1359-835x(00)00186-x

Lanxess Corporation, (2005). Plastic Metal Hybrid Technology. Retrieved January 29, 2018, from https://techcenter.lanxess.com/scp/americas/en/innoscp/tech/78310/article.jsp?docId=78310

Koch, S. F., Barfuss, D., Bobbert, M., Groß, L., Grützner, R., Riemer, M., . . . Wang, Z. (2016). Intrinsic Hybrid Composites for Lightweight Structures: New Process Chain Approaches. Advanced Materials Research, 1140, 239-246. doi:10.4028/www.scientific.net/amr.1140.239

10 Appendix

10.1 Material properties for FE Analysis of metal Inserted Specimens

Table 10.1*: Material properties of the metal insert that are used in FE Analysis*

True Stress (MPa)	Plastic Strain
202	0 *
246	2,37E-02 *
294	4,78E-02 *
374	9,44E-02 *
480	0,18 *
Elastic Modulus o	210 MPa
Poisson's Ratio	0.3

* Taken from Zareh 2011, Material non-linearity tutorial [37]

10.2 Calculation of bearing stress and strain of reference specimens

Table 10.2*: Calculation of area under stress*

Parameter	Symbol	Equation	Value
Hole Diameter	D	Measured	19 mm
Specimen Thickness	t	Measured	3 mm
Area under stress	A	A=D.t	54 mm^2
Pin pull-through force	F	Measured	[0, ~25,000 N]
Bearing Stress*	σ	$\sigma = \frac{F}{2\,.\,D\,.\,t}$	$\frac{\text{F [N]}}{2\,.\,54\,\,.\,3\,[\text{mm}^2]}$
Pin Displacement	δ	Measured	[0, ~12 mm]
Bearing Strain*	ε	$\varepsilon = \frac{\delta}{D}$	$\frac{\delta\,[\text{mm}]}{19\,[\text{mm}]}$

** For every data point at force-displacement plots*

Equation 2.1 ($\sigma = \frac{F}{2\,.\,D\,.\,t}$), becomes $\sigma\,[\text{MPa}] = \frac{F\,[\text{N}]}{2\,.\,54\,\,.\,3\,[\text{mm}^2]}$ under given D and t values where is bearing stress and is exerted force on the reference composite specimen.

Equation 2.2 ($\varepsilon = \frac{\delta}{D}$), becomes ($\varepsilon = \frac{\delta\,[\mathrm{mm}]}{19\,[mm]}$) under given D and t values where is bearing stress and is exerted force on the composite specimen.

10.3 Elastic Modulus calculation of reference specimens

Elastic moduli of reference specimens are calculated with equation 10.1. The elastic modulus (E) is:

$$E(specimen) = \frac{\sigma_1 - \sigma_2}{\varepsilon 1 - \varepsilon 2} \qquad \textit{Equation 10.1}$$

where σ_n and ε_n are stress-strain values at selected data points from linear region.

Table 10.3: Elastic Modulus calculation of reference specimens

		Stress [MPa]	**Strain**	
Specimen W1	Data Point 1*	77.40351	0.043137	E_{W1}=2026.799 [MPa]
	DataPoint2*	21.67719	0.015642	
Specimen W3	Data Point 1*	87.46842	0.051863	E_{W3}=1993.266 [MPa]
	DataPoint2*	27.75439	0.021905	
Specimen W5	Data Point 1*	29.40877	0.021884	E_{W5}=1566.169 [MPa]
	DataPoint2*	7.31544	0.007779	
Elastic Modulus Average				**1862.078**

** Data points are chosen from the linear region of the stress-strain plots*

10.4 Stiffness Calculations of the specimens

Table 10.4: Stiffness calculation of reference specimens

		Force [N]	**Hole Displacement [mm]**	
Specimen W1	Data Point 1*	8824	0,8196	K_{W1}=**12160,8** [kN/mm]
	DataPoint2*	2471,2	0,2972	
Specimen W3	Data Point 1*	9971,4	0.9854	K_{W3}=**11959,59** [kN/mm]
	DataPoint2*	3164	0,4162	
Specimen W5	Data Point 1*	3891,6	0,4665	K_{W5}=**9593,348** [kN/mm]
	DataPoint2*	834,2	0,1478	
Stiffness Average				**11237,91**

** Data points are chosen from the linear region of the stress-strain plots*

Table 10.5: Stiffness calculation of metal inserted specimens

		Force [N]	**Hole Displacement [mm]**	
Specimen M2	Data Point 1*	8010	0,7575	K_{W1}= **11424,5** [kN/mm]
	DataPoint2*	2003	0,2317	
Specimen M3	Data Point 1*	10002,8	0,8092	K_{W3}=**13012,69** [kN/mm]
	DataPoint2*	2005,2	0,1946	
Specimen M4	Data Point 1*	4002,8	0,4949	K_{W5}=**11116,05** [kN/mm]
	DataPoint2*	2000,8	0,3148	
Stiffness Average				**11851,08**

** Data points are chosen from the linear region of the stress-strain plots*

Table 10.6: Stiffness calculation of polymer inserted specimens

		Force [N]	**Hole Displacement [mm]**	
Specimen P2	Data Point 1*	16261,2	1,8482	K_{W1}=**9350,723** [kN/mm]
	DataPoint2*	1456,2	0,2649	
Specimen P3	Data Point 1*	16130	1,6222	K_{W3}=**10554,55** [kN/mm]
	DataPoint2*	1908,8	0,2748	
Specimen P5	Data Point 1*	12766	1,4077	K_{W5}=**9302,764** [kN/mm]
	DataPoint2*	2196,2	0,2715	
Stiffness Average				**9736,012**

** Data points are chosen from the linear region of the stress-strain plots*

Table 10.7: Stiffness calculation of metal-polymer inserted specimens

		Force [N]	**Hole Displacement [mm]**	
	Data Point 1*	13109,6	1,6102	K_{W1}=**8131,473** [kN/mm]
	DataPoint2*	752,2	0,0905	
Specimen MP4	Data Point 1*	13074,8	1,5598	K_{W3}=**8445,937** [kN/mm]
	DataPoint2*	748,8	0,1004	
Specimen MP5	Data Point 1*	14279,6	1,5	K_{W5}=**9187,755** [kN/mm]
	DataPoint2*	1223,8	0,079	
Stiffness Average				**8588,388**

** Data points are chosen from the linear region of the stress-strain plots*